Escola de Camins
Escola Tècnica Superior d'Enginyeria de Camins, Canals i Ports
UPC BARCELONATECH

TREBALL FINAL DE MÀSTER

Vulnerability Assessment of Masonry Churches Including Uncertainty

Treball realitzat per:
Carles-Hug Bitlloch Martínez

Dirigit per:
Luca Pelà i Savvas Saloustros

Màster en:
Enginyeria Estructural i de la Construcció

Barcelona, juny de 2018

Departament d'Enginyeria Civil i Ambiental

You say to a brick, 'What do you want, brick?'
And brick says to you, 'I like an arch.'
And you say to brick, 'Look, I want one, too, but arches are expensive and I can use a concrete lintel.'
And then you say: 'What do you think of that, brick?'
Brick says: 'I like an arch.'

Louis Kahn,
Estonian-American Architect
Pärnu, 1901 - New York City, 1974

ACKNOWLEDGEMENTS

I sincerely thank my two supervisors, Associate Professor Luca Pelà and PhD Savvas Saloustros for their support and assistance as well as our productive conversations and criteria exchanges.

I want to thank MSc Francesca Romana Contrafatto too, whose worries and tensions I have understood by the end of this work. Even if we never meet, I admire and thank her intrepidity and overcoming of difficulties.

I cannot forget to include the Basilica de Santa Maria del Pi's staff. The sacristan Pascual for his openness and patience in showing me the not public parts of the church; the tourist guide Biel for including me in his visit; and the archivist Jordi Sacasas, for his extensive knowledge of the Santa Maria del Pi's history, his predisposal to explain every detail of the church and his passion for the monument. Monuments are dead without their passionates that endure their legacy for the present and next generations.

And last but not least, I would like to thank my boyfriend Eric for his unbreakable support and assistance, emotionally and academically. But especially for standing me up when hope seems to fly away.

CONTENTS

1. Introduction

1.1. Motivation of the Present Thesis

1.1.1. Masonry Churches in the Modern World

Masonry Churches are normally witnesses of the ancient times. Therefore, their adaptation to the modern world was at times difficult when not traumatic. However, Masonry Churches, as Historical Constructions, have a main role in the contemporaneous society. In addition to their traditional religious role, of decaying importance, they are considered monuments with a scientific, cultural and social importance. Furthermore, with the relative recent cultural-related tourist industry, they acquire a prominent economic role, attracting visitors not only to the specific city area where they were built, but also to the whole city.

In consequence, the modern concepts of structural safety should be applied to these churches. This represents a main challenge, since the modern structural codes are traditionally conceived for new buildings, whose design and construction procedures can be controlled and changed for structural convenience. Lately, several codes have included recommendations and procedures for the structural assessment and intervention of the existing masonry buildings that concentrate in the usual typologies and construction technics. However, this recommendations and procedures are not entirely applicable to the Masonry Churches, either because the structural typologies are not included or because the recommended interventions would damage the scientific and cultural value.

1.1.2. ICOMOS Recommendations and Methodology Derived

In order to fix a common methodology for the application of the structural safety in the Historical Constructions, the International Council on Monuments and Sites (ICOMOS) approved a document (ICOMOS, 2003) that set the general principles and recommendations on the matter.

In the document, a multidisciplinary scientific approach to the structural safety of a Historical Construction was prescribed, as well as non-invasive reinforcement and material characterization procedures and a balance between structural safety and authenticity loss.

In the common interpretation of the document, a four branches methodology is adopted. These four branches are intrinsically interrelated and without them a complete structural assessment cannot be performed. The four branches are:

- **Historical Study:** the study of the history of the building may inform about hidden damage or ancient construction techniques.
- **Inspection of the Present Condition:** basic for the complete knowledge of the building.
- **Monitoring of the Existing Damage**: it is important to know if the visible damage is still active or only apparent.

- **Structural Modelling:** the highest technological tools let to a highest understanding of the building behaviour, especially under exceptional loads, like seismic ones. (The present thesis is mainly based on this branch)

1.1.3. Need of an Appropriated Seismic Vulnerability Assessment

The prescriptions and recommendations of (ICOMOS, 2003) complicate the structural modelling of the Historical Construction. Not only in the determination of the structure geometry, since parts of it might be hidden, but also in the determination of the material properties.

A statistically relevant conventional material characteristics study would let to a significant cultural and scientific loss, therefore an specialized material characteristic study is required. However, such study would spend a significant amount of economic resources and, in consequence, a previous idea of the vulnerability of the building is needed in order to justify such campaign.

In conclusion, a Seismic Vulnerability Assessment that includes the uncertainty in the material properties is required in order to justify (or not) further studies.

1.2. Aim and Objectives of the Present Thesis

The aim of the present thesis is the Seismic Vulnerability Assessment of the church of Santa Maria del Pi (SMPi), in Barcelona, the case study.

This aim will be achieved through the following enabling objectives:

- To question and refine the methodology used in previous similar studies like (Petromichelakis, Saloustros and Pelà, 2014; Contrafatto, 2017). This questioning and redefining will be done in two different ways:
    - Studying and drawing conclusions from the existing knowledge (literature).
    - Validating through the development of the thesis the aspects not clear in the literature.
- To appropriately and computationally model the church of SMPi, balancing exactitude and computational cost.
- To obtain the variability of the SMPi's response to an earthquake, in terms of:
    - Structural resistance to horizontal loads depending on the displacement (capacity curves).
    - Damage provability depending on the maximum ground acceleration (PGA) during the earthquake (fragility curves).

1.3. Methodology of the Present Thesis

The Methodology of the present paper is based in the used in (Petromichelakis, Saloustros and Pelà, 2014) and (Saloustros *et al.*, 2018) –this second paper is based in the master thesis (Contrafatto, 2017).

The methodology consists in the consideration of the Material Properties as random variables that are used in a mapping model in order to obtain the seismic fragility of the church of Santa Maria del Pi (SMPi).

The mapping model consists in the application of the N2 method; this is, an incremental lateral loading of a Finite Elements Method (FEM) model of SMPi (pushover analysis) whose capacity curve is used to find an equivalent Single Degree of Freedom (SDOF) capacity curve and then this SDOF capacity curve is used to find the structure performance under an earthquake; finally the output is given in terms of Peak Ground Acceleration (PGA) necessary to achieve each Limit State (LS) or Damage Grade (DG) (Figure 1.3.A).

In other words, a large number of models (in this thesis 200) are modelled with random material properties (inside a previously selected range). Afterwards, these models are analysed through a pushover analysis and its seismic performance is obtained using the N2 Method. Finally, the necessary PGA to achieve each LS or DG is recorded.

The final results are presented using a cumulative probability function (the fragility function) that gives for each PGA the achievement of each LS or DG provability.

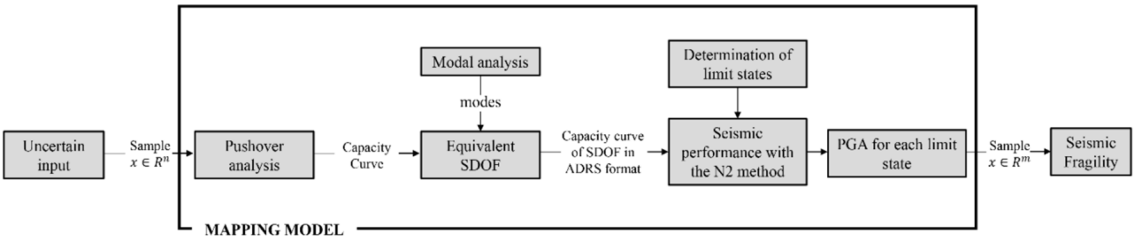

Figure 1.3.A: Methodology used in the present thesis, as it appears in (Saloustros *et al.*, 2018)

1.4. Outline of the Document

In Chapter 2 an overview of the case study (Santa Maria del Pi) is presented, with special attention to the History (Section 2.1) and the visible parts (Section 2.2) of the building.

A review of the literature oriented to the questioning of the methodology can be read in the Chapter 3. The focuses are the N2 Method (Section 3.1) and the Damage Grades (Section 3.2).

The Methodology of the thesis is explained in chapter 4 in a detailed schematic way. The main topics are the modelling (Section 4.1), the constitutive model (Section 4.2), the mechanical properties (Section 4.3), the N2 method (Section 4.4), the seismic performance (Section 4.5) and the seismic fragility (Section 4.6).

In Chapter 5 the modelling process is presented. The 3D models are described in section 5.1, the 2D model in section 5.2 and its calibration process is described in detail in section 5.3. Finally, the concerns and findings about the constitutive model behaviour are presented in section 5.4.

The results can be consulted in their own chapter, the chapter 6, where the Capacity Curves are described in section 6.1 and the Fragility ones in section 6.2.

The conclusions are explained in chapter 7, divided in conclusions (Section 7.1) and suggestions for the future work (section 7.2).

2. The Case Study - Basílica de Santa Maria del Pi

The case study is the Basílica de Santa Maria del Pi (Basilica of Saint Mary of the Pine Tree, in Catalan). The Basilica is located in the centre of the Old Town of Barcelona (Figure 2.A) near La Rambla and the Barcelona Opera House (Gran Teatre del Liceu). Main church of the homonymous parish it combines the liturgical and religious use with the guided tours and tourist visits. It is often considered one of the main gothic churches of Barcelona, with the Cathedral and Santa Maria del Mar.

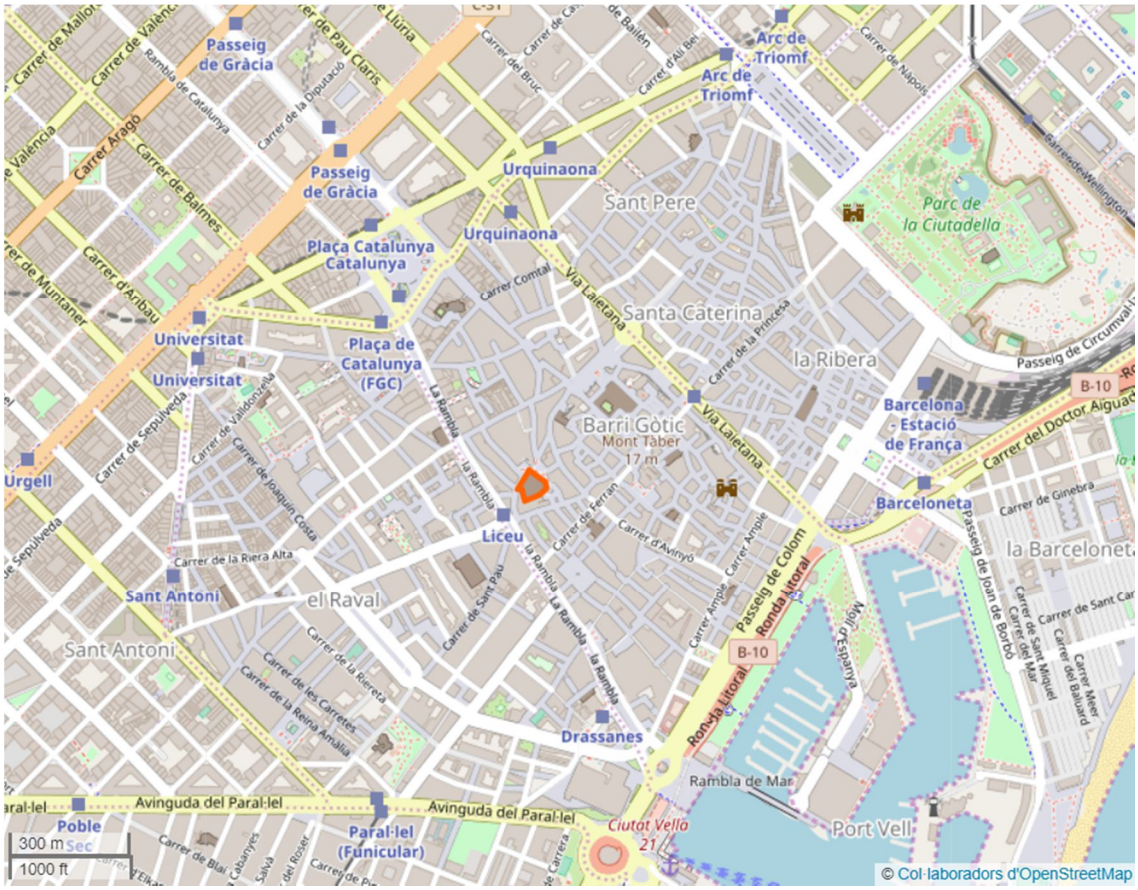

Figure 2.A: Location of the Basilica de Santa Maria del Pi in the Old Town of Barcelona © OpenStreetMap contributors

2.1. History of Santa Maria del Pi

The present chapter has been written using the information found on the Basilica's web site (*Basílica de Santa Maria del Pi*, 2017) based on the work of (Vergés, 1992) and newer research done by the Parish Archive Organization (Arxiu Parroquial de Santa Maria del Pi – APSMP).

An antecedent to the gothic church is an ancient Romanesque church located in the same place. The vestiges of that church are manly documental, however, several Romanesque capitals may be found on the northern lateral doorway of the gothic church (Figure 2.1.A). This means that several stones of the Romanesque church were used in the Gothic one.

Figure 2.1.A: Romanesque capitals in the northern lateral doorway.
(*Basílica de Santa Maria del Pi*, 2017)

2.1.1. The Construction of a Gothic Church

The construction of the gothic church is believed to have started between the years 1318 and 1320, since the first architect, Jaume Fabre, was already leading the Cathedral construction since 1317 and the first altar was under construction on 1321.

By the year 1340 half of the church (the eastern part) was already build when a big stop on the construction happened on the year 1348 because of the Great Plague. The construction restarted afterwards and the church was finished on the year 1391.

During the fifteenth, sixteenth and seventeenth centuries different annexes to the church were completed, namely the bell tower, the sacristy, the rectory and the chapel Chapter (Figure 2.1.1.A).

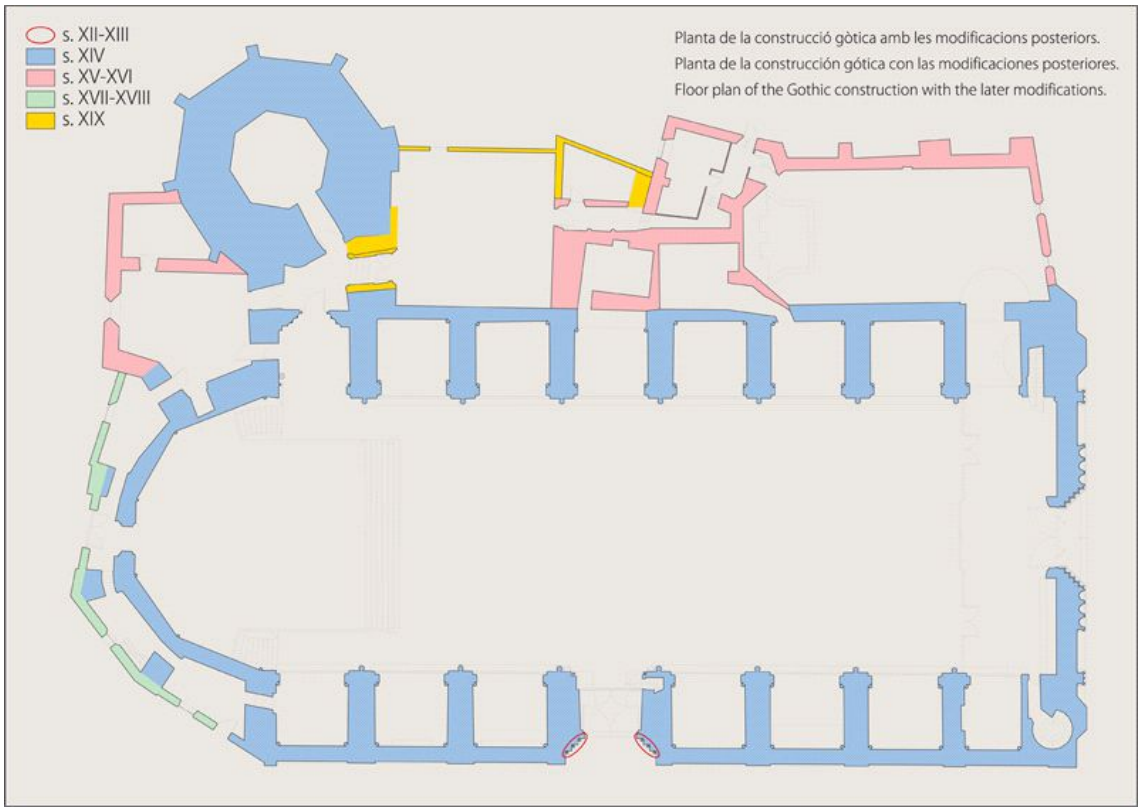

Figure 2.1.1.A: Plan of the gothic church with the later modifications.
(*Basílica de Santa Maria del Pi*, 2017)

2.1.2. The Ravages of War and Revolution

The Basílica de Santa Maria del Mar has been a mayor scenario of two different wars that affected Barcelona, the War of the Spanish Succession (1701-1714) and the Spanish Civil War (1936-1939).

By the end of the War of the Spanish Succession, Barcelona was under siege by the Bourbon France Army. In this context, the bombing of the 9th of June of 1714 caused major damage to the church. It is reported the collapse of the presbytery and some of the northern lateral chapels, as well as most of the church windows. More information about these events is available in (Navarro *et al.*, 2013).

After the failure of the coup d'état (*El Alzamiento*) of the General Francisco Franco on the 18th of July of 1936 the Spanish Civil War began. Barcelona was therefore hold by a revolutionary spirit, especially after the defeat in the city streets of the coup supporters on the 19th of July. In this context, anarchist and anticlerical groups assaulted the city churches on the 20th of July.

Santa Maria del Pi was not an exception; nearly all the burnable elements of the church were burned, causing important damage on the auxiliary elements but none remarkable on the structure. Some damage examples are observable in the figure 2.1.2.A, namely, falling of the rose window, burning of the altar and the sacristy.

Figure 2.1.2.A: State of the church after the burning on the 20th of July of 1936. (*Basílica de Santa Maria del Pi*, 2017)

2.2. Inspection of Santa Maria del Pi

On the 12th and 13th of April of 2018 a general inspection of the state and characteristics of Santa Maria del Pi was made.

2.2.1. Street Inspection

From what can be seen from the street and public space (figure 2.2.1.A), it is important the presence of vegetation in the buttresses, especially the ones corresponding to the northern façade. Nonetheless, several traces of rainwater are also visible, as well as the effects of the soil moisture, especially from a closer look (figure 2.2.1.B)

Figure 2.2.1.A: General exterior views

Figure 2.2.1.B: Northern façade details

2.2.2. Inside Inspection

In the inner general view (Figure 2.2.2.A) the efflorescence is the only observable damage. It presents itself in the upper part of the chapels roof and, therefore, it seems to be related to rainwater infiltration.

The vaults, at their turn, do not seem to be damaged (Figure 2.2.2.B) while some small damage is observed on the floor and between the chapel arch and the clerestory window (Figure 2.2.2.C)

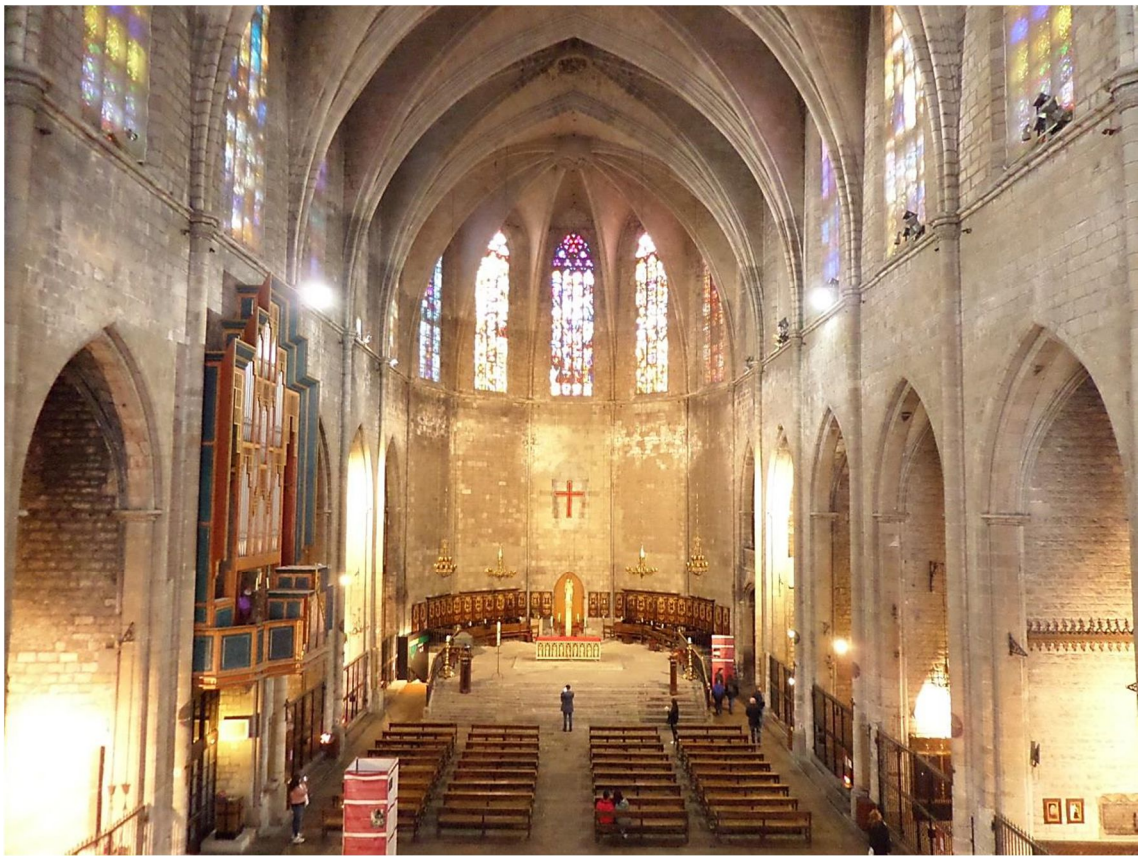

Figure 2.2.2.A: General view of the interior

Figure 2.2.2.B: Inferior views of the vaults

Figure 2.2.2.C: Observable damage in the interior, traces on the floor of the burning of 1936 (left) and cracks between the chapel arch and the clerestory window (right).

2.2.3. Roof inspection

The church roof can be divided in two different levels, the chapels' roof (with the passes through the buttresses) and the nave's roof.

The chapels' roof (Figure 2.2.3.A) presents little observable structural damage. The main damage is an old one present on the first span (Figure 2.2.3.B). This old damage was repaired and may be due the 1428 earthquake. However, it seems to have some movement, since the warner from April 1995 is broken.

The nave's roof (Figures 2.2.3.C and 2.2.3.D) has been recently renewed and, therefore, no damage is observable.

Figure 2.2.3.A: Views of the passes through the buttresses

Figure 2.2.3.B: Old repaired damage on the first span (right) and opened warner (written date: 4-1995) (left).

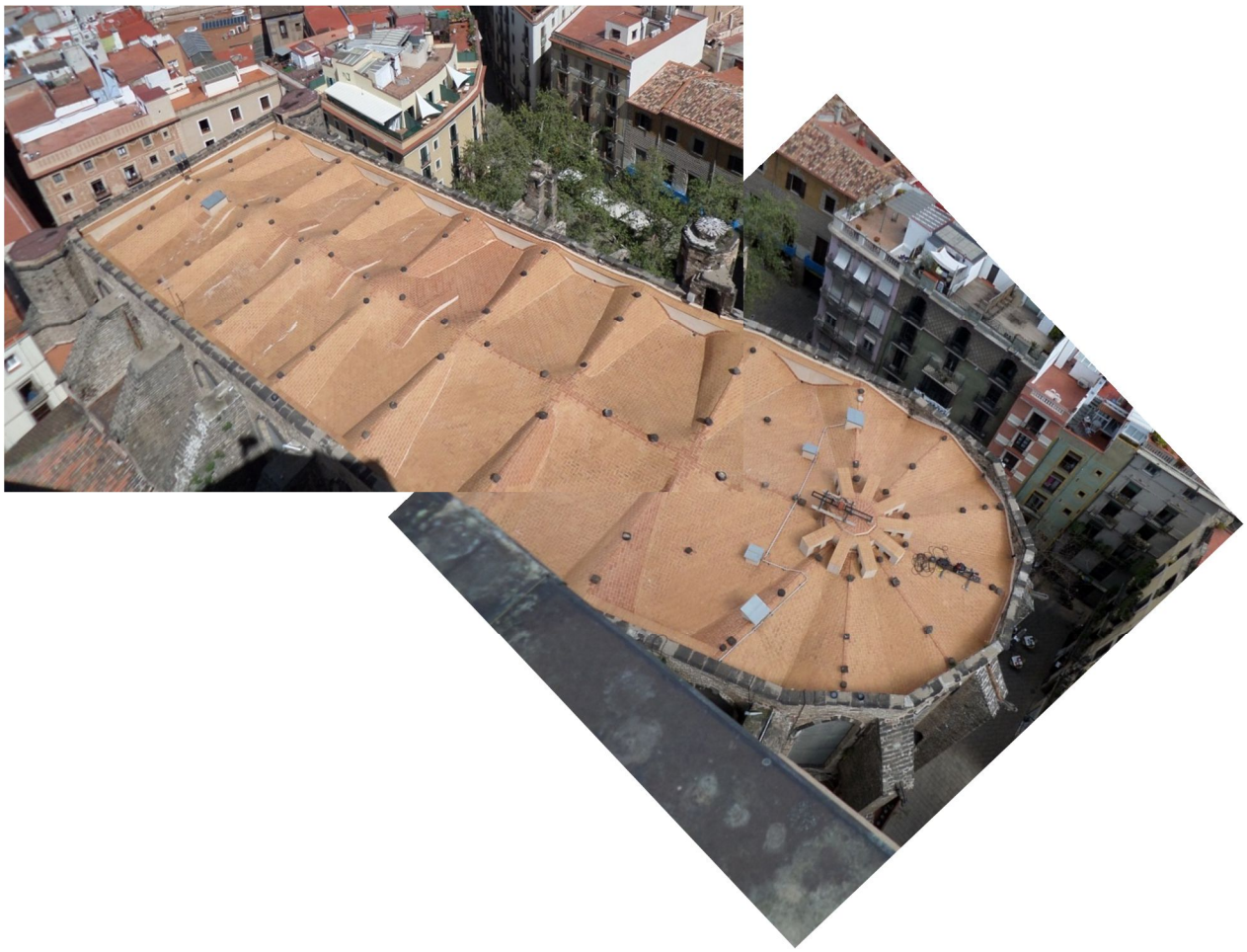

Figure 2.2.3.C: View of the roof from the bell tower.

Figure 2.2.3.D: View of the roof from the roof level.

3. State of the Art

3.1. Applicability of the N2 Method

3.1.1. Limitations of the N2 Method application

The N2 Method was proposed in (Fajfar, 2000) applied to a "Shear Frame", a simple frame made of beams and pillars, arranged in storeys. In that model, nonlinearity (plasticity) is concentrated in both ends of the linear elements. In the same way, mass is concentrated in the storeys and the control node is at the top of the structure.

The version that appears in the Eurocode 8-1 (European Committee for Standardization, 2004) confirms the limitations expressed above and goes further by considering the frame irregularity.

It's obvious then that the use of the N2 Method is not supported in a very complex masonry building in the form of the proposal of (Fajfar, 2000) or the Eurocode 8-1.

This limitations show that the use of the N2 Method in a Historical Construction should be questioned in every part of it, namely the Lateral Load Distribution, the Control Node and the equivalent SDOF structure.

3.1.2. Lateral Force Distribution (LFD)

One of the bases of the N2 Method is the "pushover" analysis, which is the incremental loading of the structure with a lateral force, distributed in height with one or more concrete rules, like the modal or mass distribution.

In the initial proposal of the N2 Method (Fajfar, 2000) a distribution according to only the first vibration mode was used. However, the Eurocode 8-1 (European Committee for Standardization, 2004) proposes the use of the mass distribution, the first vibration mode and, if significant, following vibration modes. The results of the different Lateral Force Distribution (LFD) are then used as an envelope of the structure behaviour.

Nonetheless, the Method was initially thought for steel or reinforced concrete which don't normally have huge differences in their stiffness distribution after the loading. So the use of the initial vibration modes is acceptable.

On the other hand, masonry buildings present a distributed stiffness, which may change significantly due to damage while loading. This is because the damage tends to concentrate in certain zones while other remain nearly untouched. Therefore, any use of the vibration mode shall be adaptive to the existent damage in every step, as in (Galasco, Lagomarsino and Penna, 2006).

The adaptive approach consumes a large amount of resources, though. And those should be used multiple times if we include uncertainty. Moreover, it has been proved in masonry residential buildings (Lourenço *et al.*, 2011) and bridges (Pelà, Aprile and Benedetti, 2013) that a LFD according to the mass distribution is a conservative approach compared to a Nonlinear Dynamic Analysis (Time-History).

In conclusion, a Lateral Force Distribution (LFD) according to the mass distribution seems to be conservative enough as well as not very computationally demanding, since it doesn't change during the loading.

3.1.3. Choosing of the control node

In the common definition of the control node, it is assumed to be the highest point of the structure (Fajfar, 2000). In the normative application (Eurocode 8-1) this point is redefined as the centre of mass of the roof of the building.

Contrary to regular frame concrete structures, in masonry ones the choice the control node is not straightforward. Therefore, several studies can be found in the literature that try to address this question.

One of them is (Pelà, Aprile and Benedetti, 2013), were a 3D FEM model of the San Marcello Pistoiese Bridge in Italy is analysed using a variation of the N2 method (Nonlinear Static Analysis – NSA) as well as a Nonlinear Dynamic Analysis (NDA).

For the NSA two control nodes are considered, one in the Top of the structure and another one on the Centre of Mass (Figure 3.1.3.A).

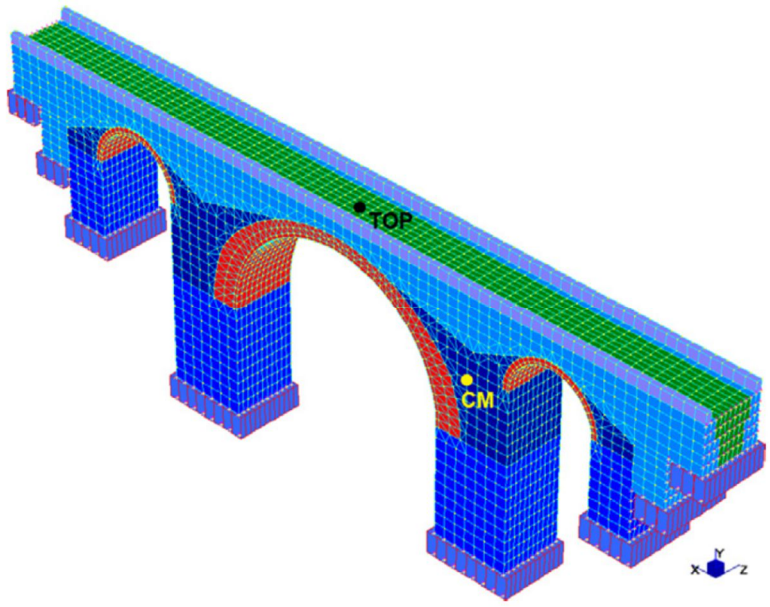

Figure 3.1.3.A: Control nodes for the NSA considered in (Pelà, Aprile and Benedetti, 2013)

For the NDA, 21 different earthquake records are used, scaled according to the EC-8 spectrum for 0.15g, 0.30g and 0.40g. Then the maximum displacements are compared to the N2 pushover curve and its performance point using the spectrum for 0.15g, 0.30g and 0.40g. In Figure 3.1.3.B the results for the 0.30g spectrum for the control node in the Top (TOP) and Centre of Mass (CM) are shown.

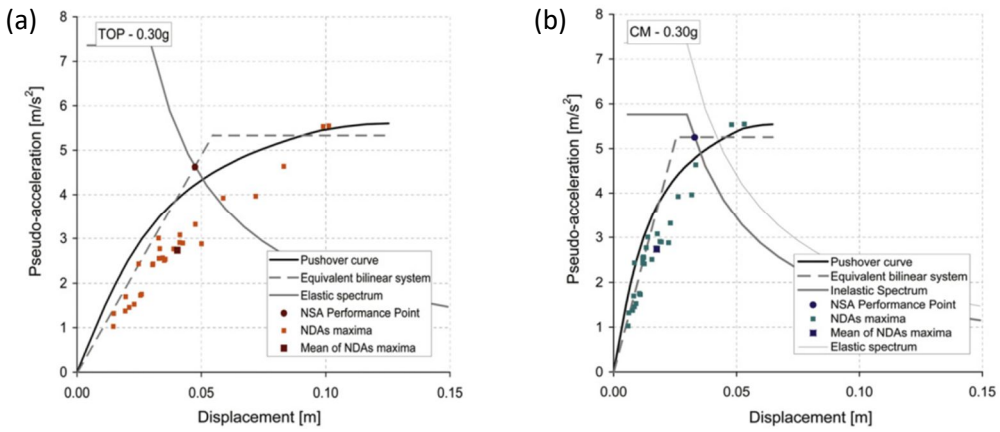

Figure 3.1.3.B: Results for the TOP (a) and the CM (b) control nodes for 0.30g in (Pelà, Aprile and Benedetti, 2013)

The results show that the control node in the Centre of Mass of the structure is more conservative in terms of ductility, since it is stiffer and its plastic branch is shorter. Furthermore, the NDA results are under or very near the capacity curve (Figure 3.1.3.B) meaning that the NSA predicts higher force demand for the same displacement compared to the NDA. That adds up with the higher displacement of the Performance Point of NSA compared with the mean of the NDA (Figure 3.1.3.C).

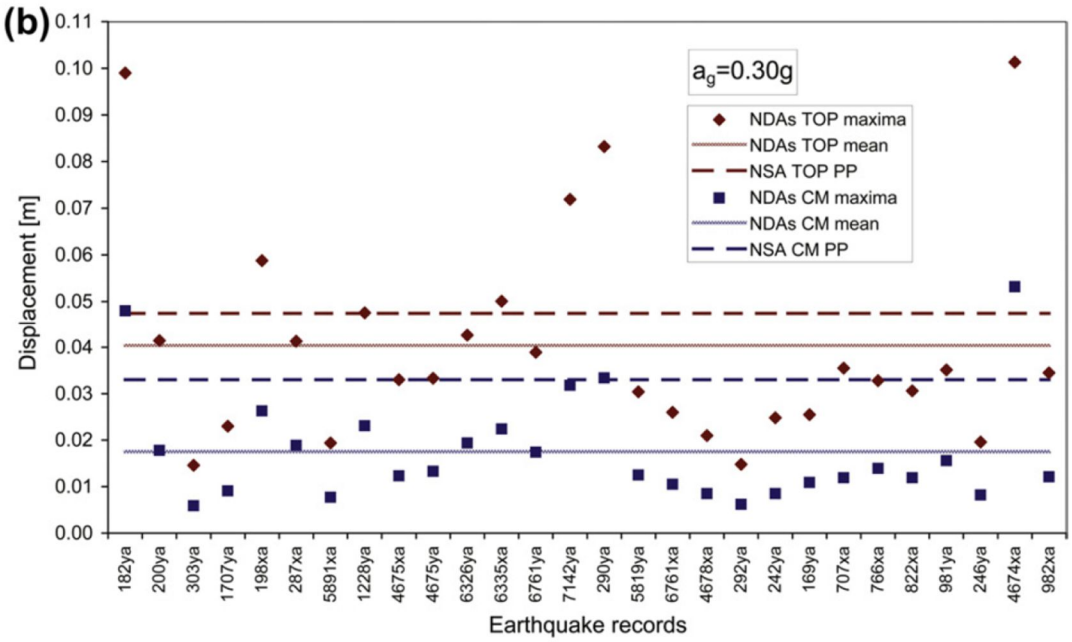

Figure 3.1.3.C: Results for 0.30g in terms of displacement in (Pelà, Aprile and Benedetti, 2013)

The work shows that the use of the CM Performance Point (PP) is more conservative than the use of the TOP Performance Point. On the other hand, the TOP PP presents a closer approximation to the NDA mean, with a higher variability on the NDA results.

A preliminary study on the same Italian bridge by the same authors (Pelà, Aprile and Benedetti, 2009) used apart from the TOP and CM control nodes, the virtual energy displacement (EN). The capacity curve of this virtual displacement is referred to the

whole energy developed (elastic and plastic) by the complete structure during the loading process. That approach seems even more conservative than the use of the CM as a control node, as the capacity curve shows in Figure 3.1.3.D.

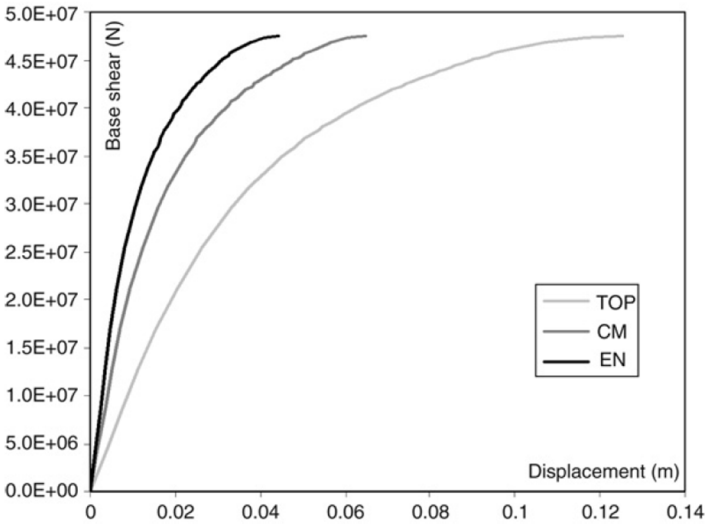

Figure 3.1.3.D: Capacity curves of the top node (TOP), the centre of mass node (CM) and the virtual energy displacement (EN) in (Pelà, Aprile and Benedetti, 2009)

Another example is an article about Mallorca's Cathedral by (Elyamani *et al.*, 2017). In this article the behaviour of the building is tested in the two axes of the plane and in each of their two directions by means of a Nonlinear Static Analysis. In other words, it is tested under X+,X-,Y+ and Y- forces.

Furthermore, 3 or 4 different control nodes are used, namely: the Top of the structure (located at the top of the gable of the west façade), the centre of gravity of the full cathedral (CG-cathedral), the centre of gravity of the naves' roof (CG-roof) and the point with the maximum displacement in the considered direction (Max-D; only in case it is none of the previous 3).

Figure 3.1.3.E and Figure 3.1.3.F present the capacity curves for loading towards the Y+ and Y- directions, which correspond to the transversal ones. The results show that the selection of the control node Max-D seems to be the least conservative while the most conservative seems the CG-cathedral. The control node TOP has a very small displacement, and therefore, its results do not seem to be accurate according to the (Elyamani *et al.*, 2017) article.

From the analysed works (Pelà, Aprile and Benedetti, 2009, 2013; Elyamani *et al.*, 2017) no definitive conclusion can be derived. However, it is shown that the less displacement the node has the more conservative it is. Nonetheless, if the displacement is too small the results might not be accurate enough.

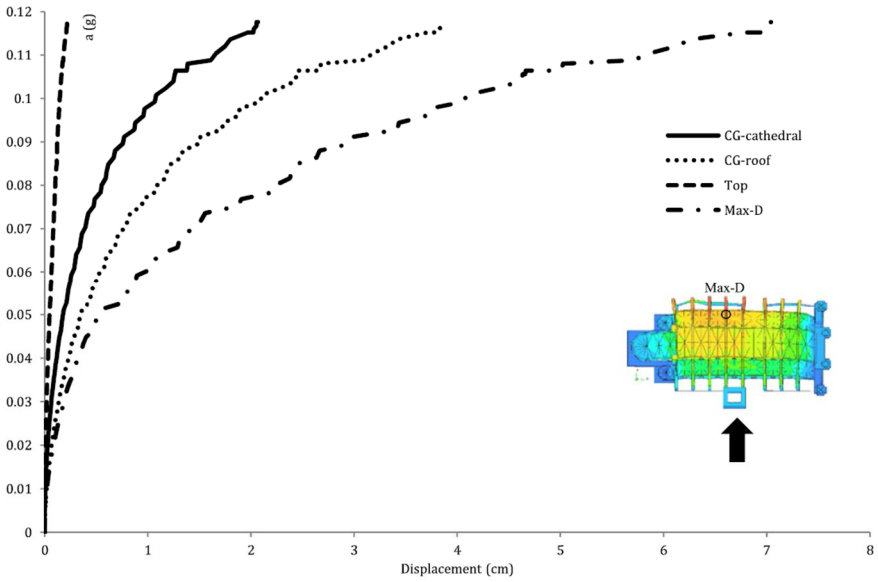

Figure 3.1.3.E: Capacity curves for the analysis in (+Y) direction. In (Elyamani *et al.*, 2017)

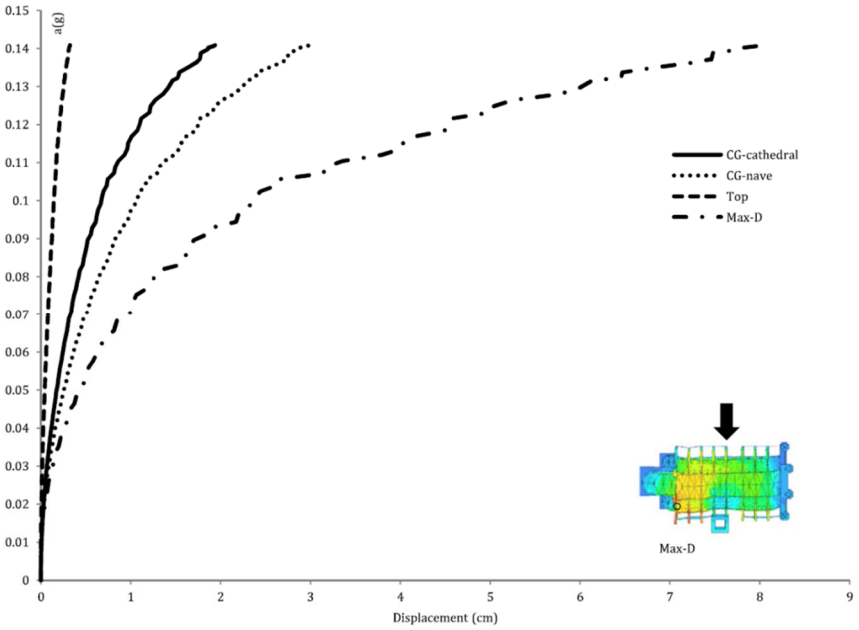

Figure 3.1.3.F: Capacity curves for the analysis in (-Y) direction. In (Elyamani *et al.*, 2017)

3.1.4. Equivalent SDOF structure

A main characteristic of the behaviour of masonry structures under horizontal load is their post-peak response, as experimental studies like (Tomaževič and Klemenc, 1997; Costa, Penna and Magenes, 2011) have shown.

Therefore, the pushover curve shall be displacement-controlled by using, for instance, the Arc Length Method (Riks, 1979). Moreover, the equivalent SDOF structure shall consider the residual strength, and not stop at the maximum resistance, as proposed in the Eurocode 8-1.

An early proposal on (Tomaževič and Žarnič, 1984) idealized the envelope of the hysteretic curve of a wall under cyclic lateral loading (equivalent to the *pushover* curve) as a bilinear elasto-plastic curve. In the Figure 3.1.4.A the envelop of the hysteretic (continuous) and the idealized (dashed) curves are shown.

The idealized curve is defined using the onset point of cracking (d_{cr},H_{cr}), the maximum resistance (H_{max}) and the maximum displacement (d_{max}). The slope of the first line (K_e) is defined as the ratio between the force in the onset point of cracking and the displacement on this moment. The elevation of the second and horizontal line (H_u) was obtained under the energetic conservation criterion, that is, the area under the bilinear curve must equal the area under the envelope of the hysterical curve.

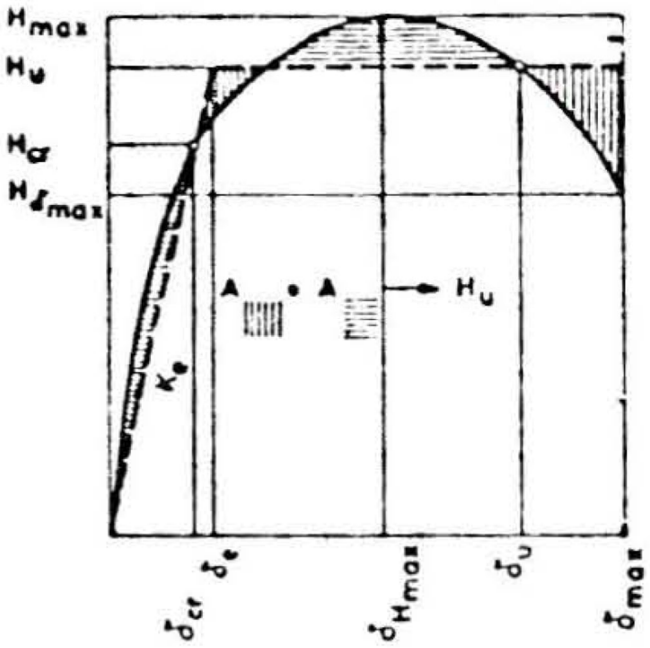

Figure 3.1.4.A: Idealization of the Hysteresis Envelope as it appears on (Tomaževič and Žarnič, 1984).

That early approach was too dependent on the maximum displacement, or collapse displacement (d_{coll}). This is problematic, since the maximum displacement in an analytical curve might be due to a numerical non-convergence.

In (Tomaževič, 2007) a more standardized approximation to the SDOF structure is proposed. Since the identification of d_{coll} might be problematic, d_u is identified conventionally as the displacement where the resistance of the structure degrades a

20% of the maximum resistance (H_{max} or R_{max}). Then only the curve section between the origin and d_u is used to obtain H_u or $R_{max,i}$ and K_e is obtained as the ratio R_{cr}/d_{cr}. In Figure 3.1.4.B the resistance (continuous) and the idealized (dashed) curves are represented using the above definition.

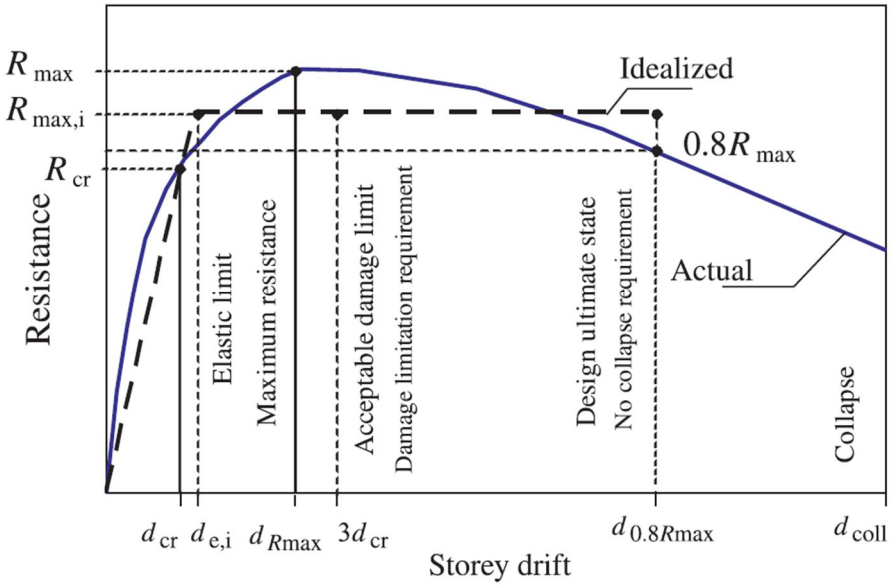

Figure 3.1.4.B: Idealization of resistance curve and definition of Limit States as it appears on (Tomaževič, 2007)

Even after the correction, the idealization method presents a problem in its application; the identification of the onset point of cracking must be done experimentally. Because the analytical models are not realistic enough to determine that point in a complex building, especially if a simplified model is used.

In the Comments (Italian Ministry of Infrastructure and Transport, 2009) of the Italian Standard NTC-08 (Italian Ministry of Infrastructure, 2008) a conventional identification of the onset point of cracking is proposed, as the displacement where the 60% of the maximum resistance (F^*_{bu}) is reached. At the same time the d_u is also identified as the displacement where the resistance of the structure degrades a 20% of the maximum resistance. In the Figure 3.1.4.C the resistance (bold) and idealized (light) curves are shown.

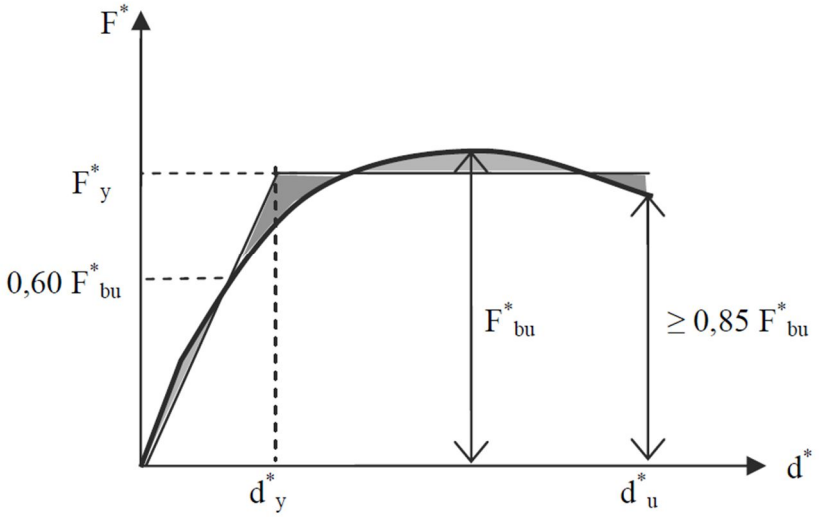

Figure 3.1.4.C: Idealization of the resistance curve as it appears on the Comments to the NTC-08, for masonry d^*_u is identified as $0.8F^*_{bu}$.

This method will be explained in detail in the Section 4.4.3.

3.2. Damage Grade Identification

After an earthquake most of the previously existing structures will have been damaged. In order to process this damage a classification or scale is needed. Obviously this scale will depend on the objectives of the person or institution that made it. This is, an insurance company will base it in the repair cost, while a NGO might base it in the structural safety or life losses.

Focusing on the structure, the damage is normally classified using damage grades. In short, a damage grade is something reached when a concrete event occurs. This might be a hair-line crack, a stiffness change, a relative displacement or a partial collapse. Therefore, the identification of the different damage grades has been, and still is, a controversial issue.

3.2.1. European Macroseismic Scale 1998 (EMS-98)

Most of the used grades are adapted from the proposal of EMS-98 (European Seismologic Commission, 1998). According to this, the damage grades were thought as a way to determine the intensity of an earthquake in terms of its effect over existing structures. Therefore, the criteria for the identification are rather vague and observation-based.

The grades and their description for masonry buildings are, according to EMS-98, as follows:

- **Grade 1: Negligible to slight damage** (no structural damage, slight non-structural damage):
    - Hair-line cracks in very few walls.
    - Fall of small pieces of plaster only.
    - Fall of loose stones from upper parts of buildings in very few cases.

- **Grade 2: Moderate damage** (slight structural damage, moderate non-structural damage):
    - Cracks in many walls.
    - Fall of fairly large pieces of plaster.
    - Partial collapse of chimneys.
- **Grade 3: Substantial to heavy damage** (moderate structural damage, heavy non-structural damage):
    - Large and extensive cracks in most walls.
    - Roof tiles detach.
    - Chimneys fracture at the roof line; failure of individual non-structural elements (partitions, gable walls).
- **Grade 4: Very heavy damage** (heavy structural damage, very heavy non-structural damage):
    - Serious failure of walls; partial structural failure of roofs and floors.
- **Grade 5: Destruction** (very heavy structural damage):
    - Total or near total collapse.

Even considering that the EMS-98 quantifies the terms "few", "many" and "most" the grades are very dependent on the effect over non-structural entities and other effects difficult to include in a structural model.

3.2.2. Numerical Scales Based on the EMS-98

In order to determine the possible effects of earthquakes to different European cities in the project RISK-UE (Mouroux and Le Brun, 2006), including Barcelona (Lantada *et al.*, 2010), a numerical scale based on the EMS-98 and the N2 Method was developed (Lagomarsino and Giovinazzi, 2006).

The proposed scale uses the conventional values of yielding (d_y) and ultimate (d_u) displacements of the equivalent SDOF structure (Table 3.2.2.A). However, little information is given over the mechanical events that identify each limit state. Only the two first grades are related to assumed mechanical events. In the same way, the grades 4 and 5 of the EMS-98 are considered to be difficult to distinguish using the N2 Method and therefore merged in the damage grade 4, which corresponds to the ultimate displacement (d_u).

Table 3.2.2.A: Damage grades and their equivalence with the EMS-98 Grades according to (Lagomarsino and Giovinazzi, 2006)

EMS-98 Grade	Proposed damage grade	Displacement	Assumed mechanical event
Grade 1	1-Slight	$0,7*d_y$	Beginning of non-linear behaviour
Grade 2	2-Moderate	$1,5*d_y$	Maximum resistance
Grade 3	3-Extensive	$0,5*(d_y+d_u)$	-
Grade 4	4-Complete	d_u	-
Grade 5			

3.2.3. Mechanical Scales Based on the EMS-98

Other approximations more adjusted to masonry structures have been developed. An example is the one developed in (Lang, 2002) for the assessment of the existing buildings of the city of Basel, Basle-City, Switzerland.

The application of the POR method (Tomaževič, Turnšek and Terčelj, 1978) enables a more precise description of the five EMS-98 grades as seen below:

- **Grade 1: Negligible to slight damage**:
  - Point of onset of cracking.
  - Stress distribution becomes zero at the extreme fibre of the wall section.
- **Grade 2: Moderate damage**:
  - Behaviour of the building becomes nonlinear, the stiffness of the building starts to reduce.
  - Yield of the first wall.
- **Grade 3: Substantial to heavy damage:**
  - Increased nonlinear behaviour of the building, the stiffness of the building tends to zero.
  - Yield of the last wall.
- **Grade 4: Very heavy damage:**
  - Failure of first wall.
- **Grade 5: Destruction**:
  - Drop of the base shear of the building below 2/3 of the maximal.

This scale is more easily applicable than the one of EMS-98, and has been used in other works like (Karbassi and Lestuzzi, 2012). However, it is oriented to the use of the POR method.

3.2.4. Performance-Based Earthquake Engineering (PBEE)

A contemporary (and similar) idea to the EMS-98 is the Performance-Based Earthquake Engineering (PBEE). PBEE means identifying an acceptable seismic damage level of an engineered facility for a particular return period according to its importance.

As it is acknowledged since its early stages (Krawinkler, 1999) the development of this idea in specific requirements and Damage Grades or Limit States (as they are normally referred) is not a simple task.

The complexity is found not only in the rather vague definition of the Limit States (e.g. "collapse", "near collapse", "collapse prevention", "life safety", "operational", "fully operational", "damage control", "immediate occupancy", and "serviceability"); but also in the identification of the facility importance. For this last concept many parameters can be used, like: Building Life Cycle, direct life losses, indirect life losses (for medical facilities or facilities containing life threating products as nuclear, chemical, etc.), containing goods value, losses when not operative (social and economic), etc.

This concept was incorporated in the last version of the Eurocode 8-1 (European Committee for Standardization, 2004). The Eurocode 8-1 distinguishes two different Limit States, namely: (1) **Ultimate (No-collapse requirement)** (ULS) and (2) **Damage limitation** (DLS). Each of them has a defined return period regarding the building importance.

However, the verifications according to the Eurocode 8-1 for each Limit State are rather different. Whereas the ULS is verified in terms of resistance and ductility (energy dissipation), the DLS is verified in terms of inter-storey drift.

Some researchers identify implicitly in the Eurocodes documents a third Limit State, the **Serviceability Limit State** (SLS), that might be verified when the structure maintains itself in the elastic zone during the earthquake (Tomaževič, 2007).

3.2.5. Mechanical Scales Based on PBEE

In the application of the PBEE principles to common unreinforced masonry buildings, four Limit States are identified among researchers —according to (Ortega *et al.*, 2018):

- **LS1: Light Damage or Immediate Occupancy**:
    - Point of onset of cracking.
    - Behaviour of the building becomes nonlinear, the stiffness of the building starts to reduce.
- **LS2: Damage Limitation**:
    - Structure still functional.
    - Minor structural damage but with the need of significant repair.

- **LS3: Life Safety Limit State**:
    - Displacement corresponding to the maximum building strength (Maximum Base Shear).
- **LS4: Ultimate Limit State or Near Collapse Limit State**:
    - The building strength deteriorates below an acceptable limit, usually set at 80% of the maximum.

From the above list the only Limit State that seems under discussion is the LS2. Actually, several works try to find its location using different approaches. Below, two different approaches are described:

(1) **An experimental approach** in (Rota, Penna and Magenes, 2010):

In this work LS2 (or DS2) is identified as the drift corresponding to the first shear cracking of a single masonry pier (Figure 3.2.5.A). The drift value was obtained experimentally.

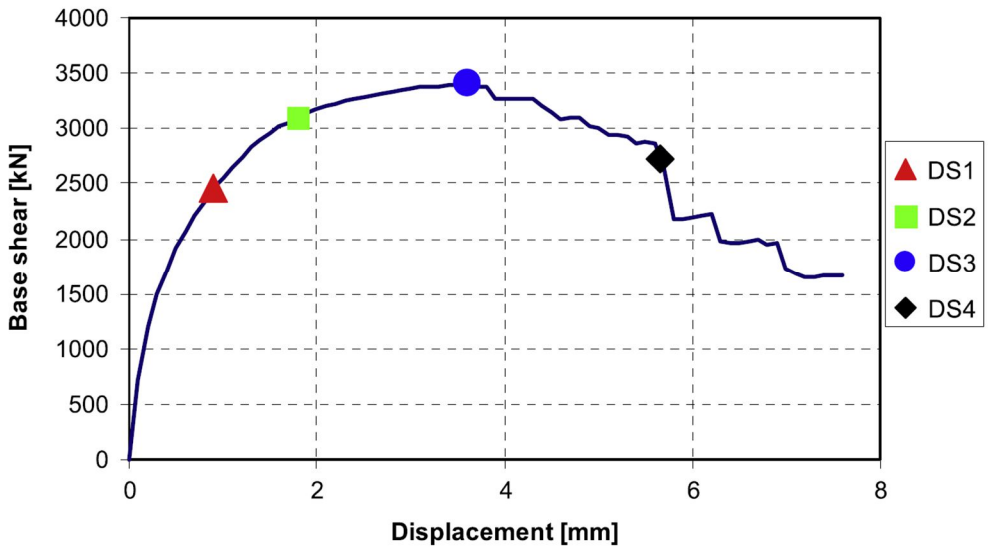

Figure 3.2.5.A: Damage States (Limit States) used in (Rota, Penna and Magenes, 2010).

(2) **An energetic approach** in (Ortega *et al.*, 2018):

In this work LS2 is calculated based on energy criteria so that the area below the bilinear curve formed by the points LS1, LS2 and LS3 coincides with the area below the pushover curve from LS1 to LS3. The criterion also involves that the point that defines the limit state LS2 is on the slope associated to the secant stiffness corresponding to 70% of the maximum strength (Figure 3.2.5.B). Since the point LS2 might be outside the pushover curve only its displacement (drift) is used as a defining criterion.

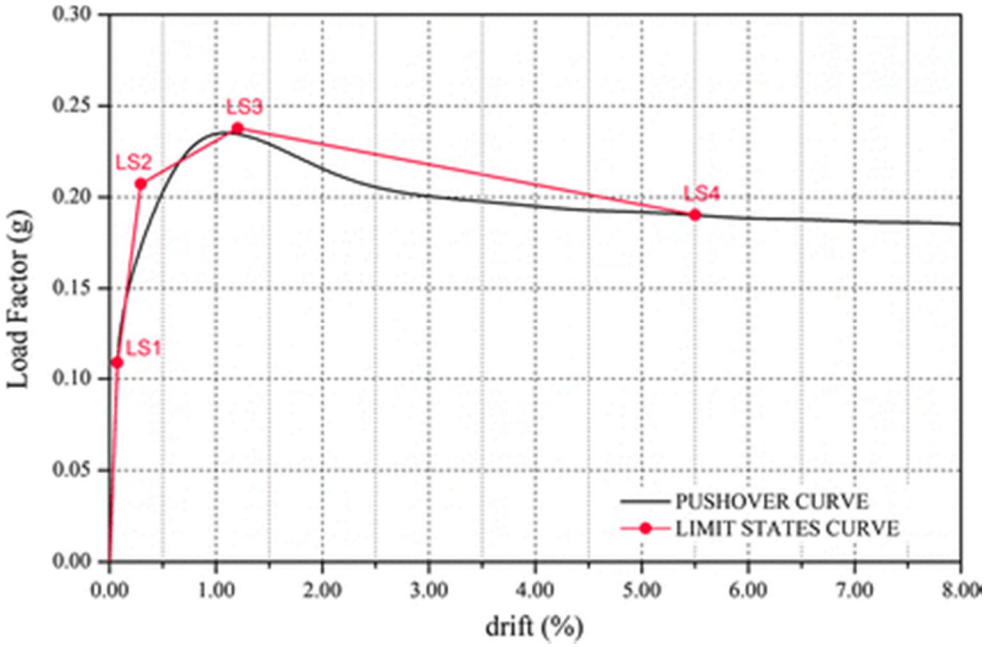

Figure 3.2.5.B: Limit States used in (Ortega *et al.*, 2018).

Finally, an extensive and rigorous analysis of the criteria to identify the four different Limit States (Mouyiannou *et al.*, 2014) concluded that only three could be identified with precise and stable criteria, namely:

- **LS1: Light Damage or Immediate Occupancy**:
    - The first pier attains its maximum shear resistance.
- **LS2: Damage Limitation Limit State**:
    - The average weighted storey drift corresponding to the attainment of the maximum base shear behaviour.
- **LS3: Life Safety Limit State**:
    - The maximum inter-storey drift corresponding to a 20% degradation from the maximum value of base shear

The article exposes that the LS4 is too close to collapse to be analysed and, therefore, was not included on the study. However, the proposed LS2 and LS3 correspond to the LS3 and LS4 of the previous studies (Rota, Penna and Magenes, 2010; Ortega *et al.*, 2018).

As exposed in (Krawinkler, 1999) the definition of the Limit States is at times vague and the same requirement may take different names. However, in the analysed studies three limit states have the same requirements, LS1, LS3 and LS4 in (Rota, Penna and Magenes, 2010; Ortega *et al.*, 2018) and LS1, LS2 and LS3 in (Mouyiannou *et al.*, 2014).

3.2.6. Mechanical-Experimental Scales Based on EMS-98 and PBEE

In (Tomaževič, 2007) an effort to associate the experimental behaviour of different kinds of masonry buildings with the analysis possibilities and the EMS-98 and the PBEE scales as included in the Eurocode 8-1 is presented.

According to this work, four main Limit States or significant points are found on any masonry building under lateral loading, namely:

(1) Crack (damage) limit state, were the first cracks occur in the walls causing a change in the system stiffness. — identified as Serviceability Limit State.

(2) Maximum resistance.

(3) Design ultimate limit state, where the resistance of the system degrades below the acceptable level —conventionally settled in a 20% of degradation from the maximum resistance.

(4) Limit of collapse, defined by partial or total collapse of the structure.

In the work a correlation among the EMS-98 scale, the Eurocode 8-1 Limit States and the Mechanical events is developed. In the Table 3.2.6.A this correlation is presented in a schematic way (See also Figure 3.1.4.B).

Table 3.2.6.A: Schematization of the correlations presented in (Tomaževič, 2007)

EMS-98 Grade	EC-8-1 Limit State	Mechanical event	Displacement
Grade 1	-	No Structural Damage	$<d_{cr}$
Grade 2	Serviceability	System Stiffness change (cracking)	d_{cr}
Grade 3	Damage Limitation	Maximum resistance or slightly beyond	d_{Rmax} or $3d_{cr}$ (highest d)
Grade 4	Ultimate	20% degradation from maximum resistance	$d_{0.8Rmax}$
Grade 5	-	Collapse	d_{coll}

In the work it is appointed that any design should not rely on the displacement corresponding to Grade 4 ($d_{0.8Rmax}$) since once the structure goes beyond the Grade 3 is unsafe to the earthquake replica due its existing damage. Therefore, it is recommended that the displacement and ductility capacity used in the design corresponds to the Damage Grade 3, using the smallest displacement between $3d_{cr}$ and $d_{0.8Rmax}$.

3.2.7. Other Mechanical Scales

The EMS-98 and PBEE are not always used as reference scales. There have been defined other scales for particular buildings.

For instance, in (Petromichelakis, Saloustros and Pelà, 2014) a three grades scale was used. The scale identified 3 different limit states, based on the structural damage on the building. This was given by the form of the pushover curve, which present 2 clear vertices (Figure 3.2.7.A). Those vertices correspond to the cracking sequence of the building and the consequent loss of stiffness. Therefore, the scale represents the real behaviour of the building and gives precise information of its state.

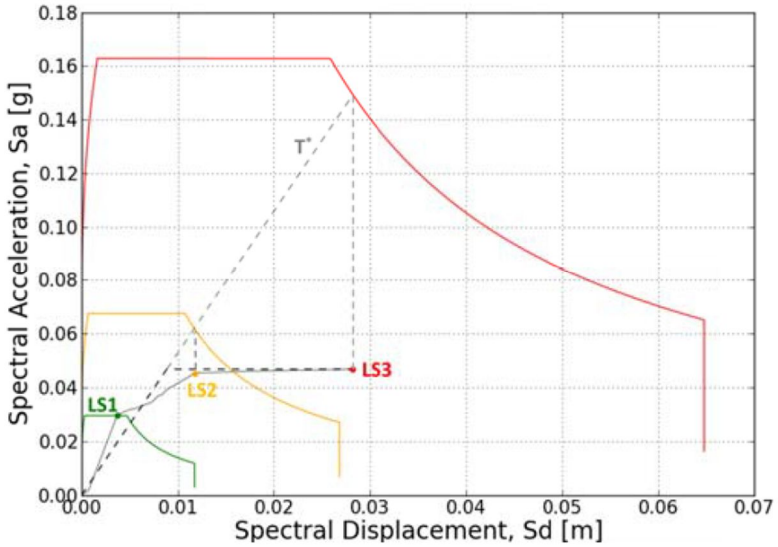

Figure 3.2.7.A: The model pushover curve and the limit states used in (Petromichelakis, Saloustros and Pelà, 2014)

It is worth saying that the three Limit States present in the work are located in a very similar place than the ones in (Tomaževič, 2007).

4. Methodology

The Methodology used in the present paper is based in the used in (Petromichelakis, Saloustros and Pelà, 2014) and (Saloustros *et al.*, 2018) –this second paper is based in the master thesis (Contrafatto, 2017).

The main characteristics of the methodology are descrived in figure 4.A.

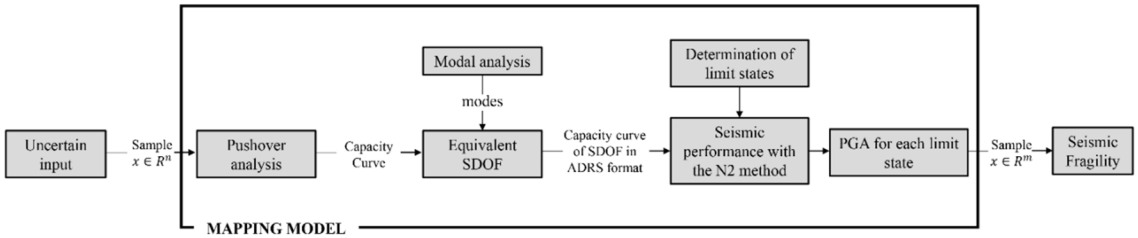

Figure 4.A: Schematic view of the adopted methodology in the present thesis, as it appears in (Saloustros *et al.*, 2018)

In a resumed way, the methodology of the vulnerability assessment consists in modelling the uncertainties of the existing building through the random determination of the material properties (uncertainty modelling) and after a process obtaining the seismic fragility of the building. In other words, there is an uncertain input in the space R^n (the material properties) to a mapping model that gives an output in the space R^m (the seismic fragility).

In the following sections, the methodology is explained in detail.

4.1. Finite Element Method (FEM) Modelling

The seismic modelling of an existing historical construction is not a simple task. A priori it seems that a good approach might be the modelling of the whole building, so all the possibilities are included. However, this is a very demanding task, since it would require an exhaustive survey and consume lots of computational resources. Furthermore, the historical constructions are normally adjacent to other constructions, so a whole modelling should include them too.

Another approach is to identify the parts that have a different or independent behaviour under an earthquake. As is explained in (D'Ayala and Speranza, 2003; Politecnico di Milano, 2010) the parts of an historical masonry building have this independent behaviour since they are not usually well connected, especially in churches. Therefore each of these parts can be analysed separately.

A common way to analyse these parts is the use of representative macroelements FEM (Lourenço, 2001). This macroelements are usually modelled using 3D FEM elements. However, this approach is still very computationally demanding, especially when a Stochastic Simulation is made, i. e. a large number of models are calculated (see section 4.3.7 of the present thesis for more information).

In order to made the Stochastic Simulation affordable computationally speaking, an equivalent Plane-Stress 2D FEM to the 3D FEM model can be used, as it was in

(Petromichelakis, Saloustros and Pelà, 2014; Endo *et al.*, 2015; Contrafatto, 2017; Saloustros *et al.*, 2018).

In the present thesis, an equivalent Plane-Stress 2D FEM model of the transversal bay of Santa Maria del Pi has been used. In order to calibrate this 2D model, a 3D model has been modelled. The details about the modelling and calibration are explained in chapter 5 of the present thesis.

4.2. Constitutive Model

The constitutive model used is a Total Strain Based Smeared Crack Model, present in the software DIANA FEA v.10.1. In this section, the chosen characteristics are presented. More information about its possibilities can be found in (Manie and Kikstra, 2017), the Material Library User's Manual for DIANA FEA.

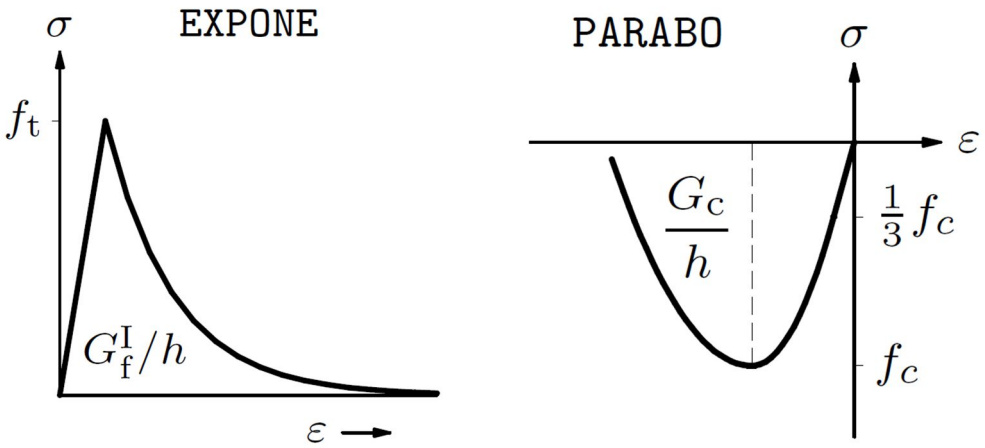

Figure 4.2.A: Strain(ε)-stress(σ) diagram in tension (left) and compression (right) chosen in the present thesis as they appear in (Manie and Kikstra, 2017)

4.2.1. Cracking Behaviour

The crack orientation is chosen as rotating with the Crack Bandwidth (*h*) specification of (Rots, 1988) specifically designed for and implemented in the DIANA FEA software. This specification assumes a value of *h* related to the area or volume of the element.

4.2.2. Tensile Behaviour

The chosen tensile behaviour is the exponential one (Figure 4.2.A). This means the curve in the strain(ε)-stress(σ) diagram is described by an exponential function. This function is defined by the Tensile Strength (f_t) the Mode-I Fracture Energy (G_f^I) and the Crack Bandwidth (*h*), as well as, the Young Modulus (*E*).

4.2.3. Compressive Behaviour

The chosen compressive behaviour is the parabolic one (Figure 4.2.A). This means the curve in the strain(ε)-stress(σ) diagram is described by a parabolic function. This function is defined by the Compressive Strength (f_c) the Compressive Fracture Energy (G_c) and the Crack Bandwidth (*h*), as well as, the Young Modulus (*E*).

4.3. Mechanical Properties (Uncertainty Modelling)

Since no information about the church materials has been found, and no tests have been held, any consideration about the mechanical properties of the church materials is intrinsically uncertain. Furthermore, even with a significant amount of information, it might be inaccurate, since is not possible to know all the details of the church construction and it could be hidden damage in the church structure (in section 1.1.3 more information about this topic is given).

Consequently, the mechanical properties are modelled as random variables and its values defined though its range of variation, as well as its distribution.

4.3.1. Identification of the Church Materials

It is assumed that the church materials are similar to the ones used in Santa Maria del Mar (SMM), another contemporary gothic church in Barcelona.

In (Murcia, 2008) the materials of SMM were determined, based in multiple and profound prior studies. And in (Contrafatto, 2017) the variability and properties of those materials was established, based in (Petromichelakis, Saloustros and Pelà, 2014) as well as the i-NTC-08 (Italian Ministry of Infrastructure and Transport, 2009) and CNR-DT 212/2013 (Advisory Committee on Technical Recommendations for Construction, 2013).

The materials considered in the present thesis for Santa Maria del Pi (SMPi) are three (Table 4.3.1.A)

Table 4.3.1.A: Materials considered in the present thesis

Nr.	Material Name
1	Vaults and single-leaf walls
2	Three-leaf walls
3	Vaults infill

It is worth noticing that the materials considered in (Murcia, 2008; Contrafatto, 2017) are 4 because in SMM there are pillars, with an outstanding masonry quality. On the contrary, in SMPi there are no pillars and, therefore, only 3 materials have been considered.

4.3.2. Kinds of Uncertainty Considered

According to CNR-DT 212/2013 (Advisory Committee on Technical Recommendations for Construction, 2013) there are two kinds of uncertainties in an existing building. One is the aleatoric uncertainty and the other is the epistemic uncertainty. The aleatoric uncertainty is the one related to the intrinsic variability of the material properties, while the epistemic uncertainty is related to the knowledge of the structure – from its exact geometry to the role that each element has in the structural system.

In order to express these two kinds of uncertainty and at the same time reduce the amount of variables, one material has been considered a reference one, namely the Vaults and Single-leaf Walls, while the characteristics other two have been defined as proportional to the reference one.

This way, the aleatoric uncertainty is concentrated in the characteristics of the reference material while the epistemic one is distributed between the reference model and the ratio between the reference material and each one of the other materials. This simplification is not far away from reality, since all the stones presumably come from the same quarry and the difference their behaviour is manly based in the different bond; and this is an epistemic uncertainty.

4.3.3. Obtaining of the Material Properties Values

As in (Contrafatto, 2017) the reference property of the materials is its compressive strength. To obtain this value, the church materials have been associated with the ones present in the Italian standard i-NTC-08 (Italian Ministry of Infrastructure and Transport, 2009).

According to the i-NTC-08, the reference value of the compressive strength is determined using the Table C8A.2.1 of this standard, and the final value is determined after being affected by the coefficients of the Table C8A.2.2 as is shown in Table 4.3.3.A of the present thesis.

Table 4.3.3.A: Correlation between the Church Materials, the ones from the i-NTC-08 and its coefficients.

	Church Material	Standard Material (C8A.2.1)	Used coefficient (C8A.2.2)	Coefficient justification	$f_{c,max}$ [MPa]	$f_{c,min}$ [MPa]
1	Vaults and Single-leaf Walls	Squared stone masonry	1	No special consideration	6.0	8.0
2	Three-leaf Walls	Roughly cut stone masonry, having wythes of limited thickness and inner core	1.4*1.5 = 2.1	Good transversal connection and good quality of the mortar	4.2	6.3
3	Vaults Infill	Irregular stone masonry	1	No special consideration	1.0	1.8

From the values of f_c in table 4.3.3.A, the coefficients for the dependent materials Three-leaf Walls (W_c) and Vaults Infill (I_c) are determined. Since the values of f_c are defined through a range, the coefficients are defined through a range too. The coefficient's values are shown in table 4.2.3.B.

Table 4.3.3.B: Dependent materials' coefficients regarding the reference material, the Vaults and Single-leaf Walls.

	Church Material	Coefficient Name	Coefficient Value
2	Three-leaf Walls	W_c	0.70 ÷ 0.80
3	Vaults infill	I_c	0.17 ÷ 0.23

The other material properties ranges are defined using the f_c ranges. This way, the Young Modulus (E) is defined as between 300 and 500 times f_c to cover the values suggested in i-NTC-08 and the tensile strength (f_t) is defined as between 0.02 and 0.05 times f_c based on common assumptions.

The values of (G_f^I) and (G_c) are defined as a function of the compressive strength too, but in this case using the 1990 Model Code (Euro-International Comitee for Concrete, 1990) as suggested for homogenised masonry in (Lourenço, 2009).

In the equation (4.3.3-1) the value of (G_f^I) is given, assuming an aggregate size of 8mm, the lowest one. In the equation (4.3.3-2) the value of (G_c) is given, assuming a ductility index of 1.6mm, corresponding to the lowest compressive strength.

$$G_f^I[Nmm/mm^2] = 0.025 * \left(\frac{f_c}{10}\right)^{0.7} \qquad (4.3.3\text{-}1)$$

$$G_c[Nmm/mm^2] = 1.6 * f_c \qquad (4.3.3\text{-}2)$$

Table 4.3.3.C resumes the process to obtain the material properties range.

Table 4.3.3.C: Process to obtain the material properties range.

	Materials	f_c [MPa]	f_t [MPa]	E [MPa]	G_f^I [J/m^2]	G_c [J/m^2]
1	Vaults and single-leaf walls (V)	6.0 ÷ 8.0	0.02*$f_{cV,min}$ ÷ 0.05*$f_{cV,max}$	0.70*$f_{cV,min}$ ÷ 0.80*$f_{cV,max}$	$25 * \left(\frac{f_{cV}}{10}\right)^{0.7}$	1600*f_{cV}
2	Three-leaf walls (W)	0.70*$f_{cV,min}$ ÷ 0.80*$f_{cV,max}$	0.70*$f_{tV,min}$ ÷ 0.80*$f_{tV,max}$	0.70*$E_{V,min}$ ÷ 0.80*$E_{V,max}$	$25 * \left(\frac{f_{cW}}{10}\right)^{0.7}$	1600*f_{cW}
3	Vaults infill (I)	0.17*$f_{cV,min}$ ÷ 0.23*$f_{cV,max}$	0.17*$f_{tV,min}$ ÷ 0.23*$f_{tV,max}$	0.17*$E_{V,min}$ ÷ 0.23*$E_{V,max}$	$25 * \left(\frac{f_{cI}}{10}\right)^{0.7}$	1600*f_{cI}

4.3.4. Mechanical Properties Range

From the equations of table 4.3.3.C, table 4.3.4.A is obtained.

Table 4.3.4.A: Mechanical properties range.

	Materials	f_c [MPa]	f_t [MPa]	E [MPa]	G_f^I [J/m^2]	G_c [J/m^2]
1	Vaults and Single-leaf walls	6.0 ÷ 8.0	0.12 ÷ 0.40	1800 ÷ 4000	17.5 ÷ 21.4	9600 ÷ 12800
2	Three-leaf Walls	4.2 ÷ 6.4	0.08 ÷ 0.32	1260 ÷ 3200	13.6 ÷ 18.3	6720 ÷ 10240
3	Vaults Infill	1.0 ÷ 1.8	0.02 ÷ 0.09	306 ÷ 920	5.0 ÷ 7.5	1600 ÷ 2880

4.3.5. Mechanical Properties Reference Values

The reference values used in the present thesis are described in the table 4.3.5.A:

Table 4.3.5.A: Reference values of the mechanical properties.

	Materials	f_c [MPa]	f_t [MPa]	E [MPa]	G_f^I [J/m^2]	G_c [J/m^2]	v	γ [kg/m^3]
1	Vaults and Single-leaf Walls	7.00	0.26	2900	19.5	11200	0.2	2200
2	Three-leaf Walls	5.30	0.20	2230	16.0	8480	0.2	2200
3	Vaults Infill	1.43	0.06	613	6.4	2288	0.2	2200

The reference values considered in table 4.3.5.A are the arithmetic mean of the maximum and minimum values of table 4.3.4.A for the compression (f_c) and tensile strength (f_t) as well as the Young Modulus (E). However, the Mode-I Fracture Energy (G_f^I) and the Compressive Fracture Energy (G_c) have been calculated using the mean value of the f_c of each material and the equations 4.3.3-1 and 4.3.3-2 respectively. Finally, the last two values, the Poisson Ratio (v) and the Density (γ) are based in common assumptions, as in (Petromichelakis, Saloustros and Pelà, 2014; Contrafatto, 2017).

4.3.6. Random Variables and Distribution

The random variables considered in the present thesis are: the reference material basic properties –namely compressive strength (f_{cV}), tensile strength (f_{tV}) and Young Modulus (E_V) of the Vaults and Single-leaf Walls– as well as the dependent material ratios –namely Three-leaf Walls (W_c) and Vaults Infill (I_c). All these five variables are considered to be independent.

The reference material properties are assumed to be lognormally distributed as in the Italian Guide for the Probabilistic Assessment of the Seismic Safety of Existing Buildings (CNR-DT 212/2013) (Advisory Committee on Technical Recommendations for Construction, 2013). Other works as (Park *et al.*, 2009; Sýkora and Holický, 2010) use the same distribution.

In order to obtain the parameters of the lognormal distribution –namely the lognormal mean and deviation– the parameters of a normal distribution of the material properties have been obtained. This is because a lognormal distribution is a continuous probability distribution whose logarithm is normally distributed, as shown in figure 4.3.6.A.

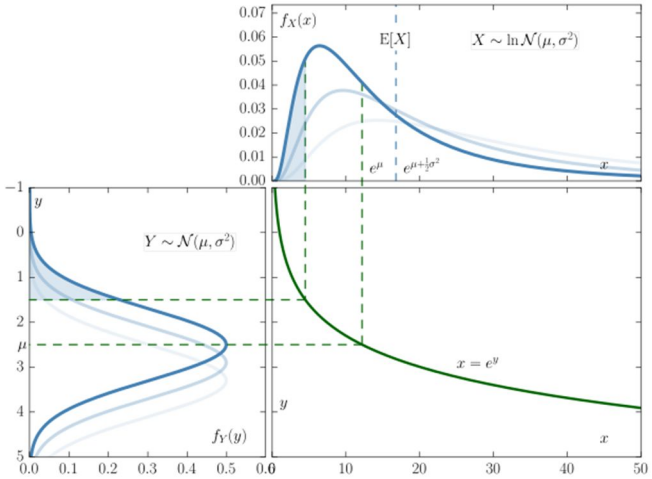

Figure 4.3.6.A: Relation between normal and lognormal distribution (StijnDeVuyst, 2016)

The parameters of a normal distribution whose extreme values are known (Table 4.3.4.A) are simple to obtain. The mean (μ) is set as the arithmetical mean between the extremes (Table 4.3.5.A) and the standard deviation (σ) is approximated as the difference between the maximum and the minimum divided by 6. Technically this includes only the 99.7% of the data, but it is approximate enough (Figure 4.3.6.B).

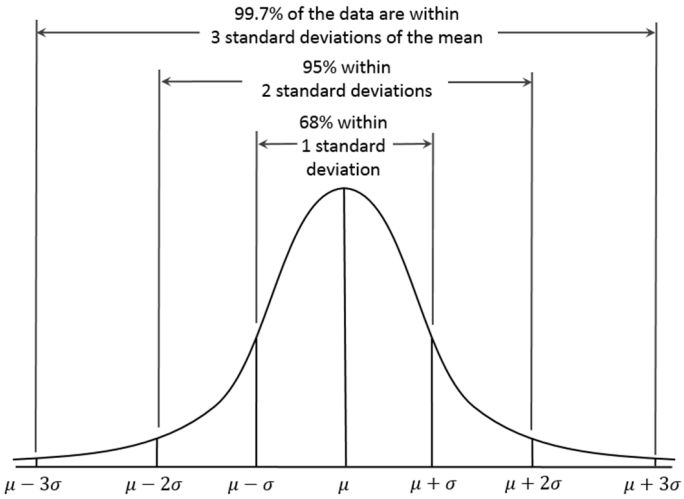

Figure 4.3.6.B: Representation of the 68-95-99.7% Empirical Rule (Kernler, 2014)

The parameters of the normal distribution (μ, σ) are transformed in the parameters of the lognormal distribution –namely the lognormal deviation (σ_{ln}) and the lognormal mean (μ_{ln})– using the equations 4.3.6-1 and 4.3.6-2 respectively.

$$\sigma_{ln} = \sqrt{\ln\left(1 + \frac{\sigma^2}{\mu^2}\right)} \qquad (4.3.6\text{-}1)$$

$$\mu_{ln} = \ln \mu - \frac{1}{2}{\sigma_{ln}}^2 \qquad (4.3.6\text{-}2)$$

The dependent material ratios (W_c, I_c) are assumed to be uniformly distributed as in (Petromichelakis, Saloustros and Pelà, 2014). The defining parameters for this distribution are the maximum and minimum, set in table 4.3.3.B.

Table 4.3.6.A shows the random variables used in the present thesis as well as their distribution and defining parameters.

Table 4.3.6.A: Random Variables, Distribution and Defining Values.

Random variable	Distribution	Mean (μ_{ln}) [MPa]	Deviation (σ_{ln}) [MPa]
Vaults Compression Strength (f_{cV})	Lognormal	1.94	0.05
Vaults tensile strength (f_{tV})	Lognormal	-1.37	0.22
Vaults Young Modulus (E_V)	Lognormal	7.96	0.13
Random variable	**Distribution**	**Minimum Value [-]**	**Maximum Value [-]**
Three-leaf Walls Coefficient (W_c)	Uniform	0.7	0.8
Vaults infill Coefficient (I_c)	Uniform	0.17	0.23

4.3.7. Stochastic Simulation

The effect of the uncertainties (random variables) in the seismic response of the structure is evaluated in the present thesis using a stochastic simulation. The validity of the stochastic methods is provided by statistical laws, namely the Central Limit Theorem and, especially, the Strong Law of Large Numbers. According to these laws, the number of samples N required to simulate a combination of random variables should approach infinity ($N \to \infty$).

Therefore, the number of samples should be sufficiently large. The definition of sufficiently large is problem dependent and strongly influenced by the number of uncertain parameters. However, it is commonly accepted in similar problems to the present thesis that $N = 200$ is a sufficiently large number of random samples (Vamvatsikos and Fragiadakis, 2009; Jalayer, Iervolino and Manfredi, 2010; Petromichelakis, Saloustros and Pelà, 2014; Contrafatto, 2017).

In order to model the 200 random samples, the Monte Carlo Simulation (MCS) method has been used as in similar works like (Singhal and Kiremidjian, 1996; Dymiotis, Kappos and Chryssanthopoulos, 1999; Petromichelakis, Saloustros and Pelà, 2014; Contrafatto, 2017). The MCS generates a specified number of N (in this case 200) independent and identically distributed random variables within the input space $\mathrm{X} \subseteq \mathbb{R}^n$, where n is the number of independent variables (in this case 5). The distribution of each random variable is taken into account in the sampling process.

The sampled values of the reference material properties used in the present thesis are shown in figure 4.3.7.A.

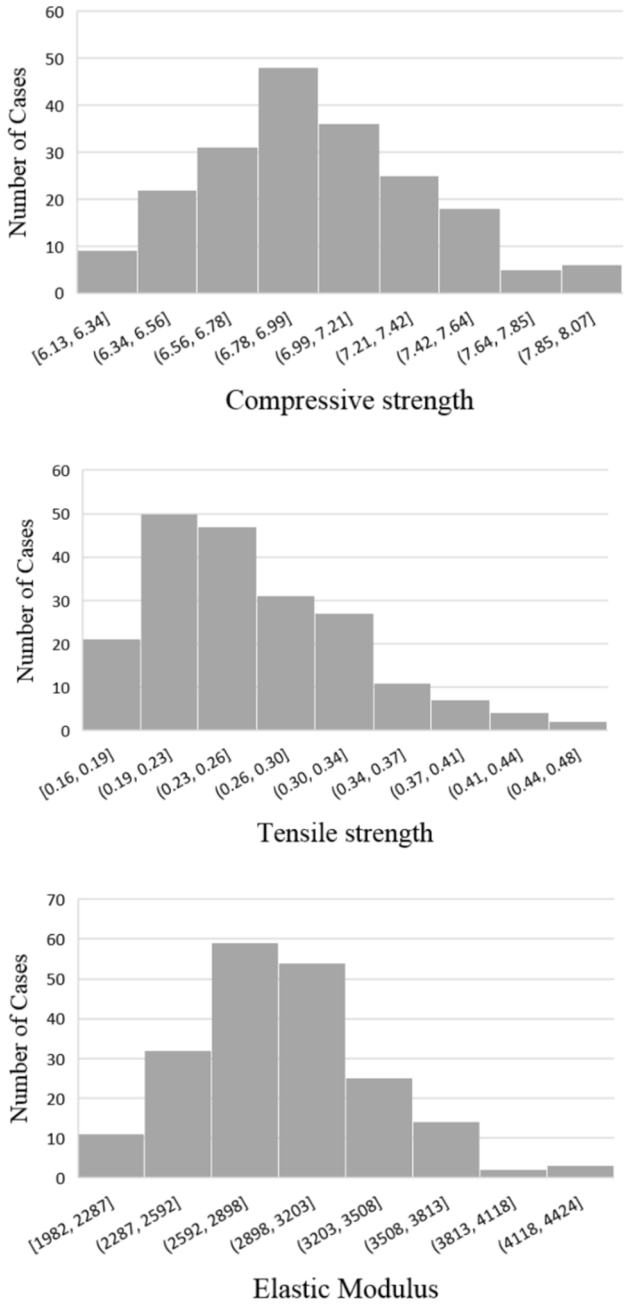

Figure 4.3.7.A: Sampled values of the reference material properties.

4.4. N2 Method Adaptation

The N2 Method Adaptation used is the one described in the Comments to the Italian Standard (i-NTC-08) (Italian Ministry of Infrastructure and Transport, 2009); with some changes in the Lateral Force Distribution (LFD) and the control node. More details about the literature on the matter can be found on the section 3.1 of the present thesis.

The choice of such adaptation is justified by the post peak behaviour of the masonry structures, as described in the section 3.1.4 of the present thesis. In the same way, the Arc Length Method (Riks, 1979) is used to obtain the post peak behaviour.

4.4.1. Lateral Force Distribution

As is written in the first paragraph of the section C7.3.4.1 (Nonlinear Static Analysis) of the i-NTC-08, this method is only valid for constructions were in a seismic situation there is a principal vibration mode with a significant mass participation, as the case study.

As is explained in the section 3.1.2 of the present thesis, a LFD proportional to the mass is a conservative approach and, therefore, such LFD is used in the present thesis.

4.4.2. Control Node

As exposed in section 3.1.3, the choice of the Control Node (CN) for the N2 Method is not a trivial decision. Since no strong conclusion may be found in the literature, the key of the nave vault is chosen as the reference one as in (Petromichelakis, Saloustros and Pelà, 2014; Saloustros *et al.*, 2015), and the final results for this and four more are considered.

The considered control nodes are the following (figure 4.4.2.A):

(A) **The Reference Node**, the key of the nave vault.

(B) **The Right spring of the Nave Vault**.

(C) **The Lower Top-Right corner of the right Buttress**.

(D) **The Higher Top-Right corner of the right Buttress**.

(E) **The Higher-Right point of the Macroelement**.

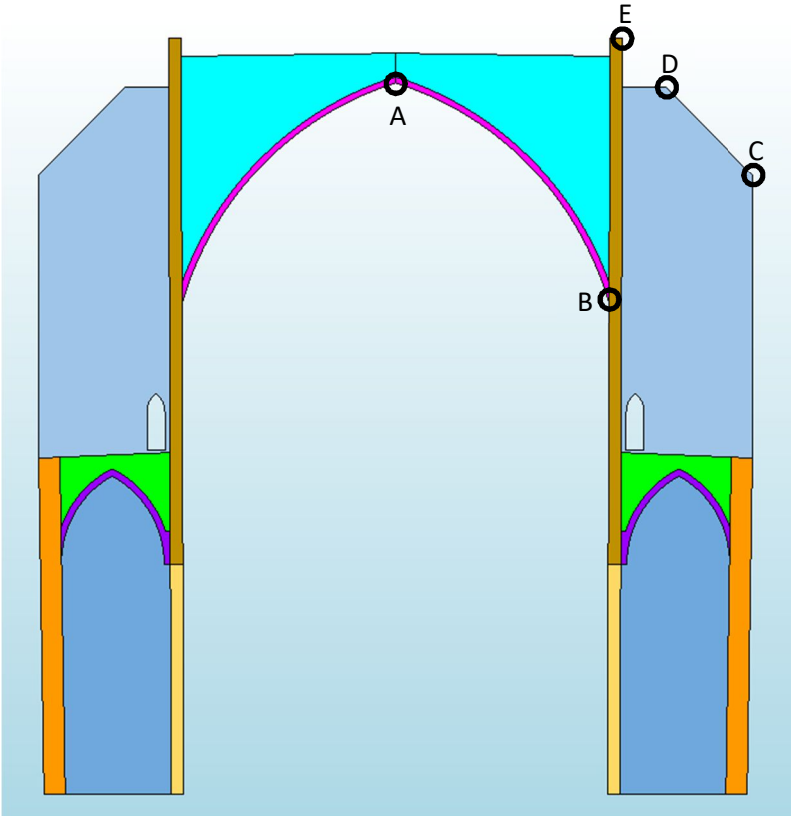

Figure 4.4.2.A: Control Nodes considered in the present thesis

4.4.3. Equivalent SDOF Structure

The equivalent SDOF Structure is defined as described in the i-NTC-08. The procedure is explained below and in figure 4.4.3.A:

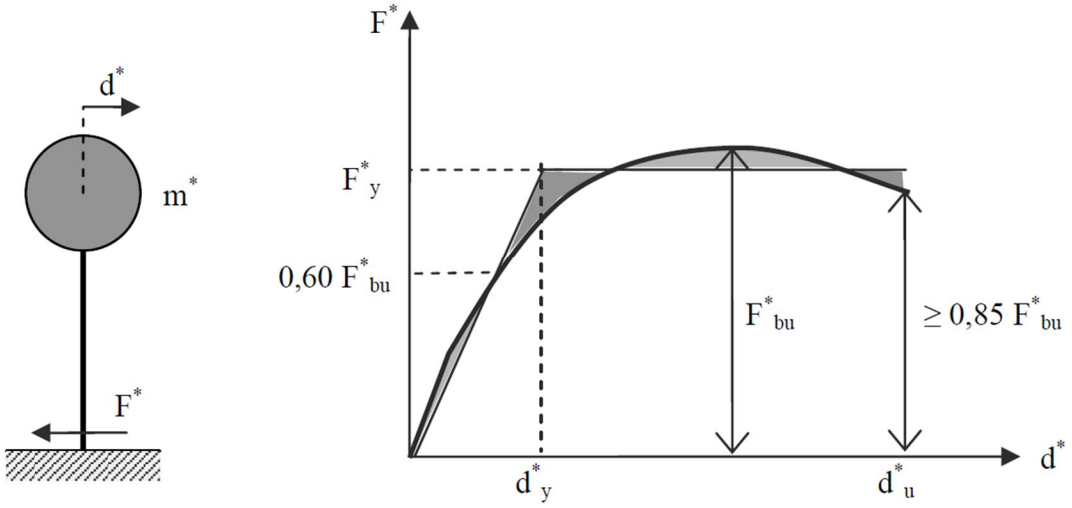

Figure 4.4.3.A: Equivalent SDOF (left) and bilinear force-displacement diagram (right) as they appear in (Italian Ministry of Infrastructure and Transport, 2009)*. In the case of masonry the d*$_u$ corresponds to ≥0.8F*$_{bu}$.*

The force (F*) and the displacement (d*) of the equivalent system are related to the base shear (Vb) and displacement in the control node (d) using the equations (4.4.3-1) and (4.4.3-2):

$$F^* = \frac{V_b}{\Gamma} \qquad (4.4.3\text{-}1)$$

$$d^* = \frac{d}{\Gamma} \qquad (4.4.3\text{-}2)$$

Were Γ is the modal participation factor, defined using the equation (4.4.3-3):

$$\Gamma = \frac{\sum_1^n \varphi_i * m_i}{\sum_1^n \varphi_i{}^2 * m_i} \qquad (4.4.3\text{-}3)$$

Were φ_i is the modal displacement of each node, normalized so the highest one equals 1, and m_i the mass of each node, obtained as the sum of the repercussion of the adjacent elements' mass.

It is worth noticing that the equation (4.4.3-3) differs from the one in the i-NTC08 in two aspects, (1) Γ is defined according to the scalar approach since the use of the matrix approach would be demanding because of the big amount of nodes, and (2) the nodal displacement considered (φ_i) is the one of the reference case.

Then, a simplification of the system behaviour is made so the force-displacement diagram becomes bilinear (Figure 4.4.3.A). This simplification is obtained defining the initial stiffness of the equivalent system (k*) as the secant to the force-displacement curve in the point where the 60% of the maximum strength ($0.6F^*_{bu}$) is reached. Moreover, the simplified curve must dissipate the same energy than the original one till the maximum displacement (d^*_u) is reached. This displacement corresponds to a 20% decrease of the maximum strength in the case of masonry. In other words, the area under the original and simplified curves from zero to d^*_u must be the same.

The elastic period of this simplified equivalent structure is:

$$T^* = 2\pi\sqrt{\frac{m^*}{k^*}} \qquad (4.4.3\text{-}4)$$

Were m* is the mass of the equivalent structure, defined using the equation 4.4.3-5:

$$m^* = \sum_1^n \varphi_i * m_i \qquad (4.4.3\text{-}5)$$

4.5. Seismic Performance

The evaluation of the Seismic Performance in the present thesis is done like the common practice but switching the input and output parameters.

Normally the ground acceleration (a_g) for the chosen return period is considered the input parameter that, using the Elastic Response Spectrum and the bilinear capacity curve in SDOF, determines a concrete equivalent displacement (S_{De} to d^*); then this d^* is compared to the equivalent displacement for the different Damage Grades (DG) in order to know the structure performance.

However, in the present thesis the a_g is considered the output parameter for each of the DG whose input parameter is the d^* for each Damage Grade (DG). This process is obviously applied for each capacity curve individually.

4.5.1. Identification of the Damage Grades

After an intensive bibliographic research described in section 3.2, three Damage Grades (DG) and a previous zone (DG0) have been identified though all of the works, specially (Tomaževič, 2007). These are the following:

(DG0) **Elastic Zone,** no structural damage zone.

(DG1) **Inelastic Zone**, from the Onset Point of Cracking (OPC).

(DG2) **Post Peak Zone**, from the Point of Maximum Resistance.

(DG3) **Near Collapse Zone**, from the Point where Resistance drops more than 20% from Maximum Resistance.

These three DG can be easily related to grades 2 to 4 of Damage in the EMS-98 (European Seismologic Commission, 1998) as well as the three limit states of the Eurocode 8-1 (European Committee for Standardization, 2004).

The only problem of application of the three DG is the determination of the Onset Point of Cracking (OPC). This is done mostly mechanically like in (Lang, 2002; Rota, Penna and Magenes, 2010; Petromichelakis, Saloustros and Pelà, 2014; Ortega *et al.*, 2018) but also experimentally in (Tomaževič, 2007) and numerically in (Lagomarsino and Giovinazzi, 2006).

It is also done implicitly in i-NTC-08 (Italian Ministry of Infrastructure and Transport, 2009) were the OPC is set when the 60% of the maximum resistance is reached. This is because the OPC is considered to be the last elastic point of the capacity curve, and therefore, used for the determination of the equivalent SDOF bilinear structure stiffness. For the simplicity of calculation, the OPC has been considered for the DG1 as where the 60% of maximum resistance is reached.

In table 4.5.A the Damage Grades, their equivalence with EMS-98 and EC-8-1, resistance and displacements are presented.

Table 4.5.A: Damage Grades used in the present thesis, equivalences and definition.

Damage Grades		EMS-98 Grade	EC-8-1 Limit State	Resistance	Displacement
DG0	No Structural Damage	Grade 1	-	-	$< d_{0.6Rmax}$
DG1	Inelastic Zone	Grade 2	Serviceability	60% of maximum resistance is reached	$d_{0.6Rmax}$
DG2	Post Peak Zone	Grade 3	Damage Limitation	Maximum resistance	d_{Rmax}
DG3	Near Collapse Zone	Grade 4	Ultimate	20% degradation from maximum resistance	$d_{0.8Rmax}$

4.5.2. Horizontal Elastic Response Spectrum

The Elastic Spectrum is determined, according to the Eurocode 8-1 (European Committee for Standardization, 2004), as a function of the soil type. According to a geotechnical study of Santa Maria del Pi (SMPi) (Batlle & Mascareñas Geoprojectes SL, 2007a) there is a rubble layer (of about 4 to 5m) between the foundations and the firm soil.

A rubble layer between the foundation and the resistant soil was also detected in a geotechnical study of Santa Maria del Mar (SMM) (Batlle & Mascareñas Geoprojectes SL, 2007b), a nearby church with the same soil type, according to the geological mapping (figure 4.5.2.A). In (Contrafatto, 2017) the soil type for SMM was set as type D in a conservative choice due to the presence of this rubble layer. Without this local problem, the soil would be set as type C.

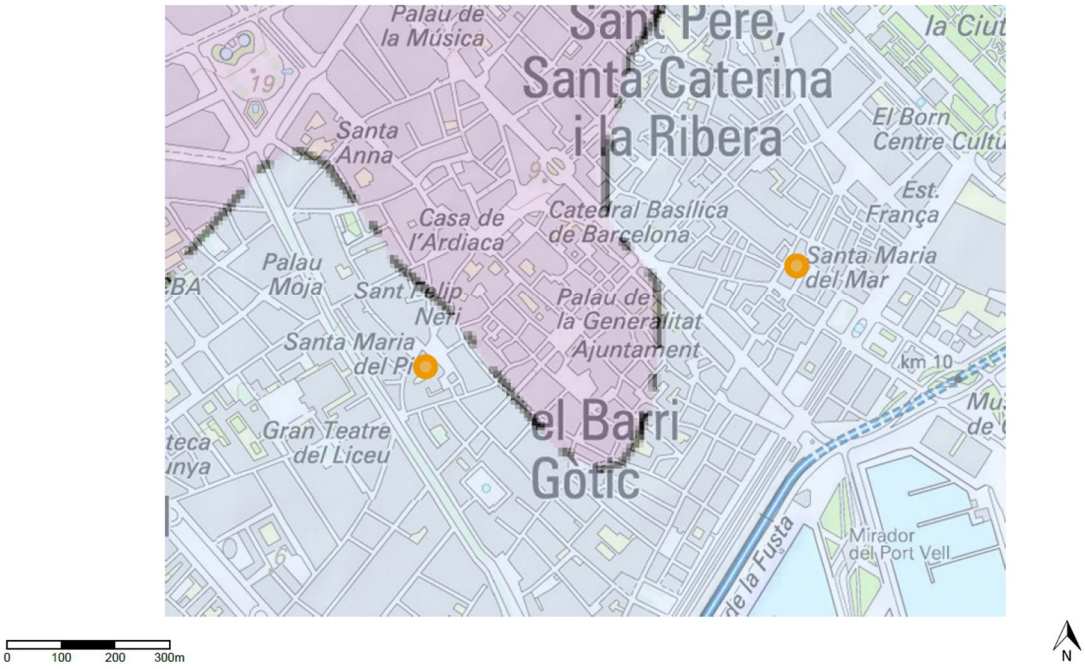

Figure 4.5.2.A: Types of soil under the old town of Barcelona. In purple the Pleistocene alluvial plane and in light blue the Superior Holocene alluvial plane. From (Institut Cartogràfic i Geològic de Catalunya, 2018)

In the present thesis the same conservative approach has been used, since the rubble layer has also very poor resistance characteristics, which recommend the characterization of the soil as type D. In table 4.5.2.A the parameters for the soil type of SMPi according to the Eurocode 8-1 are shown.

Table 4.5.2.A: Used parameters for the Elastic Response Spectrum, according to the Eurocode 8-1 for the chosen soil type.

Ground type	S	T_B (s)	T_C (s)	T_D (s)
D	1.35	0.2	0.8	2.0

With these basic parameters the Spectrum is built according to equations 4.5.2-1 to 4.5.2-4, from the Eurocode 8-1.

$$0 \leq T^* \leq T_B : S_e(T^*) = a_g * S * \left[1 + \frac{T^*}{T_B} * (\eta * 2.5 - 1)\right] \quad (4.5.2\text{-}1)$$

$$T_B \leq T^* \leq T_C : S_e(T^*) = a_g * S * \eta * 2.5 \quad (4.5.2\text{-}2)$$

$$T_C \leq T^* \leq T_D : S_e(T^*) = a_g * S * \eta * 2.5 * \left[\frac{T_C}{T^*}\right] \quad (4.5.2\text{-}3)$$

$$T_D \leq T^* \leq 4s : S_e(T^*) = a_g * S * \eta * 2.5 * \left[\frac{T_C * T_D}{T^{*2}}\right] \quad (4.5.2\text{-}4)$$

Were:

$S_e(T^*)$ is the Elastic Response Spectrum in accelerations;

T^* is the vibration period of the simplified SDOF from equation 4.4.3-4;

a_g is the design ground acceleration on type A ground for the zone;

T_B, T_B, T_B and S are the parameters of table 4.5.2.A;

η is the damping correction factor with a value of 1 for the assumed viscous damping (5%).

Then, the Elastic Response Spectrum in displacements ($S_{De}(T^*)$) is obtained with the equation 4.4.2-5:

$$S_{De}(T^*) = S_e(T^*) * \left[\frac{T^*}{2\pi}\right]^2 \qquad (4.5.2\text{-}5)$$

Finally, for the application of the N2 Method, the Spectrum is represented in the ADRS (Acceleration-Displacement Response Spectrum) format so the SDOF bilinear curve and the Spectrum may be represented in the same diagram.

4.5.3. Obtaining of the Peak Ground Acceleration for each Damage Grade

The obtaining of the Peak Ground Acceleration (a_g) for each Damage Grade (DG) is done from the equivalent displacement (d^*) for each DG through the Elastic Response Spectrum in displacements ($S_{De}(T^*)$) and in accelerations ($S_e(T^*)$), in other words, doing the method described in the i-NTC-08 (Italian Ministry of Infrastructure and Transport, 2009) and the Eurocode 8-1 (European Committee for Standardization, 2004).

The first step is obtaining the $S_{De}(T^*)$ from the equivalent displacement, using the equations 4.5.3-1 to 4.5.3-3.

$$if\ T^* < T_C\ and\ \frac{F_y^*}{m^*} \geq S_e(T^*) \rightarrow d^* = S_{De}(T^*) \qquad (4.5.3\text{-}1)$$

$$if\ T^* < T_C\ and\ \frac{F_y^*}{m^*} < S_e(T^*) \rightarrow d^* = \frac{S_{De}(T^*)}{q_u} * \left[1 + (q_u - 1)\frac{T_C}{T^*}\right] \qquad (4.5.3\text{-}2)$$

$$if\ T^* > T_C \rightarrow d^* = S_{De}(T^*) \qquad (4.5.3\text{-}3)$$

Were:

$$d^* \begin{cases} \geq S_{De}(T^*) \\ \leq 3 * S_{De}(T^*) \end{cases} \qquad (4.5.3\text{-}4)$$

And:

$$q_u = S_e(T^*) * \frac{m^*}{F_y^*} \qquad (4.5.3\text{-}5)$$

Then, $S_{De}(T^*)$ is transformed into $S_e(T^*)$ using equation 4.5.2-5 and finally a_g is obtained using the Spectrum, namely equations 4.5.2-1 to 4.5.2-4.

It is important to notice that the parameter $S_e(T^*)$ is necessary to choose between equation 4.5.3-1 and equation 4.5.3-2 and to use equation 4.5.3-5. However, it can only be obtained using the output parameter ($S_{De}(T^*)$) of those equations. Therefore, an iterative process must be used.

4.6. Seismic Fragility

For the presentation of the results from section 4.5.3, this is, the seismic fragility, a lognormal cumulative probability function (the Fragility Function) is used. This is a common practice in similar works, like (Park *et al.*, 2009; Rota, Penna and Magenes, 2010; Cattari, Lagomarsino and Ottonelli, 2014; Petromichelakis, Saloustros and Pelà, 2014).

The equation that rules the fragility function for each Damage Grade (DG), is equation 4.6-1:

$$P\left[DGi\middle|a_g\right] = F_i(a_g) = \Phi\left(\frac{\ln(a_g/\theta_i)}{\beta_i}\right) \tag{4.6-1}$$

Were $F_i(Z)$ is the conditional probability that the structure will reach the damage grade *DGi* or a more severe damage grade as a function of the demand parameter a_g and Φ denotes the standard normal (Gaussian) cumulative distribution function.

The two other parameters in equation 4.5-1, namely θ_i and β_i refer to the central value and the dispersion for each DG respectively, and are defined by the equations 4.6-2 and 4.6-3.

$$\theta_i = e^{\left(\frac{1}{N}\sum_{j=0}^{N}\ln a_{g_j}\right)} = \left(\prod_{j=1}^{N} a_{g_j}\right)^{\frac{1}{N}} \approx a_{g\,50\%} \tag{4.6-2}$$

$$\beta_i = \sqrt{\frac{1}{N-1}\sum_{j=1}^{N}\left(\ln\left(\frac{a_{g_j}}{\theta}\right)\right)^2} \tag{4.6-2}$$

Were N is the total number of samples for each DG and a_{g_j} is the value of the demand parameter for $j = 1,2,\ldots,N$.

Equation 4.6-2 shows that θ_i is the geometric mean of the demand parameter a_g which is approximately the value of a_g exceeded by 50% of the data, i.e. the median value.

Equation 4.6-3, in turn, shows that β_i is the logarithmic standard deviation of a_g for each DG.

5. Finite Element Method (FEM) Modelling

Using the Finite Element Method (FEM) the modelling of the representative transversal macroelement of Santa Maria del Pi (SMPi) has been done. The representative transversal macroelement corresponds to the transversal half of one bay, since, considering the bay symmetrical and all the bays equal (see section 5.1.1), the transversal behaviour of this element under a horizontal mass force (the pushover load) is the same as the whole SMPi. This is valid if the boundary conditions are correctly defined. For the boundary conditions used in the present thesis, see section 5.1.3 and 5.2.

5.1. 3D modelling

5.1.1. Structure Idealization

Previously to any modelling of an existing structure, it has to be idealized. This means neglecting in the structural model the decorative non-structural elements (if they are not significantly weighty) but also understanding the walls in a geometrically simple way so they can be computationally modelled. However, this process cannot underestimate the influential imperfections, deformations or differential settlements present in the structure.

A general look to the Santa Maria del Pi's plan (Figure 5.1.1.A) shows the explained above. There are visible differences among the lateral chapels and the thickness and straightness of the buttresses. These differences were corroborated in situ during the elaboration of the present thesis (Figure 5.1.1.B).

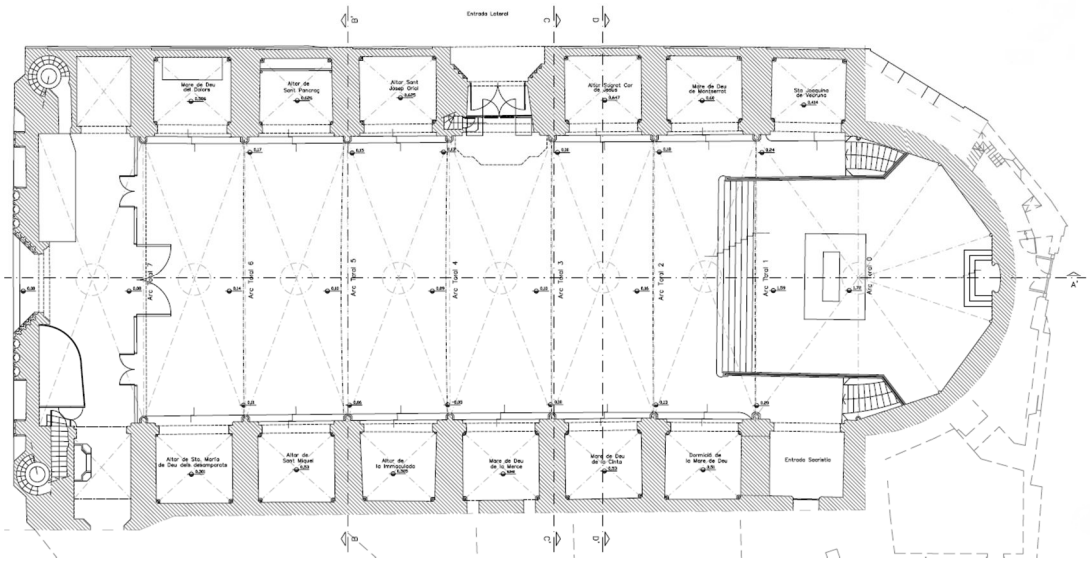

Figure 5.1.1.A: Plan of Santa Maria del Pi (Griera i Cura and Artime Alem, 2007)

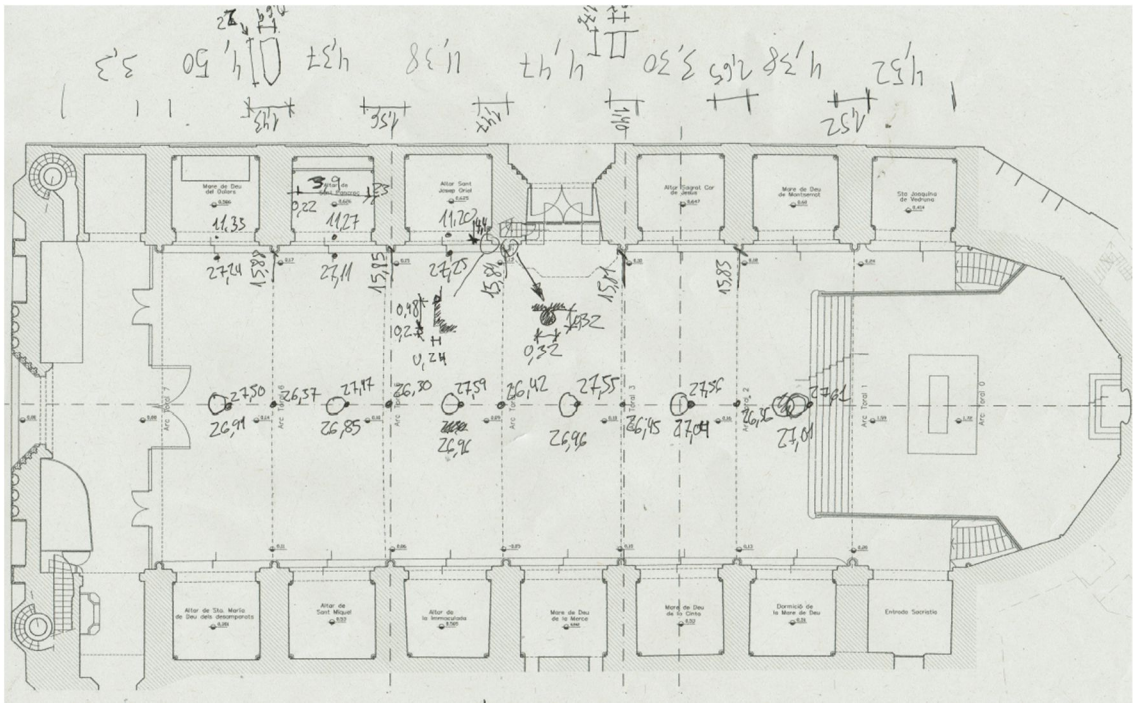

Figure 5.1.1.B: In situ measurements notations on the Santa Maria del Pi`s plan.

The idealization of the structure of Santa Maria del Mar was then made from the existing plans and corroborated by the in situ measurements. The structure was assumed to be symmetrical and the measures of the elements correspond to the average values (Figure 5.1.1.C). It has been included the leaning of the buttresses, corrected in the clerestory.

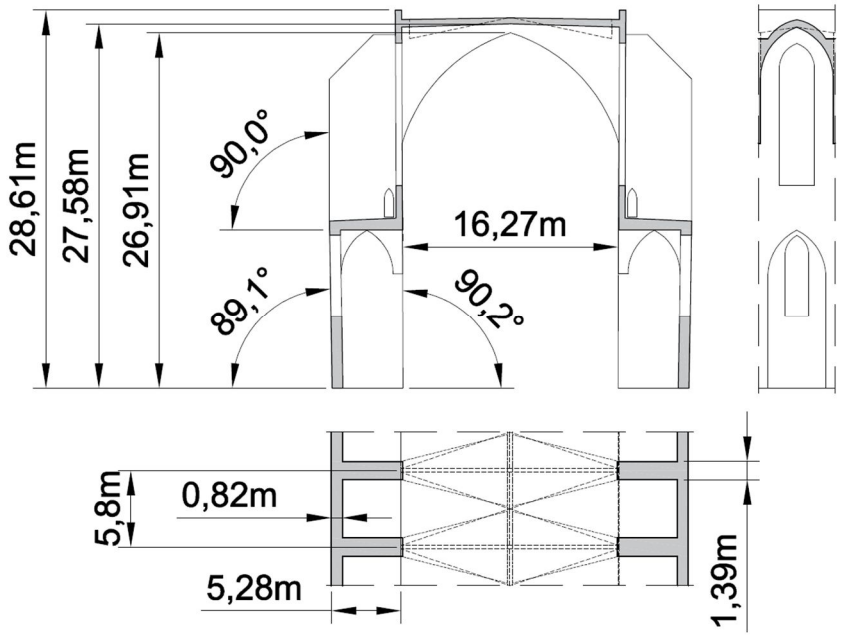

Figure 5.1.1.C: Idealization of the existing structure, taking in account the buttresses leaning

5.1.2. Materials and Parts Identification

The parts identification in the 3D model is based in the diferent materials present in the building. It has been assumed that the materials are simillar to the ones in Santa Maria del Mar (SMM), as explained in section 4.3.1.

In the same way, the distintion between the vaults and their infill has been made assuming that the external resistent leaf (Vault) is 25cm thick and the rest of the aparent volume is made of irregular stone massonry (Vault Infill). This was a common practice at the time and has been corroborated in SMM (Contrafatto, 2017).

The identified parts and materials associated are presented in Table 5.1.2.A and Figure 5.1.2.A.

Table 5.1.2.A: Parts and materials of the 3D model.

Nr.	Part	Material Name
1	Buttresses	Three-leaf Walls
2	Three-leaf Walls	Three-leaf Walls
3	Single-leaf Walls	Vaults and Single-leaf Walls
4	Chapels Vaults	Vaults and Single-leaf Walls
5	Nave Vault	Vaults and Single-leaf Walls
6	Chapel Infill	Vaults Infill
7	Nave Infill	Vaults Infill

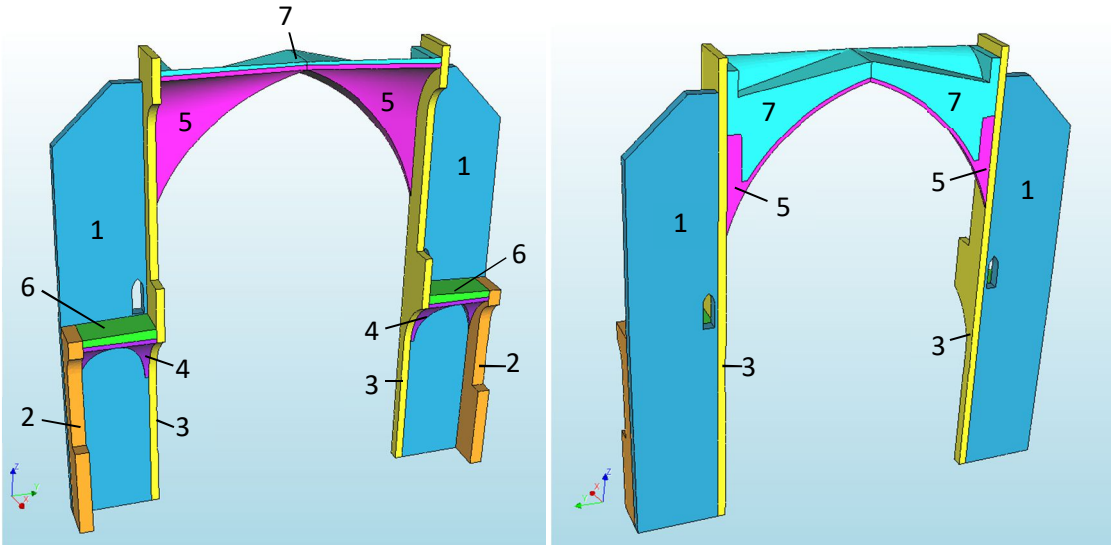

Figure 5.1.2.A: Parts of the 3D model: (1) Buttresses, (2) Three-leaf Walls, (3) Single-Leaf Walls, (4) Chapels Vaults, (5) Nave Vault, (6) Chapel Vault Infill, (7) Nave Vault Infill.

It is worth saying that in the first stages of the modelling the material of the Single-leaf Walls was identified as “pillar like” material (see section 4.3.1). The objective of such identification was to take in account the prominent church nerves and pilasters. These parts are presumably made of outstanding masonry that could not be represented by the plain “Vault” material. However, the influence of this material identification in the

general behaviour of the church was judged to be excessive, since the Single-leaf Wall has a key role in the connection between the Nave Vault and the Buttress. Therefore, the influence of the nerves and pilasters was not considered, and, in a conservative approach, the material of the Single-leaf Wall was finally identified as "Vaults and Single-leaf Walls".

5.1.3. Bondary Conditions

The applied boundary conditions in the 3D FEM model are two: (1) the total constrain of the longitudinal movement of the nodes in the transversal boundaries (the symmetry planes), and (2) the total constrain of the 3 space directions movement in the base boundaries (Figure 5.1.3.A).

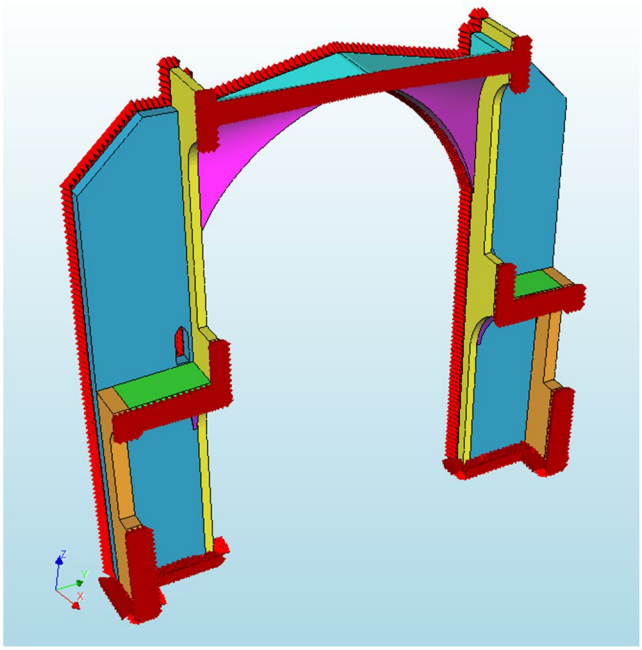

Figure 5.1.3.A: Boundary conditions of the 3D FEM Model.
The longitudinal movement (X) is constrained for the nodes in the symmetry planes and all the movements (X,Y,Z) are constrained for the base nodes.

5.1.4. Mesh Convergence Study

In order to establish a mesh for the FEM calculation, a reduced Mesh Convergence Study (MCS) was realized using the reference properties (Table 4.3.5.A).

This MCS consisted in analysing which was the relative difference in elastic deformation between having 2 or 3 elements thickness in the bending parts, since the used element was the 4 nodes tetrahedron. This meant having a maximum element dimension of 15cm in the vaults and 30cm in the other parts for the 2 elements thickness (Mesh 15-30cm) and 10cm in the vaults and 20cm in the other parts for the 3 elements thickness (Mesh 10-20cm). The two meshes are shown in Figures 5.1.4.A

and 5.1.4.B and compared in Figure 5.1.4.C. The Mesh 15-30cm has 240405 elements and 52047 nodes and the Mesh 10-20cm has 764405 Elements and 154011 Nodes.

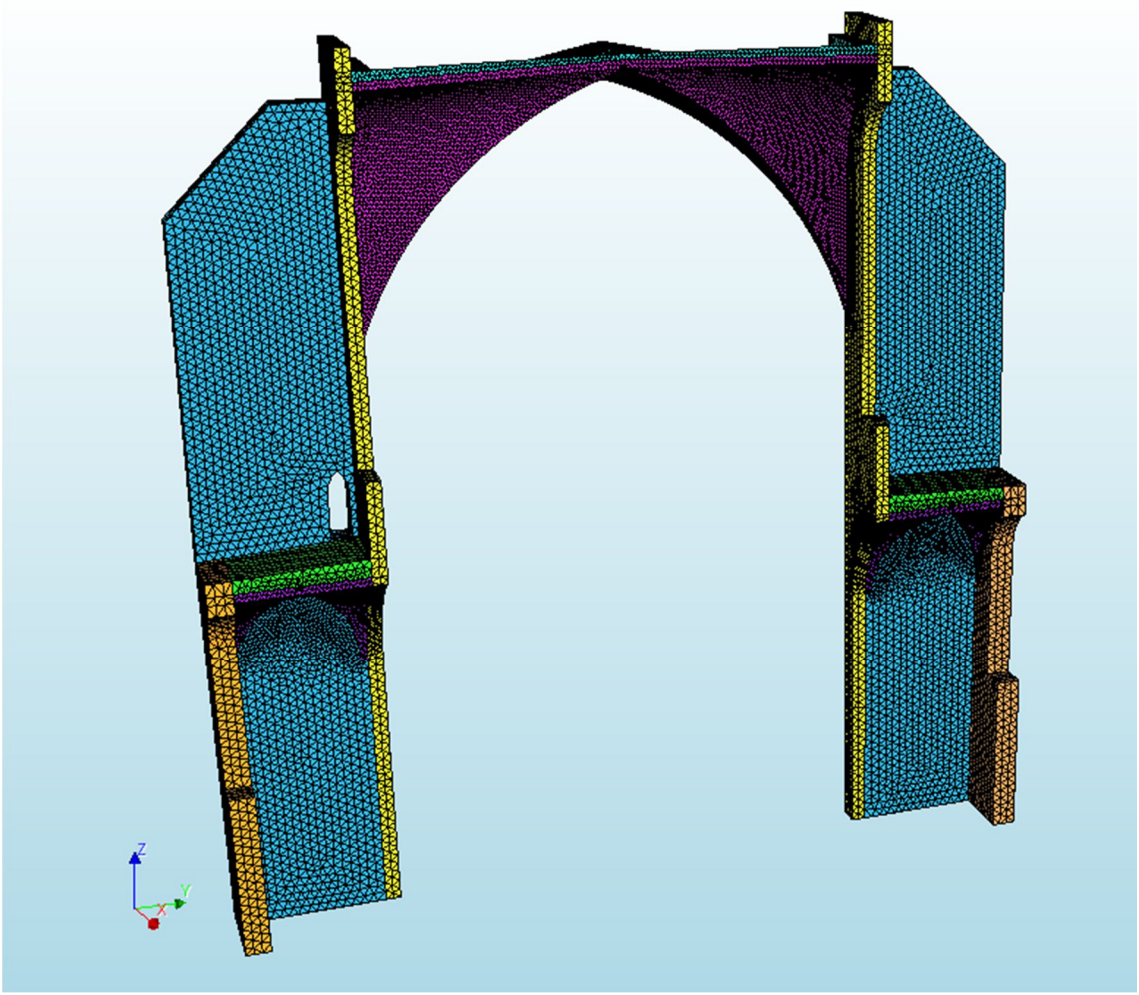

Figure 5.1.4.A: Mesh 15-30cm (average element sides), with 240405 elements and 52047 nodes

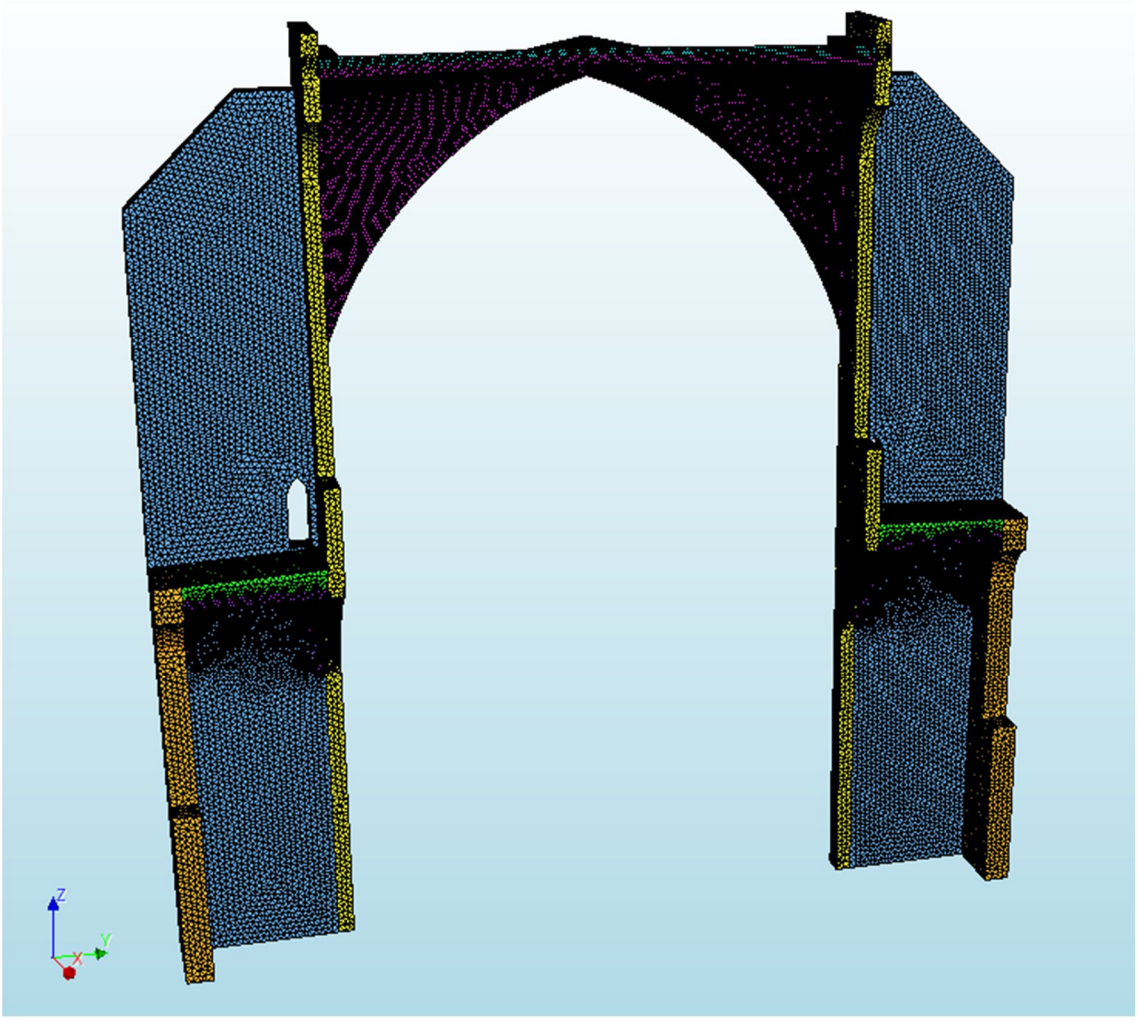

Figure 5.1.4.B: Mesh 10-20cm (average element size),
with 764405 Elements and 154011 Nodes

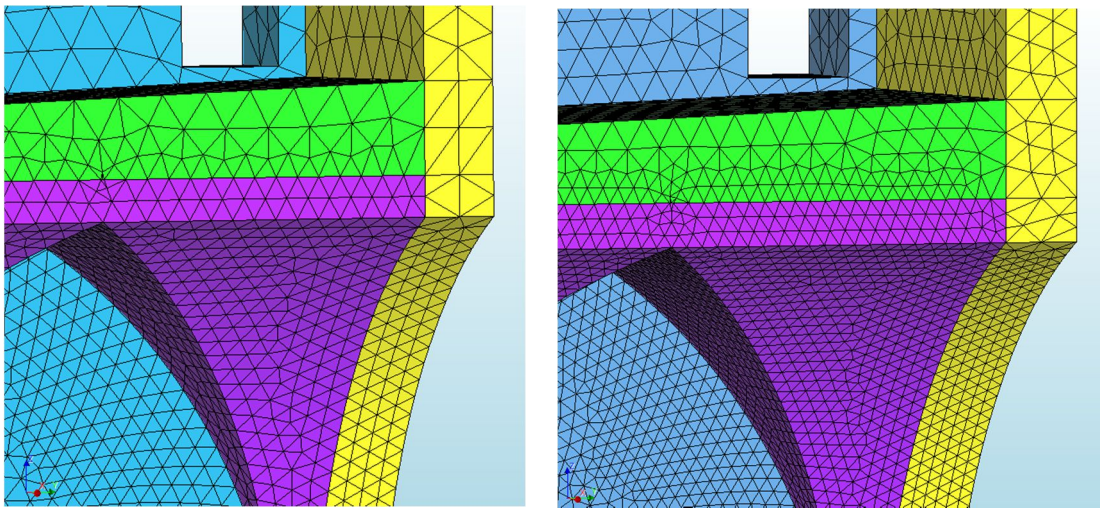

Figure 5.1.4.C: Comparison between the two meshes (detail).
Left: Mesh 15-30cm Right: Mesh 10-20cm.
The description of the flexure behaviour is done with two elements in Mesh 15-30cm and with three elements in Mesh 10-20cm.

Two load cases were applied to the two meshes with mass distributed forces equivalent to an acceleration of 1g. The first loading case was in the direction of gravity (Z-) and the second was in the Y+ direction. The resulting deformation is shown in figure 5.1.4.D and 5.1.4.E. In table 5.1.4.A the comparative and relative error between the two meshes' responses is presented.

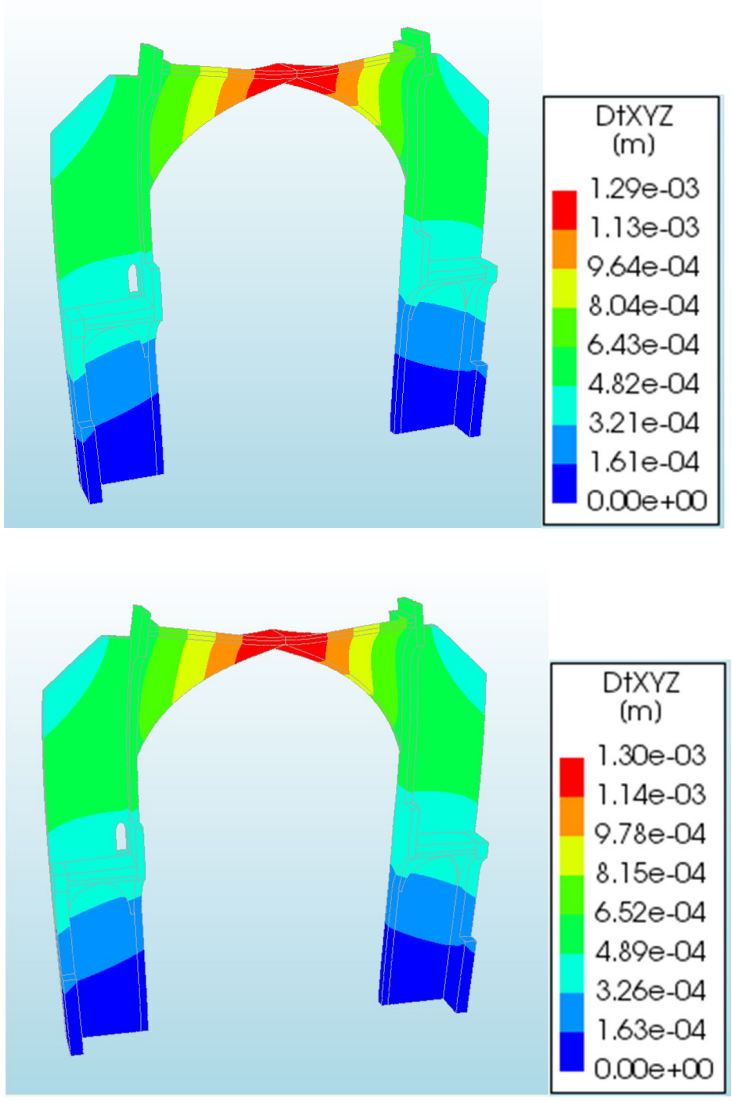

Figure 5.1.4.D: Deformation under graviational load (Z-) of 1g.
Above: Mesh 15-30cm Below: Mesh 10-20cm.
The diferences between meshes are low.

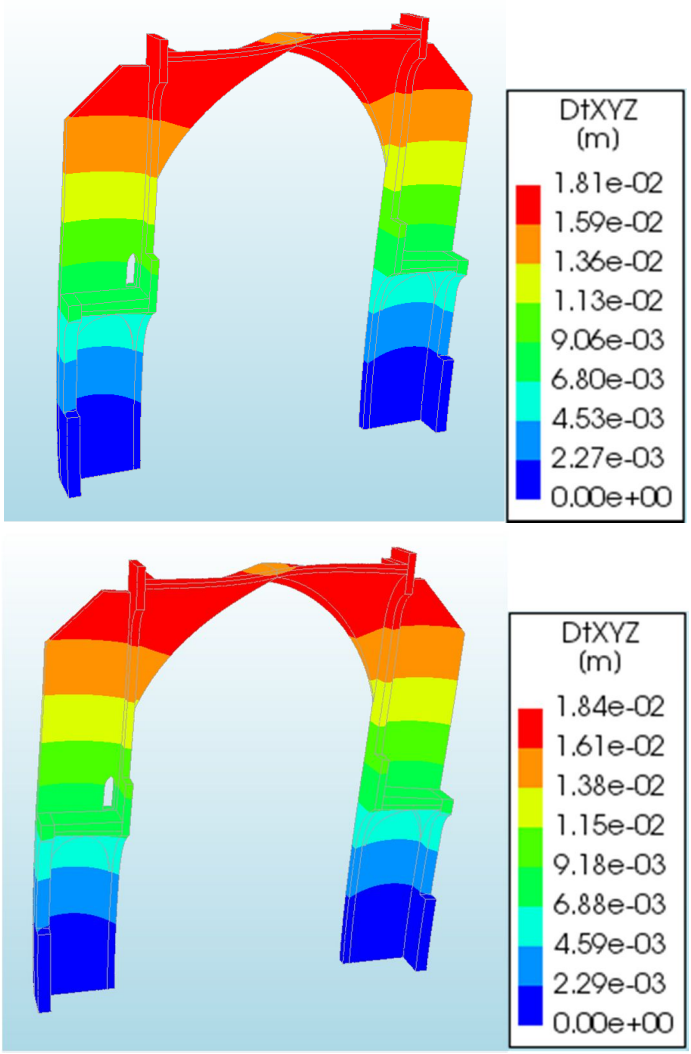

Figure 5.1.4.E: Deformation under lateral load (Y+) of 1g.
Above: Mesh 15-30cm Below: Mesh 10-20cm
The diferences between meshes are low.

Table 5.1.4.A: Comparative of the two meshes' elastic response.
The diferences between meshes are low.

Magnitude [unit]	Case	Mesh 15-30cm	Mesh 10-20cm	Relative error
Maximum deformation [m]	Gravitational (Z-)	$1{,}29 \times 10^{-3}$	$1{,}30 \times 10^{-3}$	0,78%
	Lateral (Y+)	$1{,}81 \times 10^{-2}$	$1{,}84 \times 10^{-2}$	1,66%

Magnitude [unit]	Case	Mesh 15-30cm	Mesh 10-20cm	Relative error
Vibration frequency [Hz]	1st mode	1,3636	1,3549	0,64%
	2nd mode	3,8344	3,7991	0,92%
	3rd mode	5,7998	5,7589	0,71%
	4th mode	7,0857	7,0514	0,48%
	5th mode	8,1941	8,1685	0,31%

From the values shown in table 5.1.4.A was concluded that the mesh 10-20cm was precise enough to be used as elastic reference for the 2D elastic calibration while the mesh 15-30cm would be used as inelastic reference for the 3D inelastic calibration, since it was less computationally demanding. It is worth noticing that the Mesh Convergence Study was made with the "pillar like" material in the Single-leaf Wall. The materials were changed during the calibration process (section 4.3.1 and 5.3).

5.2. 2D modelling

The 2D model is understood as a projection in a vertical plane of the 3D model. Therefore, all the 3D elements are represented in this plane stress model. The element used is the 3 nodes triangle, in order to simplify the calculations and as a projection of the 4 nodes tetrahedron. The boundary conditions consist in the displacement constraint in all the directions of the base nodes.

5.2.1. Materials and Parts Identification

The parts of the 2D model are not only defined by the material properties, but also by the different geometries and structural roles. Therefore the buttresses and Single-leaf Walls have been divided in two parts, namely the clerestory and the chapel.

The identified parts and materials associated are presented in Table 5.2.1.A and Figure 5.2.1.A.

Table 5.2.1.A: Parts and materials of the 2D model:
The material Vaults Infill has been replaced during the calibration process.

	Part	Material
A	Clerestory Buttresses	Three-leaf Walls
B	Chapels Buttresses	Three-leaf Walls
C	Three-leaf Walls	Three-leaf Walls
D	Chapels Infill	Three-leaf Walls
E	Nave Infill	Vaults and Single-leaf Walls
F	Chapels Vaults	Vaults and Single-leaf Walls
G	Nave Vault	Vaults and Single-leaf Walls
H	Chapels Single-leaf Walls	Vaults and Single-leaf Walls
I	Clerestory Single-leaf Walls	Vaults and Single-leaf Walls

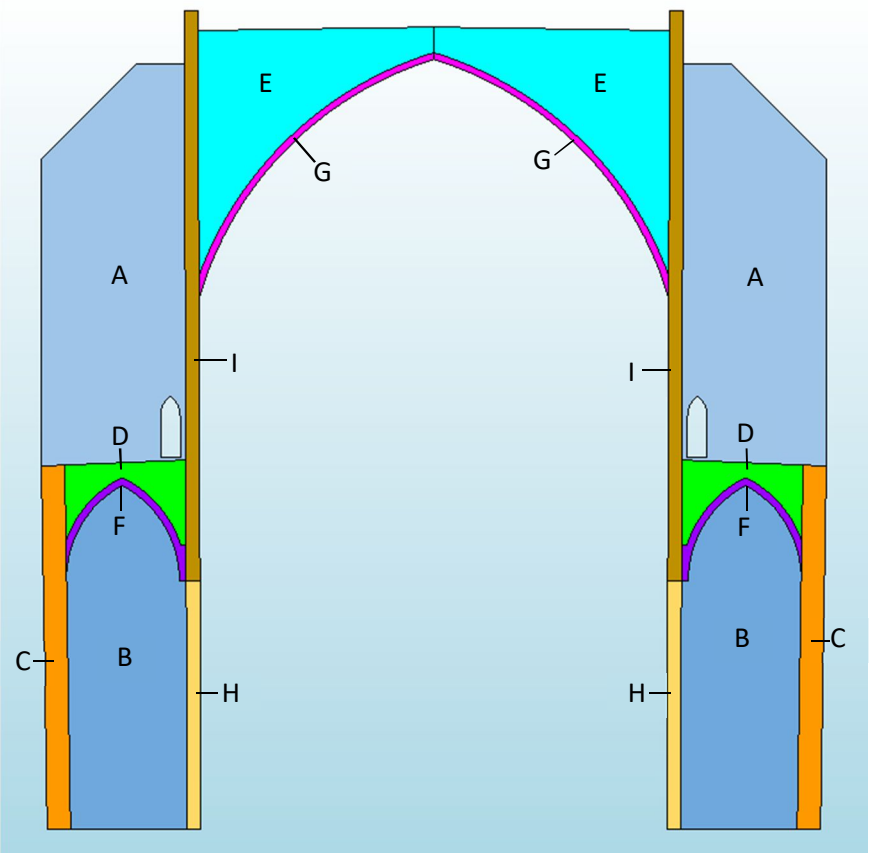

Figure 5.2.1.A: Parts of the 2D model: (A) Clerestory Buttresses, (B) Chapels Buttresses (C) Three-leaf Walls, (D) Chapels Infill, (E) Nave Infill, (F) Chapels Vaults, (G) Nave Vault, (H) Chapels Single-Leaf Walls, (H) Clerestory Single-Leaf Walls.

As shown in table 5.2.1.A, the vaults infill material has not been considered in the 2D model. This decision was made during the calibration process. It was realized that using the Vaults Infill material for the parts D and E (Chapels and Nave Infill respectively) affected strongly the structural response of key zones of the Nave Vault and the Buttresses. This is because the use of the softer material of the projected volume (the Infill is not present in all the thickness in the 3D model) weakens the 2D projection. As a solution, the stiffest material in the projected volume was used in the 2D part. Namely, the Three Leaf Walls material was used in the part D (Chapels Infill) and the Vault and Single-leaf material was used in the part E (Nave Infill).

5.2.2. Mesh Description

As explained above, the 2D FEM model is built as a projection of the 3D FEM model. Therefore, the used mesh has the same criteria as the finest 3D mesh, namely the Mesh 10-20cm (figure 5.2.2.A). The dimension criterion is that the description of the flexural behaviour is done with 3 elements (figure 5.2.2.B). In this mesh, the number of elements is 27440 and the number of nodes is 14206.

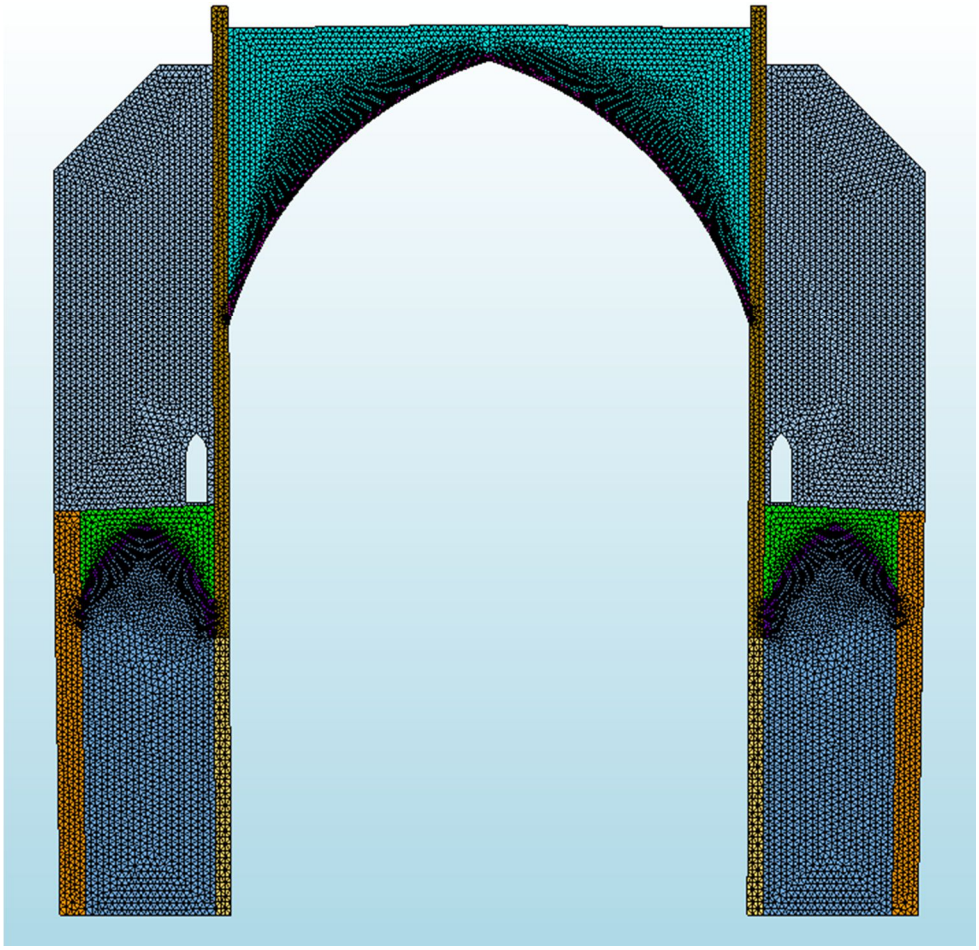

Figure 5.2.2.A: Mesh used in the 2D Plane Stress FEM model.
The element maximum dimension is 10-20cm.
The number of elements is 27440 and the number of nodes is 14206.

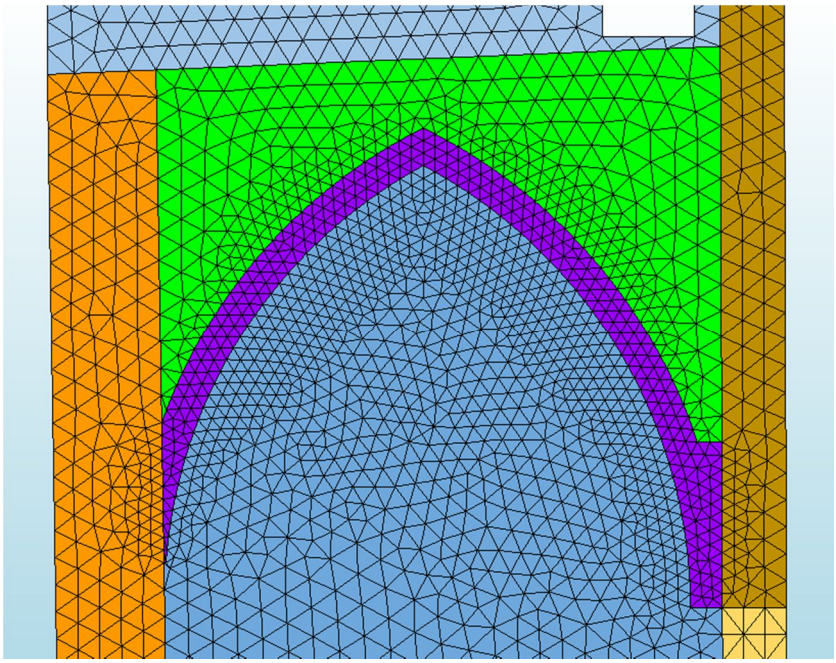

Figure 5.2.2.B: Mesh used in the 2D Plane Stress FEM model (Detail).
The description of the flexural behaviour is done with 3 elements

5.3. Calibration Process of the 2D model

The calibration process has been made first in elasticity (section 5.3.1) and afterwards in inelasticity. For the inelastic calibration, two different criteria have been used, first a Mechanism Centred Approach (section 5.3.2) and afterwards a Stiffness and Energy Centred Approach (section 5.3.3). During all the calibration process, the reference material properties (table 4.3.5.A) have been used.

5.3.1. Elastic Calibration

The elastic calibration consists in achieving the same deformation for the 3D and the 2D model under both gravitational (Z-) and lateral (Y+) mass proportional loads. The equivalent acceleration considered is 1g in both cases.

The procedure of the elastic calibration consists in changing the thickness of the different 2D parts without changing the mass of the projected zone (Table 5.3.1.A). This is equivalent in elasticity to changing the Young Modulus of the different parts without changing the applied loads (that are directly dependent on the total mass).

It is worth saying that the mass of the projected zone is normally higher than the one of the homologue 3D part, since the 3D are not usually present in all the thickness. A case apart is the Nave Vault and Infill that because of their close relationship the weight of the 2D elements is proportional to each area, considering the Nave Vault and Infill as a unique 3D part.

In order to achieve an equivalent elastic deformation in the different parts of the model, the calibration has been made by 3 successive phases. Those phases are:

(1) **The Buttress Zone**, including the Chapel and Clerestory Buttresses the Three-leaf Wall and the Chapels Vaults and Infill (figures 5.3.1.A and 5.3.1.B);

(2) **The Lateral Zone**, including the Buttress Zone and the Chapel and Clerestory Single-leaf Wall (figures 5.3.1.C and 5.3.1.D); and

(3) **The Whole Macroelement**, including all the 2D parts (figures 5.3.1.E and 5.3.1.F)

Finally a good equivalence between the 3D and the equivalent 2D is achieved, since among the 5 first vibration modes the highest error is 6.38% (table 5.3.1.B).

Table 5.3.1.A: Parts' volume, mass, area, thickness and density of the 1st 2D model. The thickness of the 2D Parts has been adjusted so the elastic deformation is the same under gravitational (Z-) and lateral (Y+) loads. This forces a change in the density in order not to alter the total mass.

3D Part		Volume [m^3]	Mass [kg]	2D Part		Area [m^2]	Thickness [m]	Mass [kg]	Density [kg/m^3]
1	Buttesses	88.24	194129	**A**	Clerestory Buttresses	63.17	0.600	96776	2553
				B	Chapels Buttresses	45.20	0.696	69235	2201
2	Three-leaf Walls	18.63	40975	**C**	Three-leaf Walls	10.37	2.493	56858	2200
3	Single-leaf Walls	21.64	47603	**H**	Chapels Single-leaf Walls	9.18	0.696	14052	2200
				I	Clerestory Single-leaf Walls	9.57	0.696	33551	5035
4	Chapels Vaults	3.15	6940	**F**	Chapels Vaults	1.96	1.950	9941	2603
5	Nave Vault	10.54	23189	**G**	Nave Vault	2.72	0.950	6900	2672
6	Chapel Infill	9.58	21071	**D**	Chapels Infill	6.03	1.950	30306	2578
7	Nave Infill	25.81	56776	**E**	Nave Infill	28.79	1.101	73064	2305
Total Mass [kg]			390683					390683	

Table 5.3.1.B: Relative error between the 3D Mesh 10-20cm and the 1st 2D models. The relative error is low in the first 5 vibration frequencies.

Magnitude [unit]	Case	3D Mesh 10-20cm	1st 2D	Relative error
Elastic deformation [m]	Gravitational (Z-)	$1{,}30 \times 10^{-3}$	$1{,}30 \times 10^{-3}$	0,00%
	Lateral (Y+)	$1{,}84 \times 10^{-2}$	$1{,}84 \times 10^{-2}$	0,00%
Magnitude [unit]	**Case**	**3D Mesh 15-30cm**	**1st 2D**	**Relative error**
Vibration frequency [Hz]	1st mode	1,3549	1,3557	0,06%
	2nd mode	3,7991	3,6199	4,72%
	3rd mode	5,7589	5,3914	6,38%
	4th mode	7,0514	6,6343	5,91%
	5th mode	8,1685	8,0798	1,09%

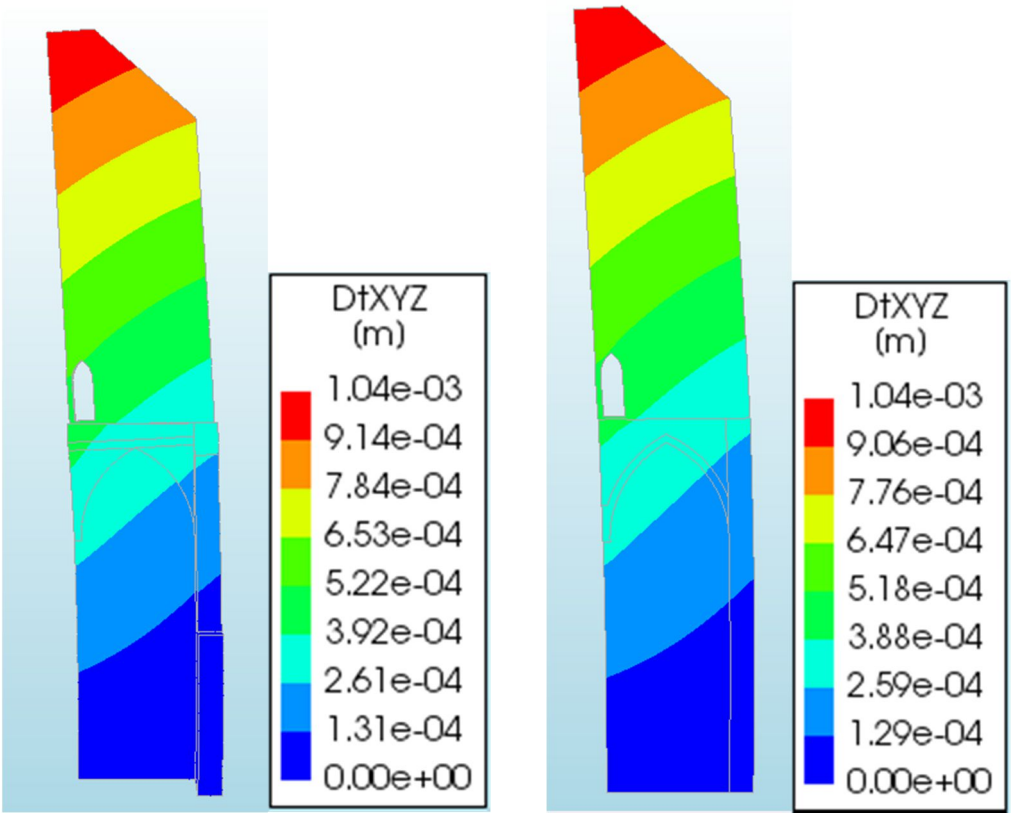

Figure 5.3.1.A: Elastic Calibration Phase 1,
Gravitational (Z-) equivalent acceleration of 1g. Left: 3D model, right: 2D model.

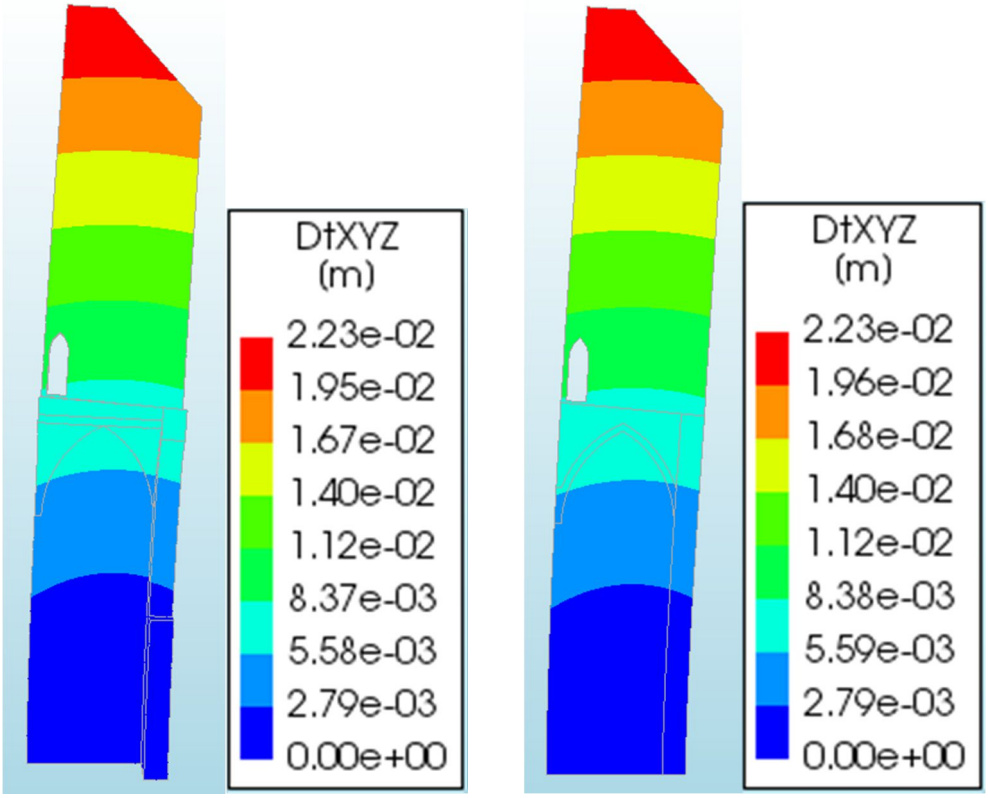

Figure 5.3.1.B: Elastic Calibration Phase 1,
Lateral (Y+) equivalent acceleration of 1g. Left: 3D model, right: 2D model.

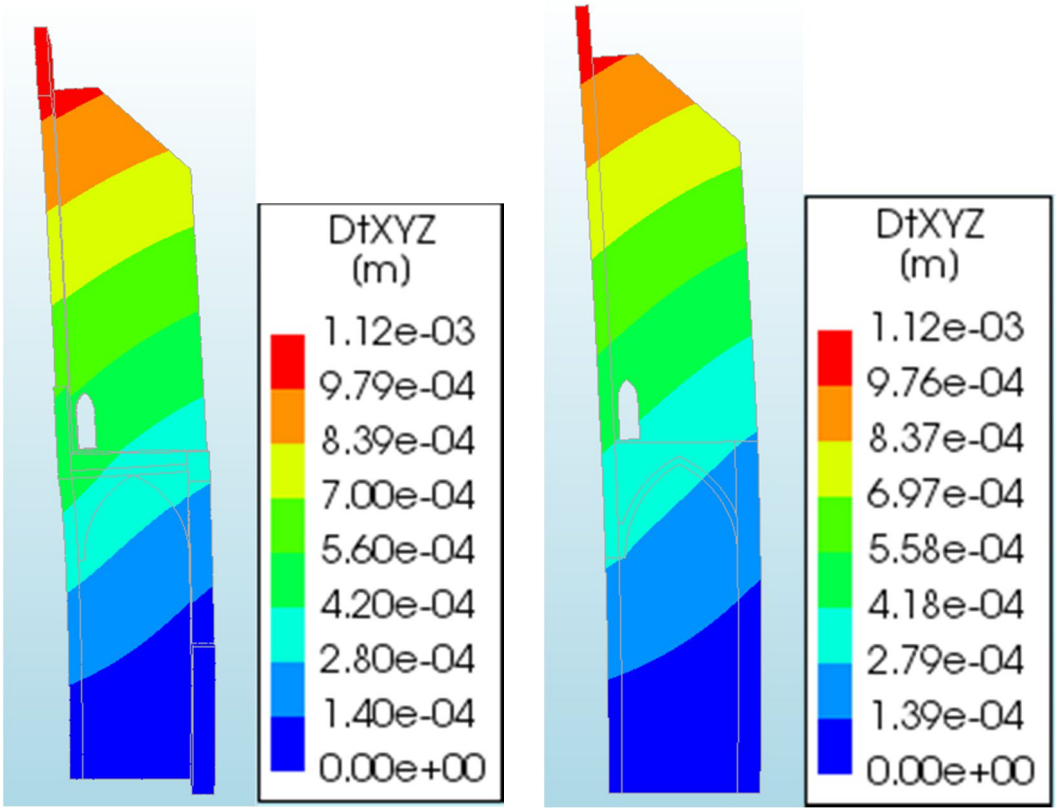

Figure 5.3.1.C: Elastic Calibration Phase 2,
Gravitational (Z-) equivalent acceleration of 1g. Left: 3D model, right: 2D model.

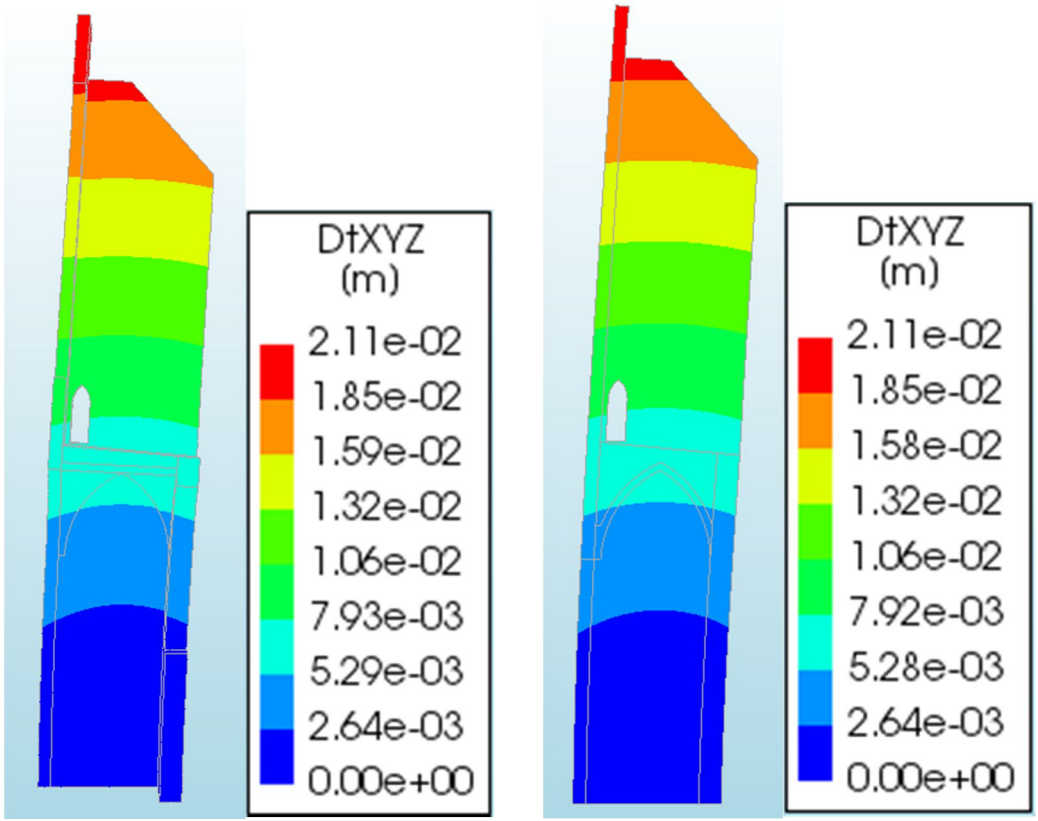

Figure 5.3.1.D: Elastic Calibration Phase 2,
Lateral (Y+) equivalent acceleration of 1g. Left: 3D model, right: 2D model.

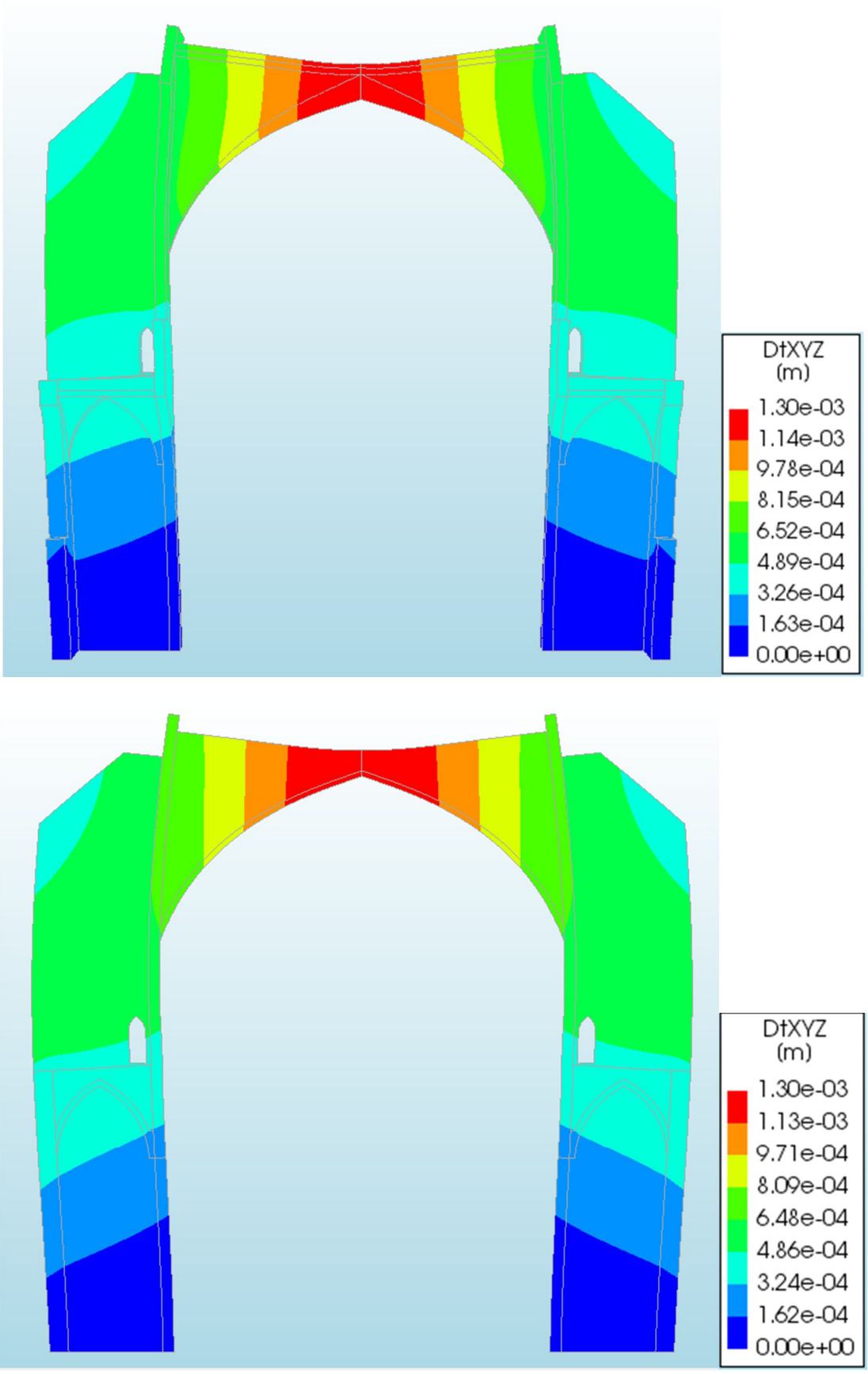

Figure 5.3.1.E: Elastic Calibration Phase 3,
Gravitational (Z-) equivalent acceleration of 1g. Above: 3D model, below: 2D model.

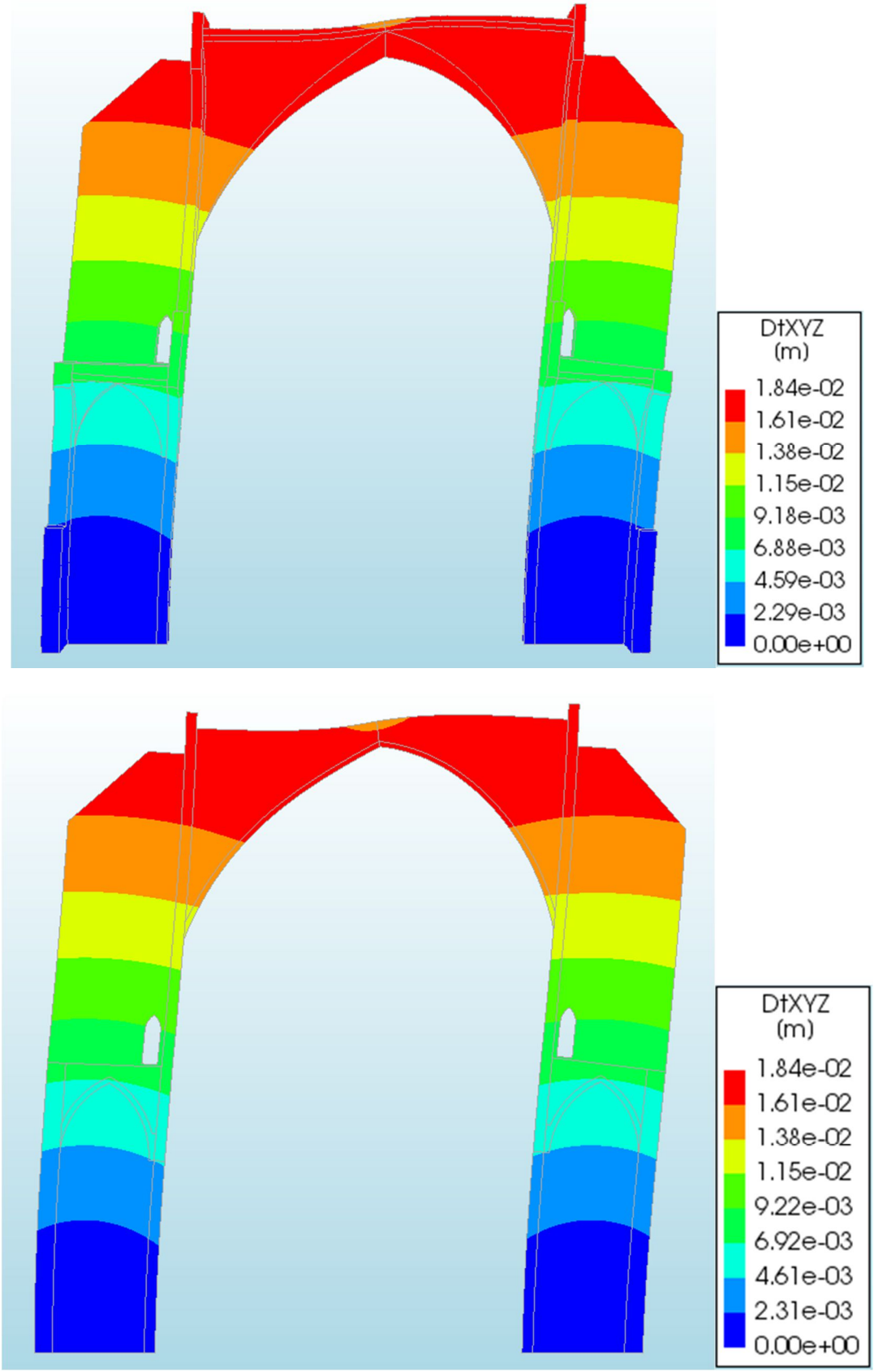

Figure 5.3.1.F: Elastic Calibration Phase 3,
Lateral (Y+) equivalent acceleration of 1g. Above: 3D model, below: 2D model.

5.3.2. First Inelastic Calibration

The first inelastic calibration can be described as a mechanism based calibration. This is because among the main objectives of the calibration was to obtain a 2D equivalent model able to reproduce the 3D (mesh 30-15cm) model Collapse Mechanism under a lateral incremental loading or Pushover (figure 5.3.2.A). The other main objectives of the calibration were the match of the maximum resistance, the elastic limit and the dissipated energy.

The procedure of this calibration is less structured and more experience based than the elastic one. Furthermore, it is iteration based and may lead to different results if different paths are followed.

In the present thesis, the first step was to perform a pushover analysis in the 1st 2D model, the output of the elastic calibration. The results of the analysis showed that it was far from developing the same mechanism (figure 5.3.2.B). Nonetheless, the pushover curves were close enough but their form was significantly different (figure 5.3.2.C).

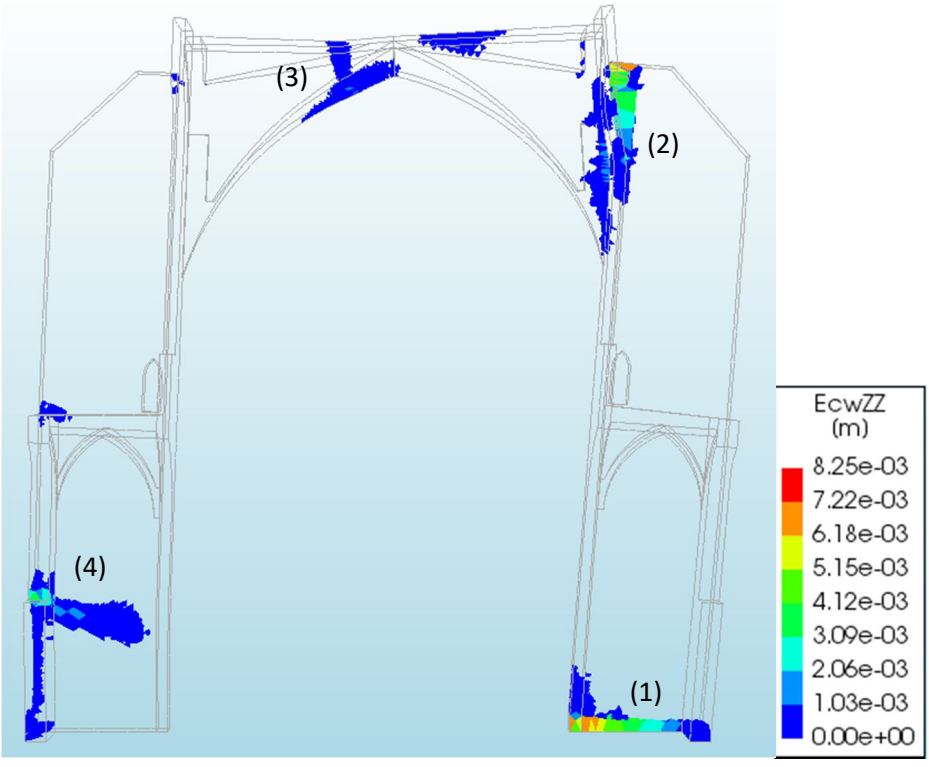

Figure 5.3.2.A: 3D (Mesh 30-15cm) model mechanism which develops 4 hinges: (1) Base of the right buttress, (2) Union between the right buttress and the clerestory wall, (3) Top left of the nave vault, and (4) Left buttress in the in the base of the lateral chapel window.

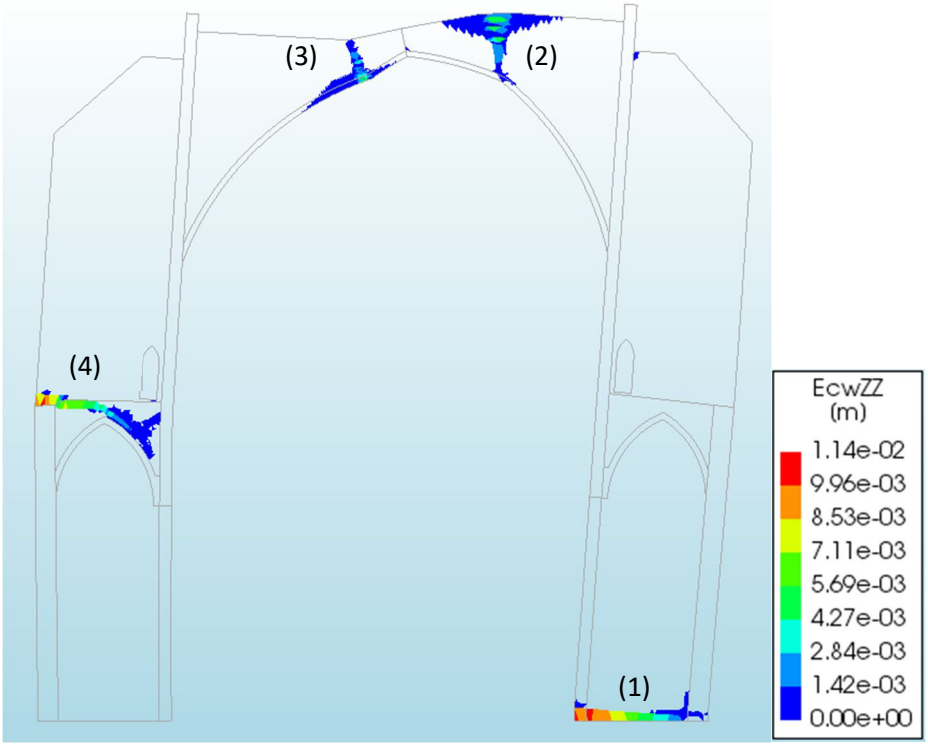

Figure 5.3.2.B: 1st 2D model mechanism which develops 4 hinges: (1) Base of the right buttress, (2) Top right of the nave vault, (3) Top left of the nave vault, and (4) Left buttress in the top the lateral chapel.

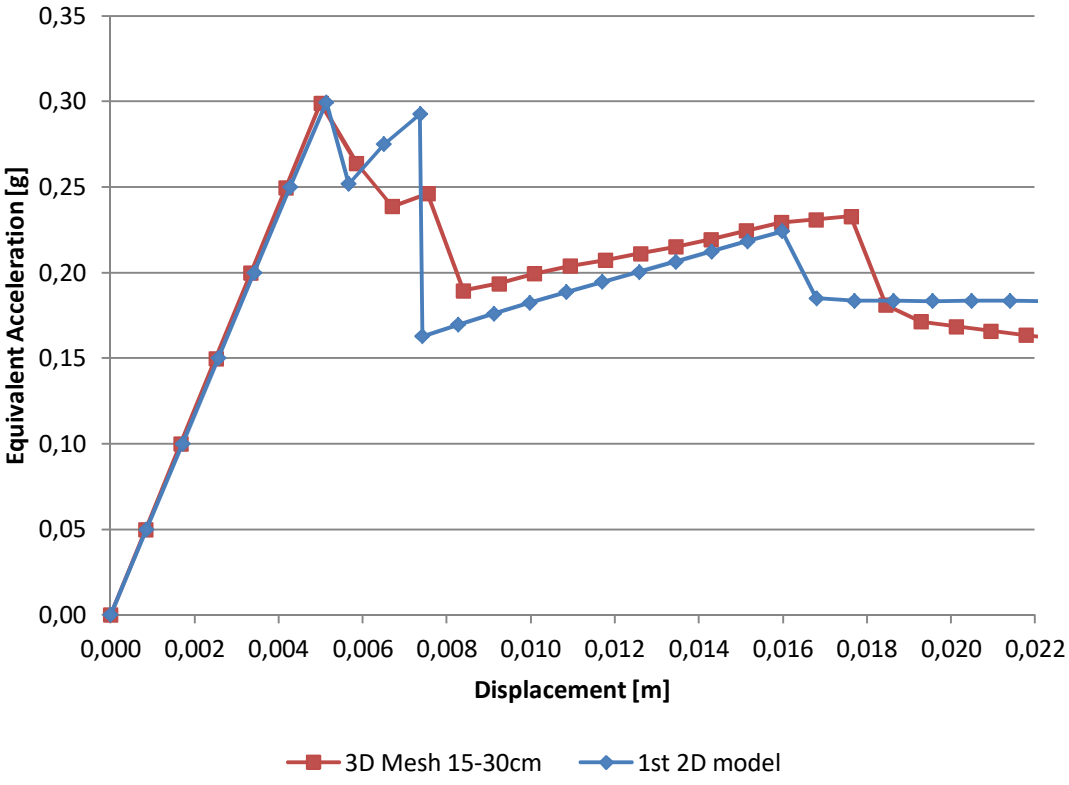

Figure 5.3.2.C: Capacity curve (pushover curve) in the reference control node for the 3D and the 1st 2D equivalent model. The curves are close enough but the form is significantly different.

The developed mechanism in the 1st 2D model (figure 5.3.2.B) consisted in 4 hinges: (1) Base of the right buttress, (2) Top right of the nave vault, (3) Top left of the nave vault, and (4) Left buttress in the top the lateral chapel. However, the objective mechanism (the one developed by the 3D model – figure 5.3.2.A) differed in the (2) and (4) hinges, being these the union between the right buttress and the clerestory wall (2) and the Left buttress in the base of the lateral chapel window (3).

Two conclusions were achieved in this first iteration, first, the (4) hinge (figure 5.3.2.B) penetrated in the left chapel vault infill, which weakened the model; and second, the (2) hinge (figure 5.3.2.B) could be due to the use of the material vault infill in the nave vault infill. Therefore, two new iterations were held, namely the 2nd and 3rd 2D models, changing in the 2nd the material of the chapels' infill to Three-leaf Wall and in the 3rd the material of the nave vault infill to Vaults and Single-leaf Walls.

In order to respect the elastic calibration of the 2D model in the new iterations, another elastic calibration procedure was used, since the using of the Phase-Based one was too demanding for an already calibrated model. The new procedure consisted in achieving a relative error between the 3D and the calibrated 2D model beyond or slightly above the 10%, in the deformation under an equivalent acceleration of 1g in Z- (gravity) and Y+ (lateral) on the 5 defined control nodes (figure 5.3.2.D).

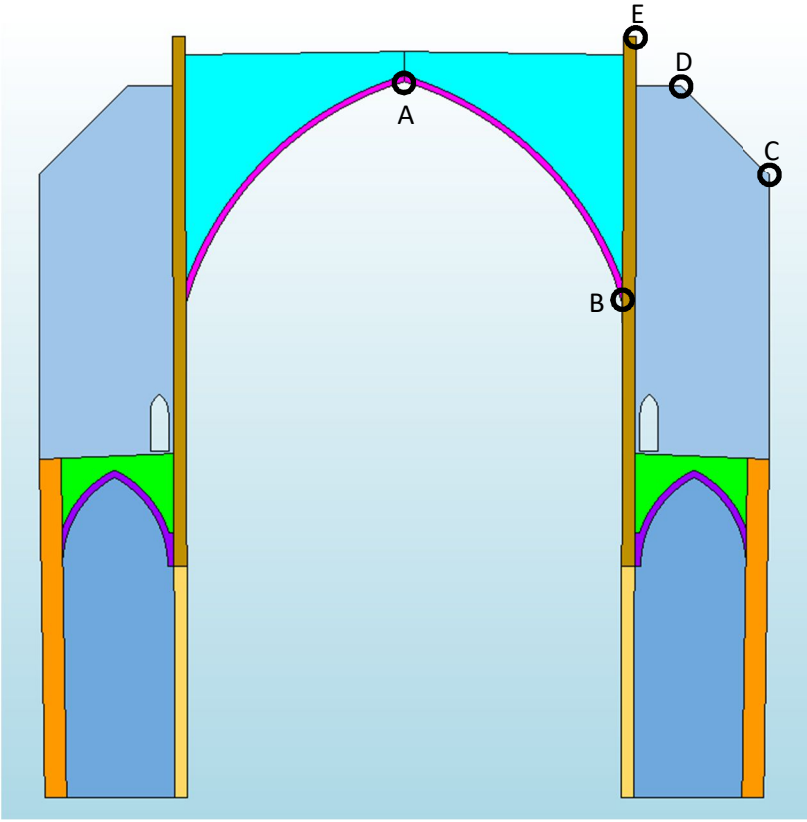

Figure 5.3.2.D: Control nodes for the N2 method. These nodes were used for the recalibration of the 2D inelastic iterations so the relative error with the 3D model was below or slightly above 10%.

The results of the 2nd and 3rd equivalent 2D models were not satisfactory, the pushover curves (figure 5.3.2.E) differed more than the 1st iteration and the mechanisms (figures

5.3.2.F and 5.3.2.G) were really similar to the one of the 1st iteration. The only difference in the mechanisms was that the hinge (4) did not enter the left chapel infill, and, therefore, did not weaken the model.

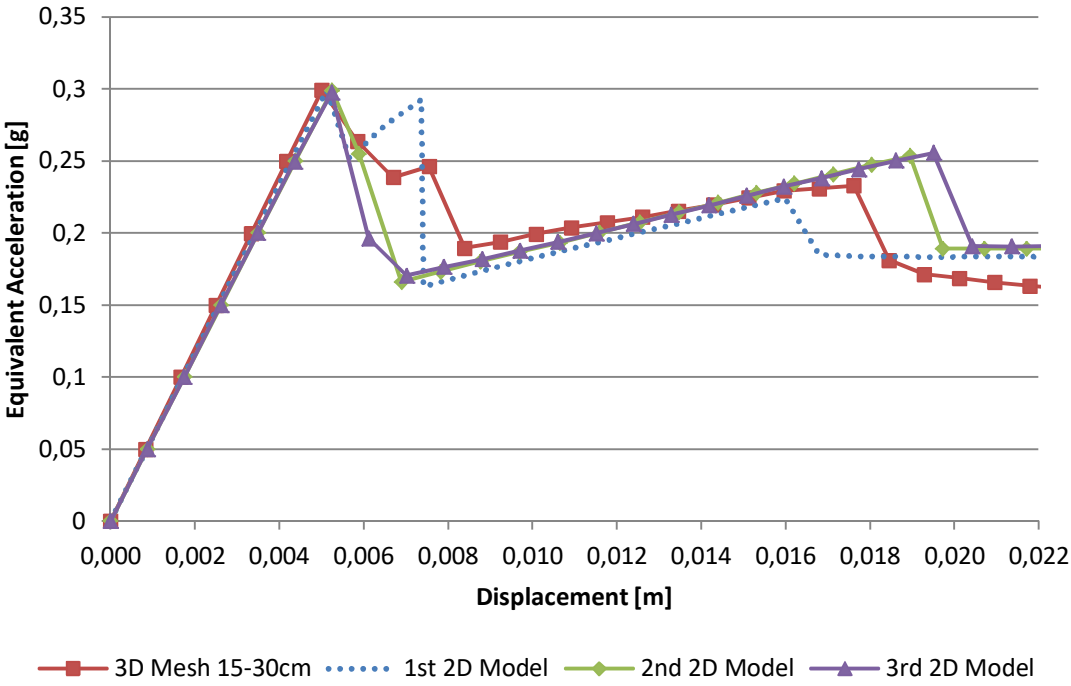

Figure 5.3.2.E: Capacity curve (pushover curve) in the reference control node for the 3D and the 1st, 2nd and 3rd 2D equivalent model. The differences intensify in the latter iterations.

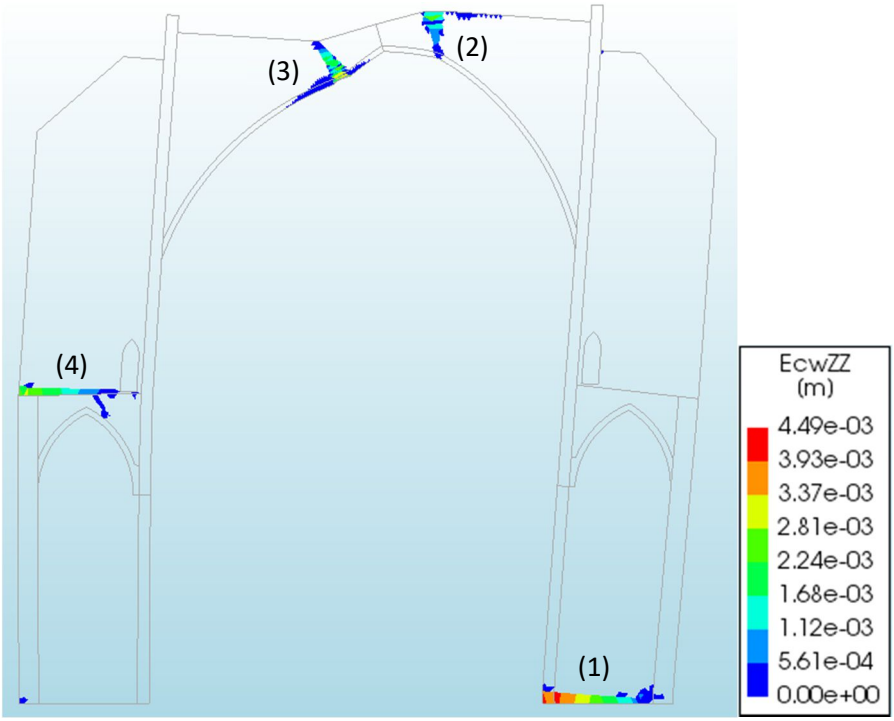

Figure 5.3.2.F: 2nd 2D model mechanism which develops 4 hinges: (1) Base of the right buttress, (2) Top right of the nave vault, (3) Top left of the nave vault, and (4) Left buttress in the top the lateral chapel.

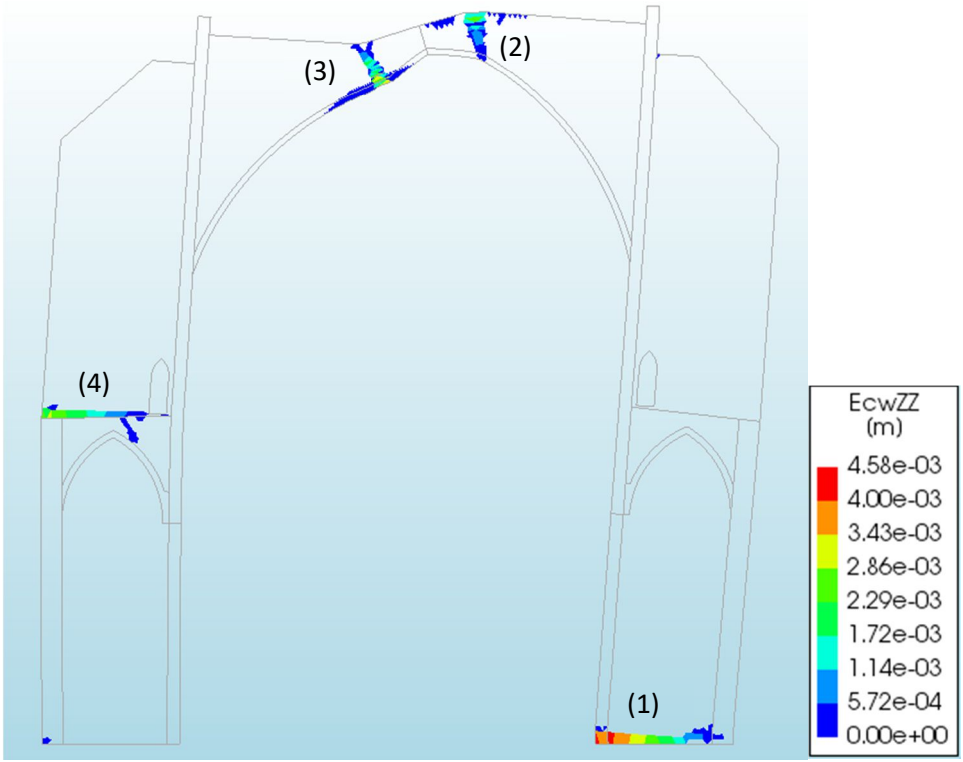

Figure 5.3.2.G: 3rd 2D model mechanism which develops 4 hinges: (1) Base of the right buttress, (2) Top right of the nave vault, (3) Top left of the nave vault, and (4) Left buttress in the top the lateral chapel.

From the 2nd and 3rd iterations was concluded that the way to achieve a correct position of the hinge (2) in the equivalent 2D model was to significantly increase the thickness of the Clerestory Single-leaf Wall, at the same time that the thickness of the nave infill was not much different from the Clerestory Buttresses thickness.

The 4th equivalent 2D model resulted in the wanted position of the hinge (2) –the union between the right buttress and the clerestory wall (figure 5.3.2.H). However, the elastic rigidity of the pushover curve (the first slope of the curve) was significantly different and the dissipated energy was lower than the 3D model (figure 5.3.2.I). Therefore, the finding of the mechanism did not seem to imply a closer approach to the pushover curve, which is basic for the application of the N2 method and the final results.

For information proposes, the characteristics of the 4th equivalent 2D model are presented in table 5.3.2.A and the relative error of the model is presented in table 5.3.2.B.

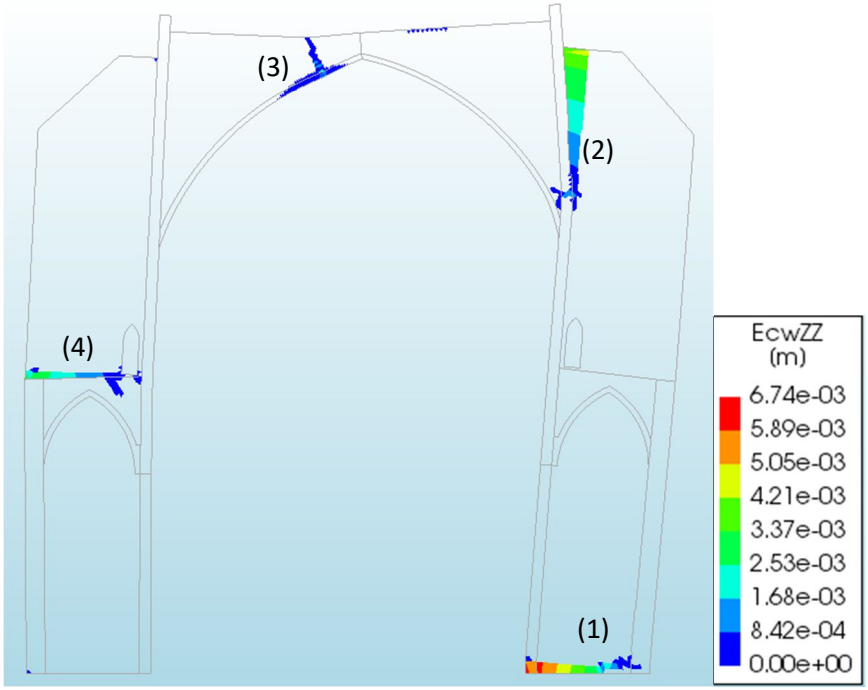

Figure 5.3.2.H: 4th 2D model mechanism which develops 4 hinges: (1) Base of the right buttress, (2) Union between the right buttress and the clerestory wall, (3) Top left of the nave vault, and (4) Left buttress in the top the lateral chapel. This is the most similar to the 3D mechanism achieved by an equivalent 2D model in the present thesis.

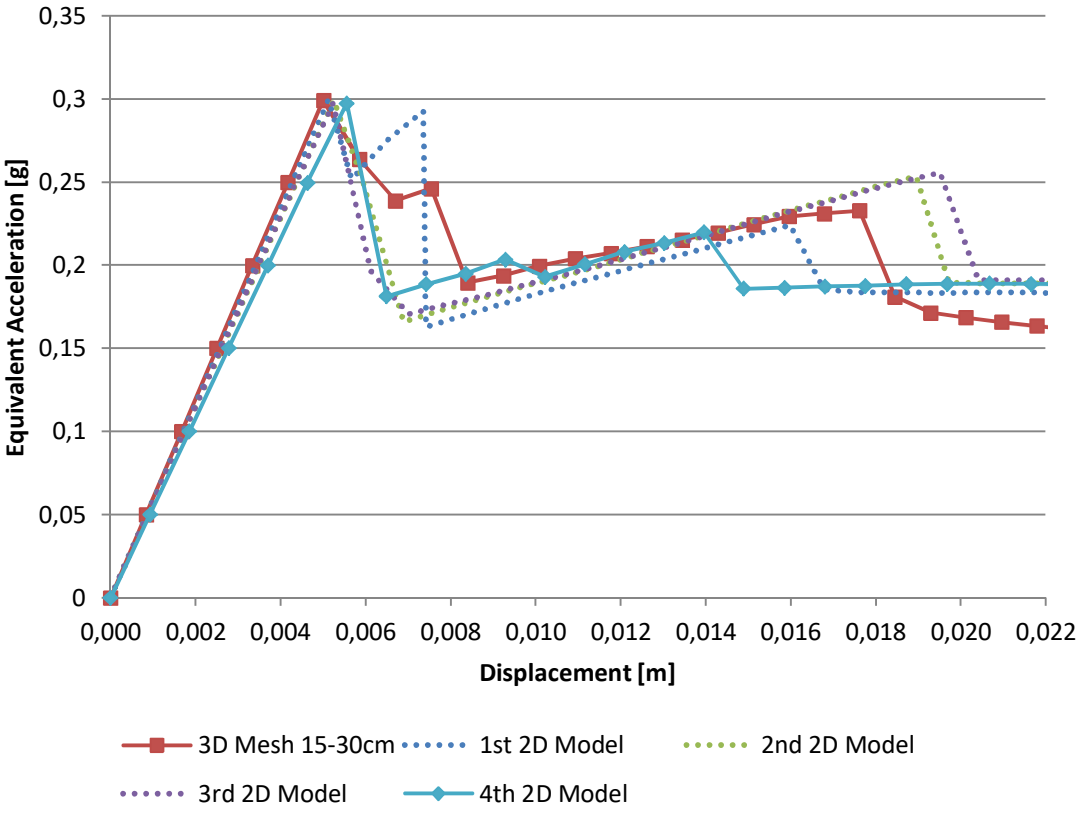

Figure 5.3.2.I: Capacity curve (pushover curve) in the reference control node for the 3D and the 1st, 2nd, 3rd and 4th 2D equivalent model. The differences intensify in the latter iterations.

Table 5.3.2.A: Parts volume, mass, area, thickness and density of the 4th 2D model. The thickness of the 2D Parts has been adjusted so the elastic deformation is the same under gravitational (Z-) and lateral (Y+) loads. This forces a change in the density in order to not alter the total mass.

3D Part		Volume [m^3]	Mass [kg]	2D Part		Area [m^2]	Thickness [m]	Mass [kg]	Density [kg/m^3]
1	Buttesses	88.24	194129	**A**	Clerestory Buttresses	63.17	0.400	96776	3830
				B	Chapels Buttresses	45.20	0.696	69235	2201
2	Three-leaf Walls	18.63	40975	**C**	Three-leaf Walls	10.37	2.200	56858	2493
3	Single-leaf Walls	21.64	47603	**H**	Chapels Single-leaf Walls	9.18	0.696	14052	2200
				I	Clerestory Single-leaf Walls	9.57	1,575	33551	2225
4	Chapels Vaults	3.15	6940	**F**	Chapels Vaults	1.96	1.000	9941	5075
5	Nave Vault	10.54	23189	**G**	Nave Vault	2.72	0.400	6900	6346
6	Chapels Infill	9.58	21071	**D**	Chapels Infill	6.03	0.75	30306	6702
7	Nave Infill	25.81	56776	**E**	Nave Infill	28.79	0.35	73064	7252
Total Mass [kg]			390683					390683	

Table 5.3.2.B: Relative error between the 3D Mesh 10-20cm and the 4th 2D models. The relative error is below or slightly above 10% in all the points.

Magnitude [unit]	Case	3D Mesh 10-20cm	4th 2D	Relative error
Point A: Elastic deformation [m]	Gravitational (Z-)	$1.30x10^{-3}$	$1.21x10^{-3}$	6.85%
	Lateral (Y+)	$1.69x10^{-2}$	$1.85x10^{-2}$	9.61%
Point B: Elastic deformation [m]	Gravitational (Z-)	$5.53x10^{-4}$	$5.61x10^{-4}$	1.34%
	Lateral (Y+)	$1.25x10^{-2}$	$1.33x10^{-2}$	6.25%
Point C: Elastic deformation [m]	Gravitational (Z-)	$4.26x10^{-4}$	$4.46x10^{-4}$	4.82%
	Lateral (Y+)	$1,59x10^{-2}$	$1.69x10^{-2}$	6.54%
Point D: Elastic deformation [m]	Gravitational (Z-)	$4.72x10^{-4}$	$5.25x10^{-4}$	11.32%
	Lateral (Y+)	$1,78x10^{-2}$	$1.89x10^{-2}$	6.11%
Point E: Elastic deformation [m]	Gravitational (Z-)	$5.67x10^{-4}$	$6.21x10^{-4}$	9.45%
	Lateral (Y+)	$1.83x10^{-2}$	$1.94x10^{-2}$	5.68%

Magnitude [unit]	Case	3D Mesh 15-30cm	4th 2D	Relative error
Vibration frequency [Hz]	1st mode	1,3549	1.3174	2.77%
	2nd mode	3,7991	3.6157	4.83%
	3rd mode	5,7589	5.5013	4.47%
	4th mode	7,0514	6.8259	3.20%
	5th mode	8,1685	7.7443	5.19%

5.3.3. Second Inelastic Calibration: Obtaining of the 2D Reference Model

In order to achieve a better 2D equivalent model, a different criteria for the second inelastic calibration was used. This time, the priority was set to achieve a close elastic stiffness and the closest possible dissipation of energy.

The new calibration was used as an opportunity to change the material used in the 3D model for the Single-leaf Wall. As explained in section 5.1.2, the used material was a "pillar like" one to take in account the prominent church nerves and pilasters, however, this was too influential in the church behaviour (especially in the determination of the mechanism) and therefore it was replaced, in a conservative approach, for the Vaults and Single-leaf Walls material.

The pushover analysis for the modified 3D model (that used the 30-15cm mesh) was done with a smaller step (0.005g) than the one of the first inelastic calibration (0.05g) in order to obtain more precise results (figure 5.3.3.A). However, the mechanism (figure 5.3.3.B), even if not entirely developed in the analysis, was very similar to the one of the first inelastic calibration.

The 5th equivalent 2D model achieved manly the objectives of the second inelastic calibration, concentrating the elastic equivalence in the lateral deformation and keeping the relative error in the gravitational deformation below 15% (table 5.3.3.A). This meant a close approach of the slope and values of the pushover curve to the modified 3D model (figure 5.3.3.A) but not in the mechanism (figure 5.3.3.C) and a still significantly lower energy dissipation (figure 5.3.3.A).

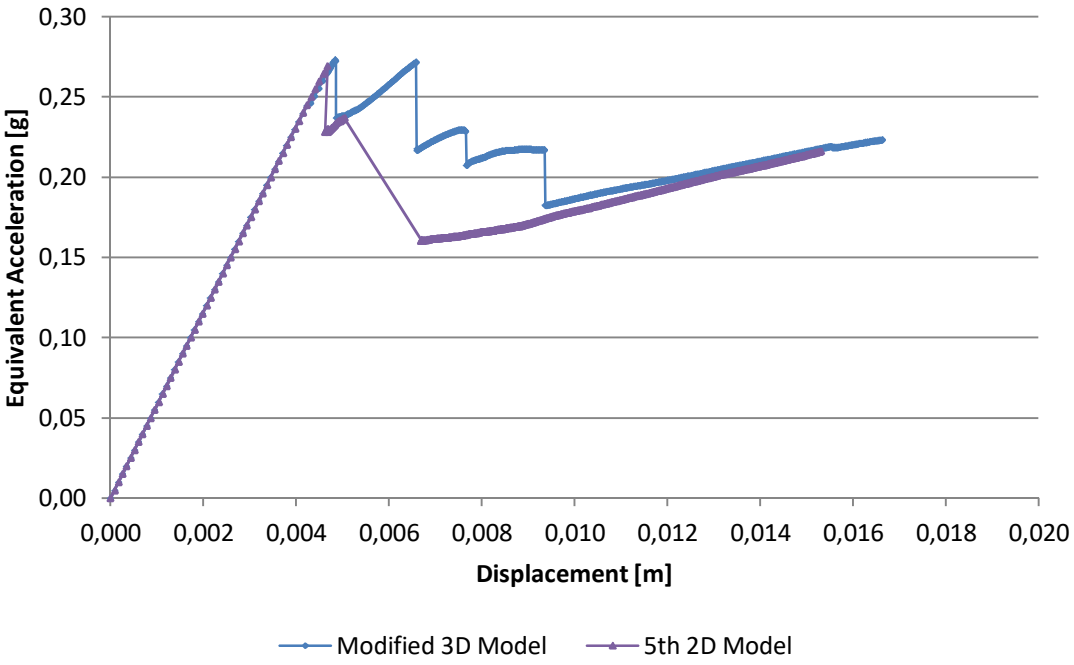

Figure 5.3.3.A: Capacity curve (pushover curve) in the reference control node for the modified 3D and the 5th 2D equivalent model. The differences are low in stiffness and resistance but significant in the dissipated energy.

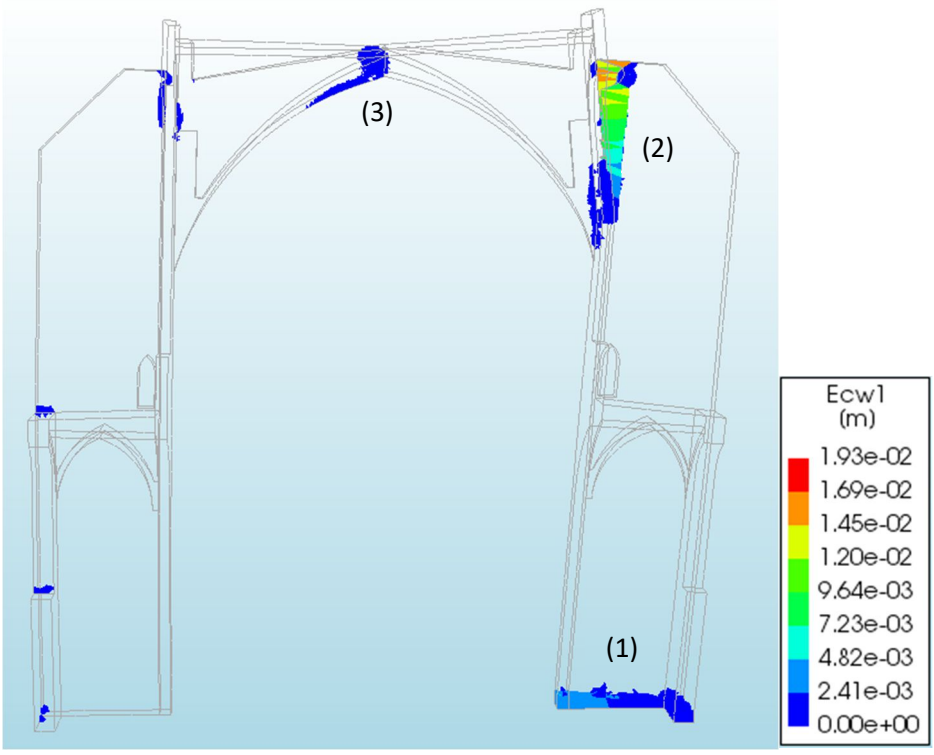

Figure 5.3.3.B: Modified 3D (Mesh 30-15cm) model mechanism not entirely developed with 3 hinges: (1) Base of the right buttress, (2) Union between the right buttress and the clerestory wall, (3) Top left of the nave vault. The final mechanism occurs at large displacements and has not a main importance for the calibration

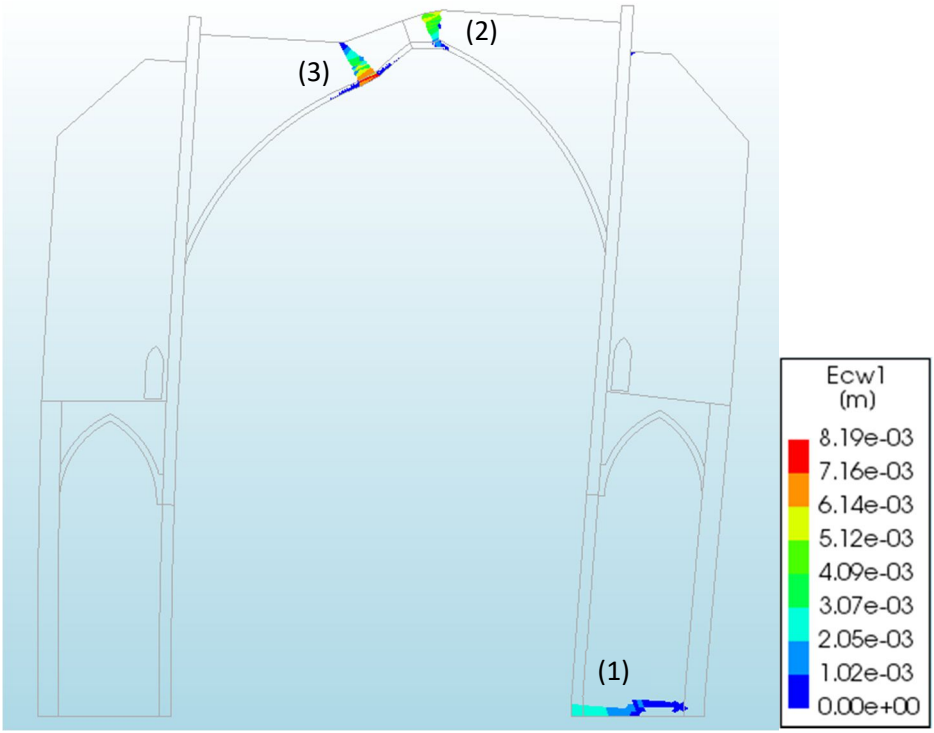

Figure 5.3.3.C: 5th 2d model mechanism not entirely developed with 3 hinges: (1) Base of the right buttress, (2) Top right of the nave vault, (3) Top left of the nave vault.

In order to correct the significantly lower dissipated energy in the curve of the 5th equivalent 2D model, a ratio was applied to the fracture energy of the different 2D parts in the same way as the density (Table 5.3.3.B).This is justified because as the density can be understood as inversely proportional to the volume at equal mass, the fracture energy is inversely proportional to the volume at equal energy dissipation. Specifically, the 2D parts have different thickness than the 3D parts. This way, the area of a crack in 2D is lower than the area of a crack in 3D. The ratio between the 2D thickness and that of the 3D gives approximately the ratio between the dissipated energy.

The resulting 6th equivalent 2D model achieved a better approach to the modified 3D (figure 5.3.3.D) but did not change the mechanism (figure 5.3.3.E). Even though this model was considered approximate enough to be used in the Stochastic Simulation.

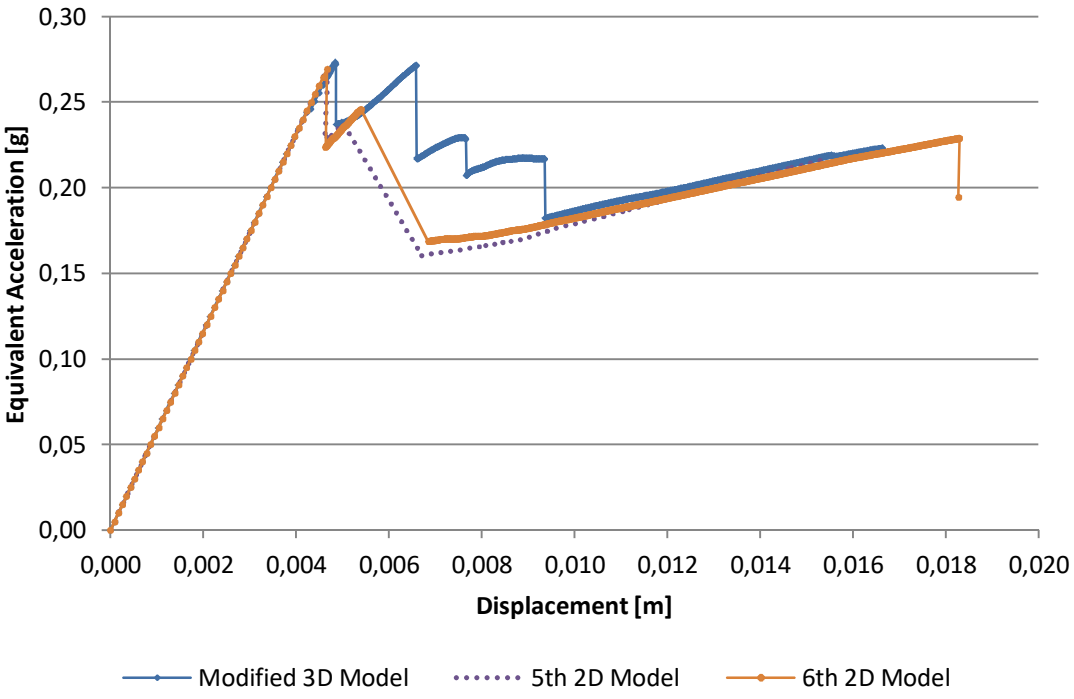

Figure 5.3.3.D: Capacity curve (pushover curve) in the reference control node for the modified 3D and the 5th and 6th 2D equivalent model. The differences are low in stiffness and resistance and the ones in the dissipated energy are corrected.

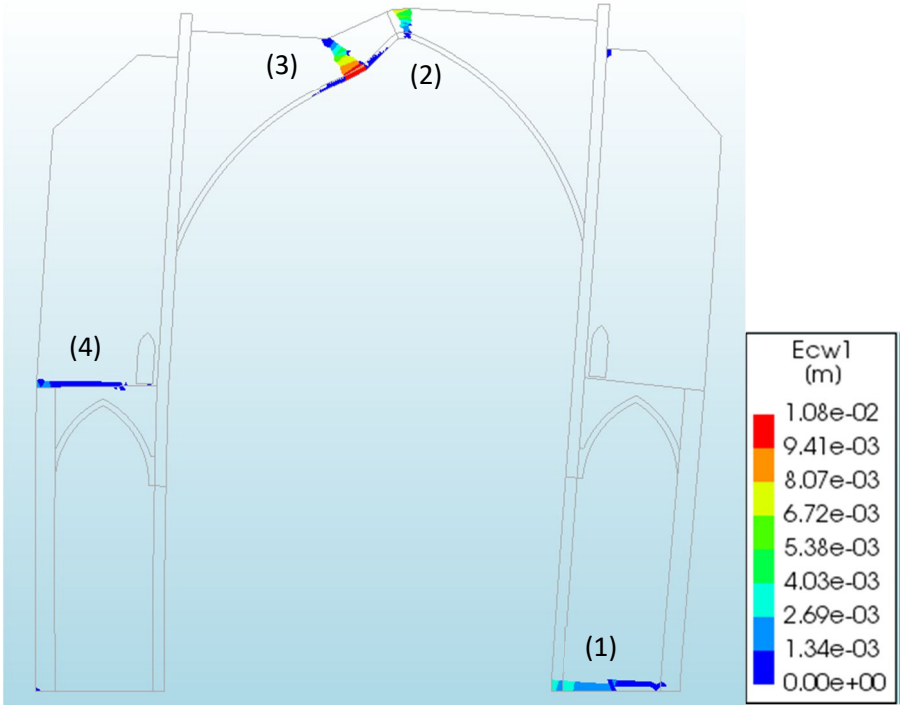

Figure 5.3.3.E: 6th 2D model mechanism which develops hinges: (1) Base of the right buttress, (2) Top right of the nave vault, (3) Top left of the nave vault and (4) Left buttress in the top the lateral chapel.

Table 5.3.3.A: Relative error between the Modified 3D and the 5th 2D models. The relative error is low under lateral loads and below 15% under gravitational loads.

Magnitude [unit]	Case	3D Mesh 10-20cm	6th 2D	Relative error
Point A: Elastic deformation [m]	Gravitational (Z-)	$1.35x10^{-3}$	$1.23x10^{-3}$	9.15%
	Lateral (Y+)	$1.74x10^{-2}$	$1.73x10^{-2}$	0.97%
Point B: Elastic deformation [m]	Gravitational (Z-)	$5.84x10^{-4}$	$6.42x10^{-4}$	9.93%
	Lateral (Y+)	$1.30x10^{-2}$	$1.29x10^{-2}$	0.92%
Point C: Elastic deformation [m]	Gravitational (Z-)	$4.37x10^{-4}$	$4.48x10^{-4}$	2.47%
	Lateral (Y+)	$1,65x10^{-2}$	$1.60x10^{-2}$	2.75%
Point D: Elastic deformation [m]	Gravitational (Z-)	$4.92x10^{-4}$	$5.63x10^{-4}$	14.41%
	Lateral (Y+)	$1,84x10^{-2}$	$1.76x10^{-2}$	4.15%
Point E: Elastic deformation [m]	Gravitational (Z-)	$6.00x10^{-4}$	$6.77x10^{-4}$	12.92%
	Lateral (Y+)	$1.89x10^{-2}$	$1.80x10^{-2}$	5.05%

Magnitude [unit]	Case	Modified 3D	6th 2D	Relative error
Vibration frequency [Hz]	1st mode	1,3408	1.3583	1.33%
	2nd mode	3,7451	3.6140	3.50%
	3rd mode	5,6814	5.5579	2.17%
	4th mode	6,9948	6.9437	0.73%
	5th mode	8,0902	7.8071	3.50%

Table 5.3.3.B: Parts volume, mass, area, thickness and ratio of the 6th 2D model (Reference model).The thickness of the 2D Parts has been adjusted so the elastic deformation is the same under gravitational (Z-) and lateral (Y+) loads. This forces a change in the density and the fracture energy using the ratio in order to not alter the total mass and dissipated energy.

3D Part		Volume [m^3]	Mass [kg]	2D Part		Area [m^2]	Thickness [m]	Mass [kg]	Ratio [-]
1	Buttesses	88.24	194129	**A**	Clerestory Buttresses	63.17	0.475	96776	1.47
				B	Chapels Buttresses	45.20	0.696	69235	1.00
2	Three-leaf Walls	18.63	40975	**C**	Three-leaf Walls	10.37	2.200	56858	1.13
3	Single-leaf Walls	21.64	47603	**H**	Chapels Single-leaf Walls	9.18	0.696	14052	1.00
				I	Clerestory Single-leaf Walls	9.57	1,100	33551	1.45
4	Chapels Vaults	3.15	6940	**F**	Chapels Vaults	1.96	1.000	9941	2.31
5	Nave Vault	10.54	23189	**G**	Nave Vault	2.72	0.550	6900	2.10
6	Chapels Infill	9.58	21071	**D**	Chapels Infill	6.03	0.750	30306	3.05
7	Nave Infill	25.81	56776	**E**	Nave Infill	28.79	0.475	73064	2.43
Total Mass [kg]			390683					390683	

5.4. Constitutive Model Comentary (Capacity Curve Decays)

As it can be observed in figures 5.3.3.A and 5.3.3.D, the capacity curves present large and abrupt (sometimes even vertical) resistance decays. This is an unexpected behaviour and it is related to the sudden opening of the hinges (progression of the fracture) once one element runs out of Mode-I Fracture Energy (G_f^I), i.e. the tension fracture energy.

This resistance decays are problematic numerically, since the lower point of the decay is extremely far away from the higher point, especially compared with the previous converging point. This supposes a major challenge for the Arc Length Method, that needs a large number of iterations (>200) in order to converge. This struggling to find the new equilibrium path may lead to a Step Back equilibrium path, i.e. a lower displacement and resistance. This is a totally logic result for the Arc Length Method, but it is not for a Capacity Curve, which should behave like a displacement dependent function (to every displacement corresponds only one resistance).

In order to corroborate that the vertical decays were a consequence of the constitutive model and not a problem of the modelling or the mesh dimensions, a numerical experiment was performed. The numerical experiment consisted in isolating one element of the zone of the hinge (1) (figures 5.3.3.C and 5.3.3.E) and vertically loading the superior node while the other two had all their displacements coerced (figure 5.4.A).

The resulting force-displacement diagrams in tension (figure 5.4.B) and compression (figure 5.4.C) reproduce the forms present in the model manual (figure 4.2.A). The results also show in figure 5.4.B that once the element runs out of Mode-I Fracture Energy (G_f^I) the distance between iterations increases quickly. This phenomena doesn't happen when it runs out of Compressive Fracture Energy (G_c) (figure 5.4.C).

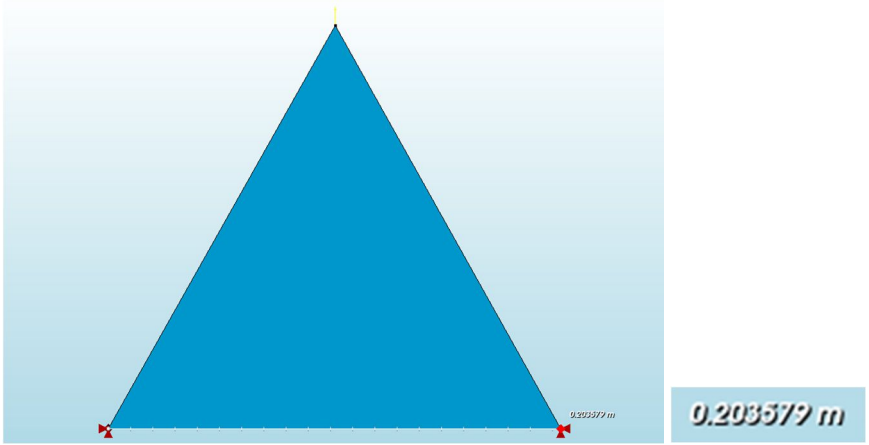

Figure 5.4.A: Performed Numerical experiment. The element is vertically loaded in the superior node while the other two had all their displacements coerced. The element side length is 0.203579m.

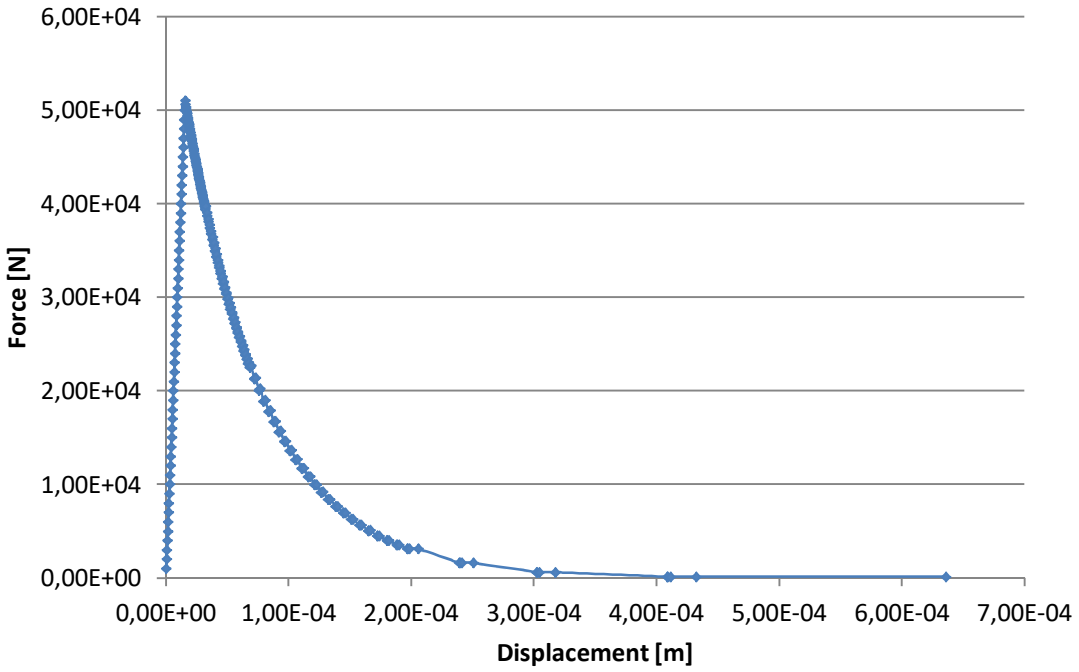

Figure 5.4.B: Force-displacement diagram under tension. Once the element runs out of Mode-I Fracture Energy (G_f^I) the distance between iterations increases quickly.

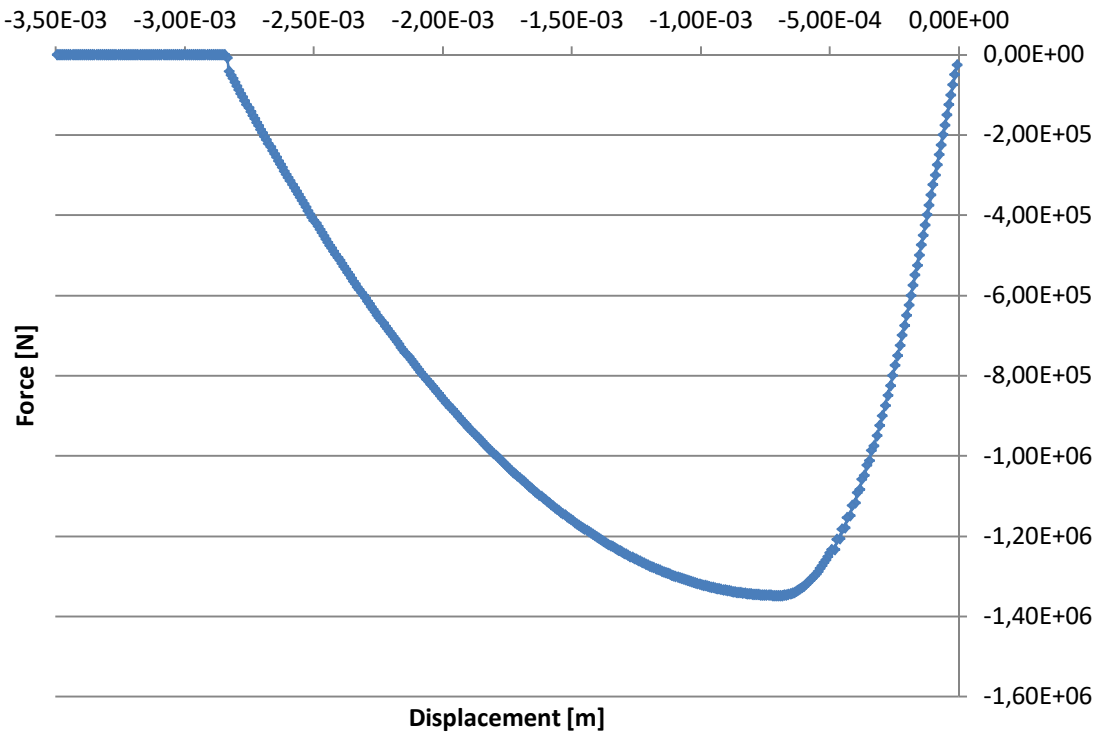

Figure 5.4.C: Force-displacement diagram under compression. Once the element runs out of Compressive Fracture Energy (G_c) the distance between iterations mantains

6. Results

6.1. Capacity curves

Figure 6.1.A shows the 200 obtained capacity curves in terms of displacement (d) against equivalent acceleration (a_e), as well as the 16%, 50% and 84% percentile curves. The last ones are curves representing the a_e level that is not exceeded by 16%, 50% and 84% of the individual capacity curves for every *d* value, referring to a normal distribution of a_e. The control node of the curves is the reference control node, the A node in figure 6.2.A.

The fact that the 16% and 50% percentile curves end prematurely is that those are the percentiles of prematurely ending capacity curves. This is most likely due to numerical instabilities consequence of the constitutive model explained in section 5.4. However, as commented in section 6.2, the influence of this is relatively low, since the resistance of a large majority of the curves has already deceased below the 80% of the maximum when the instability occurs.

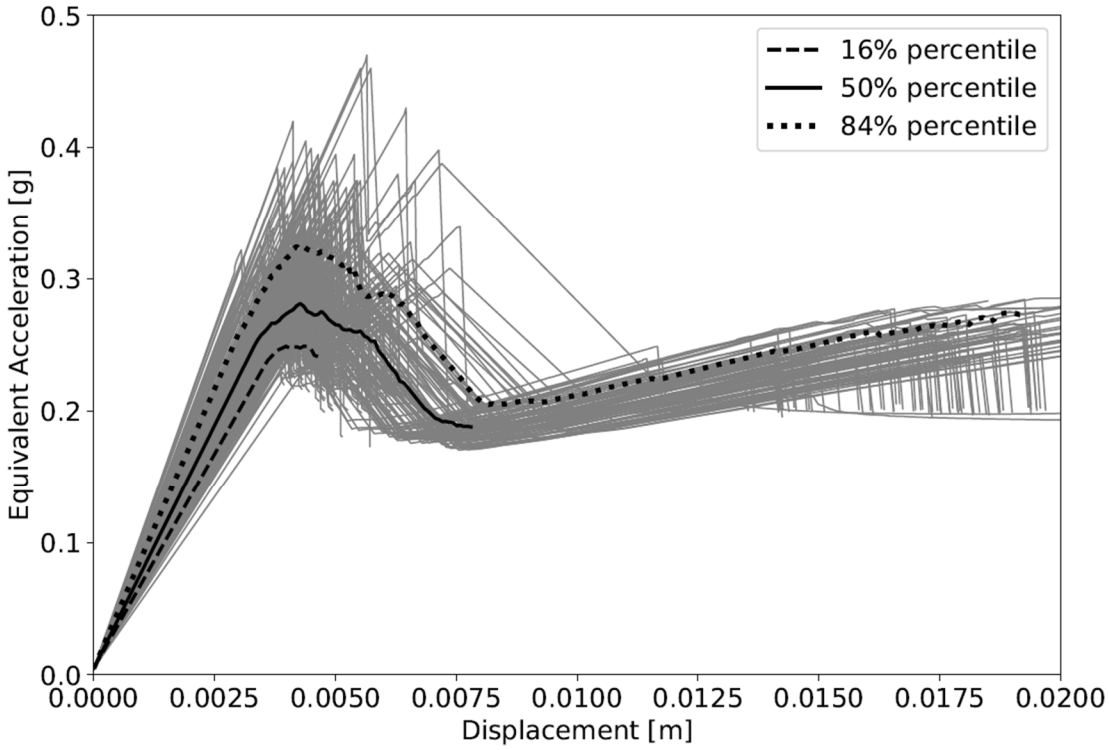

Figure 6.1.A: Obtained capacity curves for the 200 performed pushover analysis, as well as the 16%, 50% and 84% percentiles curves. The fact that several curves end prematurely is most likely due to numerical instabilities consequence of the constitutive model explained in section 5.4.

Figure 6.1.B presents the mean and the median (50% fractile) capacity curves, together with the pushover curve of the reference case, which depicts the capacity of the structure for the reference values of the material properties shown in Table 4.3.5.A.

The slightly higher elevation and significantly longer extension of the mean curve compared to the median, means that for each displacement the mean value of the curves above the median is located slightly farther from the median than the respective mean of the curves below it. This is more evident in figure 6.1.A, where the curves above the median appear significantly more dispersed than the curves below. In consequence, for the adopted distributions of the uncertain parameters, for a given d the distribution of a_e is unsymmetrical and shifted to the lower values.

Returning to figure 6.1.B, a similar conclusion can be drawn by looking at the position of the capacity curve for the reference case. The difference between the mean and the reference curve implies an unsymmetrical influence of an indeterminate number of input parameters to the structural capacity. More specifically, the samples of these input parameters that are above the mean push the capacity curve upwards more than the samples below the mean push it downwards. Therefore, the reference case becomes a significantly conservative case.

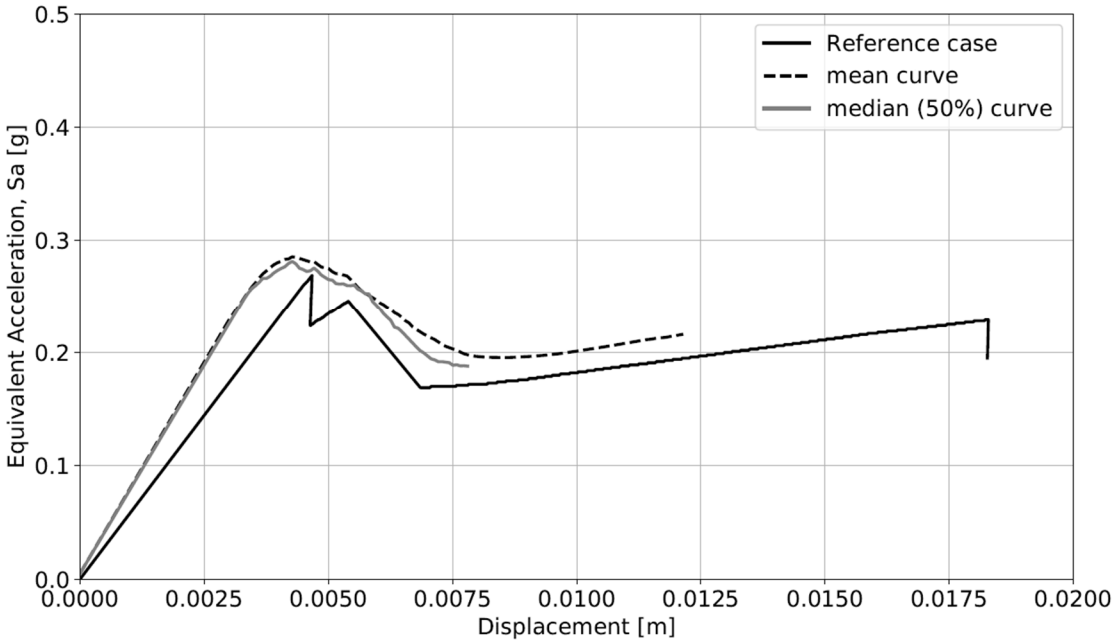

Figure 6.1.B: Mean, median and reference case capacity curves. The position of the mean and median curves implies that the curves above the median push the mean upwards more than the ones below push it downwards. A similar conclusion regarding the material properties can be drawn looking at the position of the mean and reference case curves.

6.2. Fragility curves

In figures 6.2.A to 6.2.E the fragility curves for the control nodes (figure 6.2.F) are presented. The vertical line in figures 6.2.A to 6.2.E for Peak Ground Acceleration (PGA) = 0.04g refers to the earthquake demand in the city of Barcelona (according to the Spanish code – (Spanish Ministry of Public Works, 2003)).

The demand is not enough in most of the control nodes to produce any structural damage to the structure, since the probability of achieving any Damage Grade (DG) is negligible. The exceptions are the control node B (figure 6.2.B) and the control node C (figure 6.2.C), where the provability of achieving the DG1 is of 10% and 5% respectively. This is significant and means that the provability of damage under the expected earthquake is low, and if it would be damage it could be imperceptible for the users –like minor fissures. In this way, no structural damage in the transversal bay was observed during the inspection (section 2.2) even though the church suffered a major earthquake in the late Middle Age (1428).

Another important feature in figures 6.2.A to 6.2.E is that the damage curves for DG1 and DG2 virtually maintain the same separation in terms of PGA for all the provability range. However, DG3 has a significantly different slope. This is because a significant amount of capacity curves end prematurely due to a numerical instability (Figure 6.1.A). However, the influence of this phenomenon is relatively low, since the DG3 curve only appears around PGA=0.08g, a PGA that doubles the earthquake demand.

Comparing the fragility curves for the different control nodes (Figures 6.2.A to 6.2.E) is easy to draw the conclusion that the conservativeness of the control nodes is inversely proportional to their height. This way, the nodes A, D and E (Figures 6.2.A, 6.2.D and 6.2.E) are the least conservative ones, the node C (Figure 6.2.C) holds an intermediate position and the node B (Figure 6.2.B) is the most conservative one. This is a conclusion that can be also drawn from the literature, since this is still a topic under discussion (Pelà, Aprile and Benedetti, 2009, 2013; Elyamani *et al.*, 2017). However, for the present case, seems that only one point of the three least conservatives (A, D and E) would have been necessary since they have very similar results.

In conclusion, even if several points are still necessary for the use of the N2 Method in complex masonry buildings, it is important that their heights are significantly different, in order to obtain significantly different results.

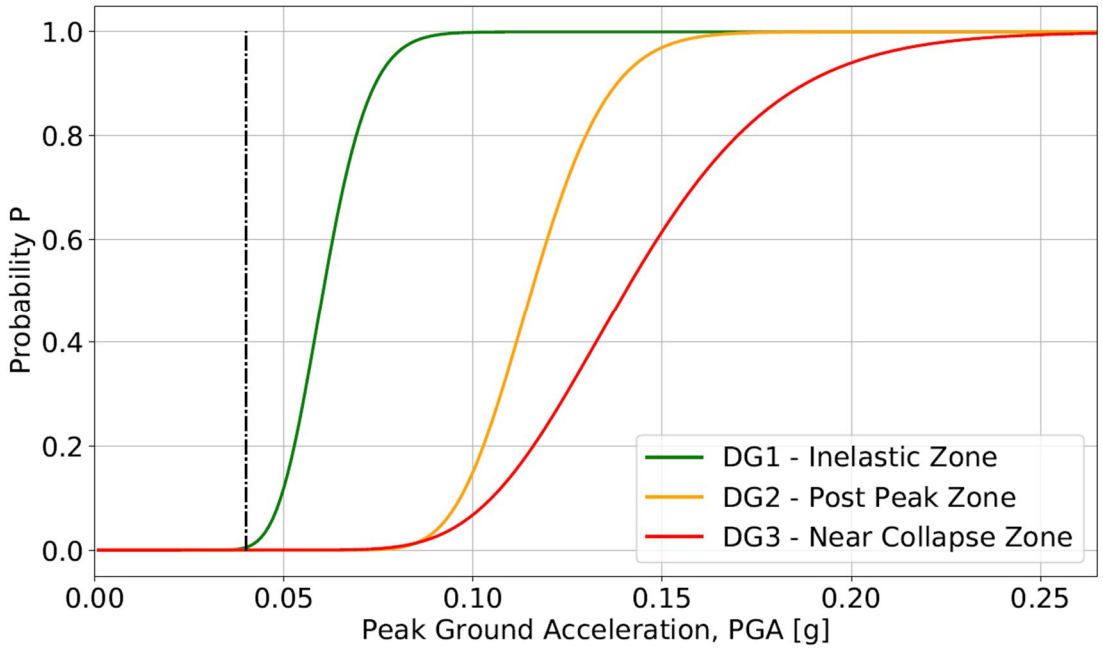

Figure 6.2.A: Fragility curves using the control node A, the provability of achieving any damage grade for the seism demand (PGA=0.04g) is negligible. This one of the least conservative chooses of Control Node.

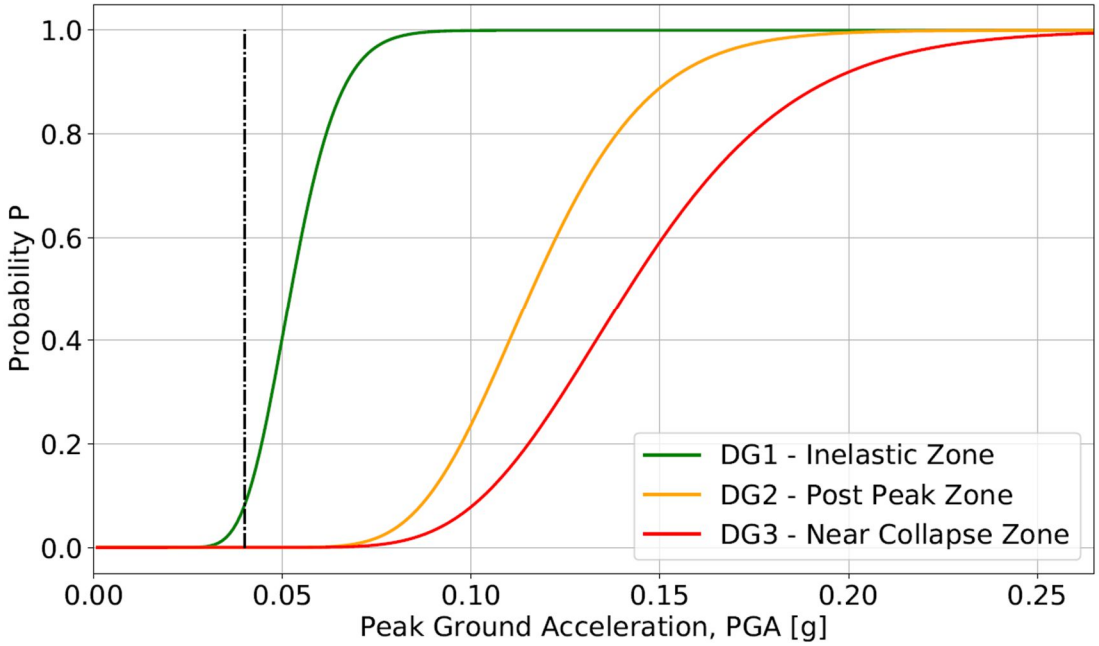

Figure 6.2.B: Fragility curves using the control node B, the provability of achieving any Damage Grade (DG) except the DG1 for the seism demand (PGA=0.04g) is negligible, the provability of achieving the DG1 is around 10%. This is the most conservative choose of Control Node.

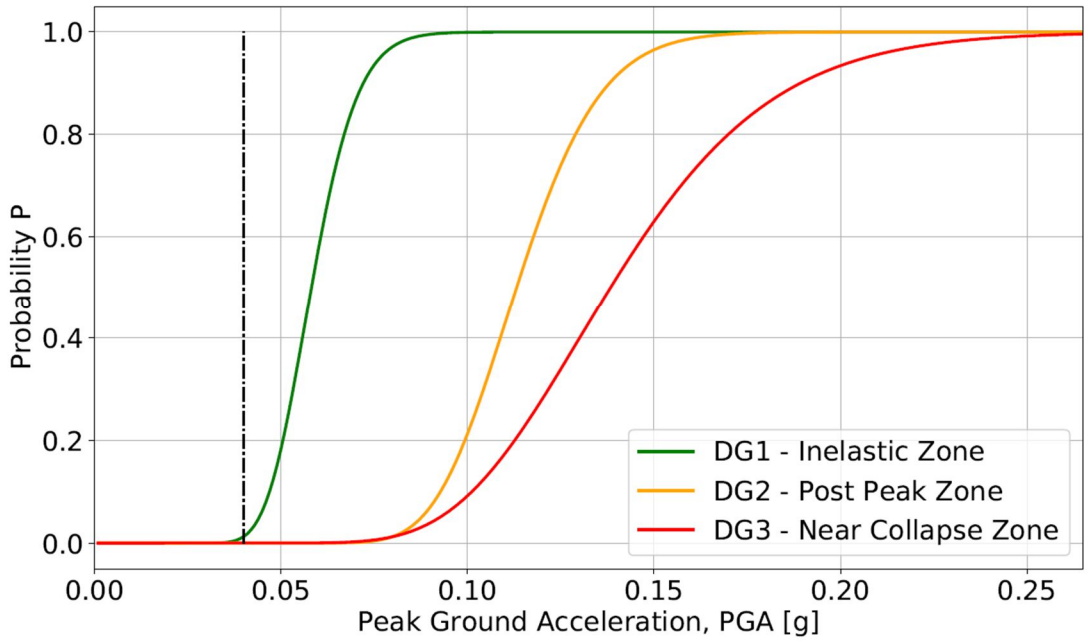

Figure 6.2.C: Fragility curves using the control node C, the provability of achieving any Damage Grade (DG) except the DG1 for the seism demand (PGA=0.04g) is negligible, the provability of achieving the DG1 is around 5%. This is the intermediate choose of Control Node.

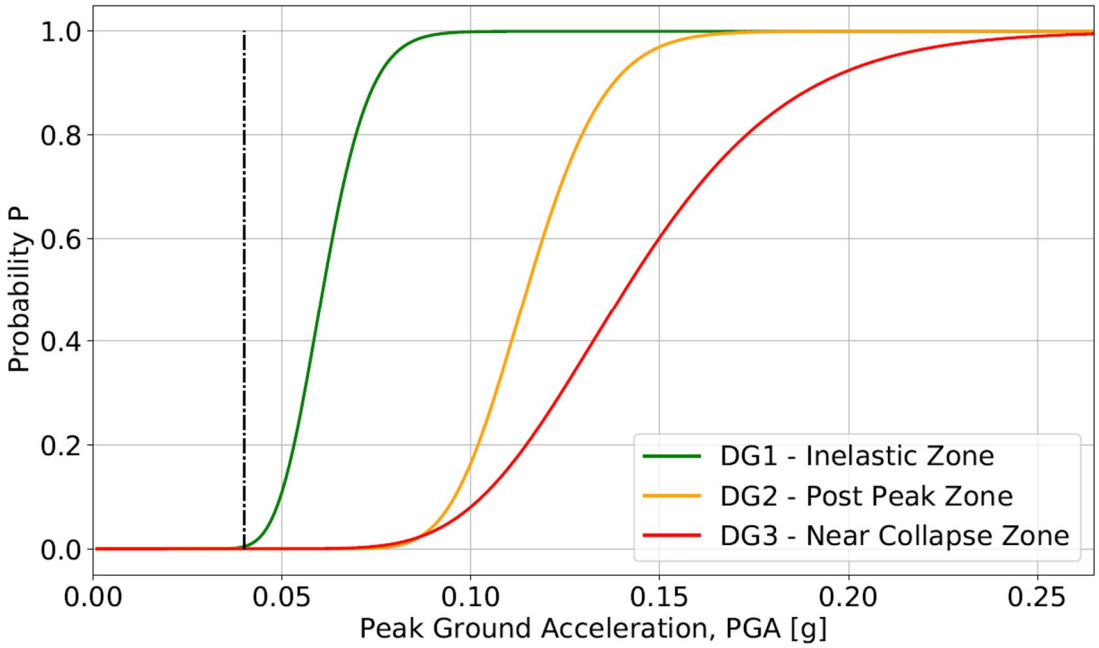

Figure 6.2.D: Fragility curves using the control node D, the provability of achieving any damage grade for the seism demand (PGA=0.04g) is negligible. This one of the least conservative chooses of Control Node.

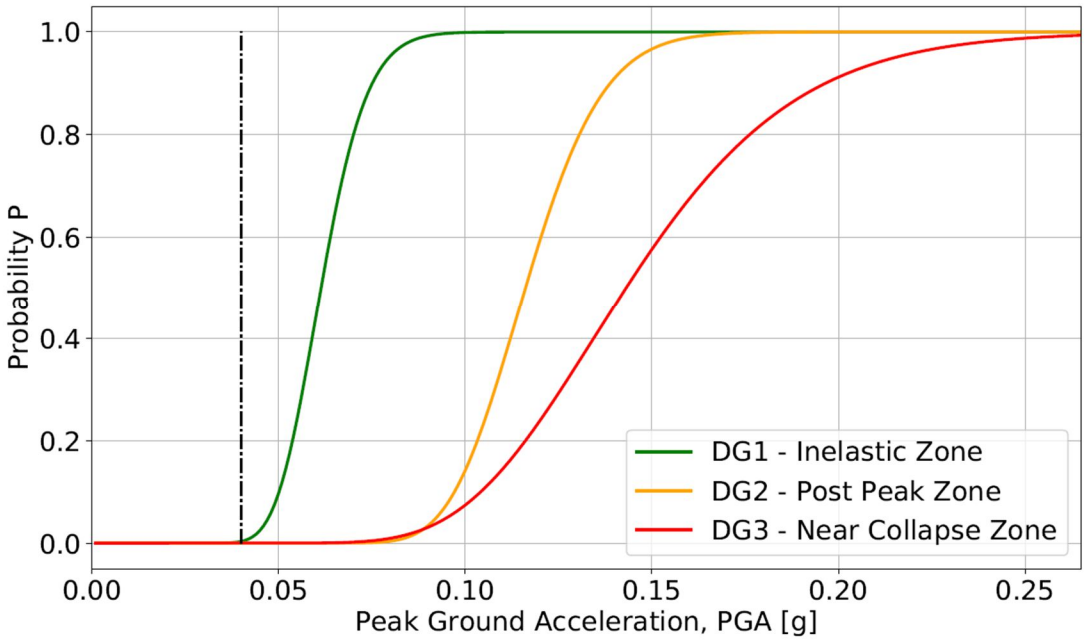

Figure 6.2.E: Fragility curves using the control node E, the provability of achieving any damage grade for the seism demand (PGA=0.04g) is negligible. This one of the least conservative chooses of Control Node.

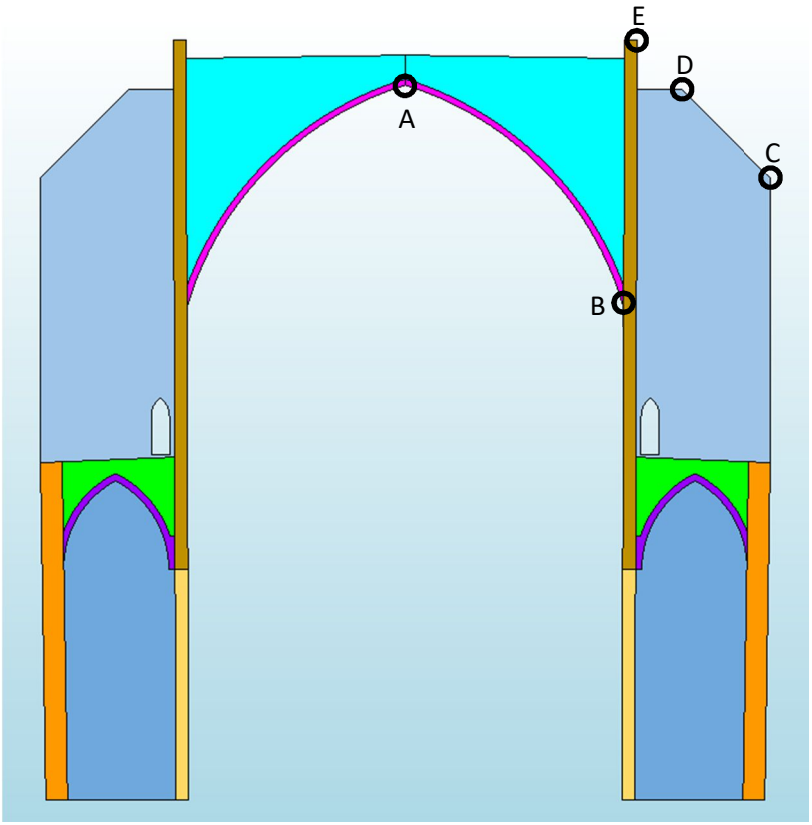

Figure 6.2.F: Control Nodes considered in the present thesis: (A) Reference Node, key of the nave vault; (B) Right spring of the Nave Vault; (C) Lower Top-Right corner of the Right Buttress; (D) Higher Top-Right corner of the Right Buttress (E) Higher-Right point of the Macroelement.

7. Conclusions

7.1. Conclusions of the Present Thesis

The main conclusion of the present thesis responds to the aim of it. The seismic vulnerability of the church of Santa Maria del Pi (SMPi) is very low in the transversal direction, since only 10% of the analysed samplings in the most conservative approach have reached the inelastic zone for the demand earthquake (Chapter 6). Therefore, the hypothetical damage that SMPi would face is low and might be inappreciable by the user –like minor fissures. Furthermore, the analysis of the capacity curves shows that the samples with better material properties achieve farer values above the mean than samples with worse material properties achieve below it. This means that SMPi is a very low seismic vulnerable church in the transversal direction, as the absence of visible structural damage in the transversal direction suggests (Section 2.2) –SMPi suffered a major earthquake in 1428.

About the methodology used in the present thesis (Chapter 4), it has been drawn he conclusion that the one used in the previous studies (Petromichelakis, Saloustros and Pelà, 2014; Contrafatto, 2017) is robust in most of its aspects. However, a significant improvement in the determination of the Damage Grades (DG) has been achieved. The DG used in the present thesis have a closer relationship with the general behaviour of the masonry structures and can be found in all the analysed literature.

Furthermore, the methodology was also improved in the use of the control nodes. In the present thesis (Chapter 6), it has been drawn the conclusion that it is necessary to use different control nodes (as in the analysed literature – section 3.1.3) and that their height should be significantly different. This last conclusion has been drawn from the obtained results.

In the present thesis, the FEM modelling procedure used (a 2D FEM model equivalent to a 3D one) has faced its limits (Chapter 5). This is mainly due to the 3D behaviour of the singular vault of SMPi and its singular relationship with the Buttresses as well as its major role in the global building behaviour. These characteristics make extremely difficult to obtain a 2D equivalent model. Nonetheless, a perfectly valid equivalent model has been obtained, in order to balance the exactitude and the computational cost of the analysis.

SMPi has resulted to be an outstanding masonry church in its transversal seismic resistance, especially compared to the similar cases in the zone (Petromichelakis, Saloustros and Pelà, 2014; Contrafatto, 2017). Therefore, the results show no worrying issues regarding the transversal seismic vulnerability of SMPi.

7.3. Suggestions for the Future Work

The suggestions for the future work, that outline the present thesis, are the following:

- A study about the possible adaptations of the constitutive model used in the methodology to the buildings where the methodology is thought to be used, in order to eliminate or minimize the vertical decays that made it slightly instable (Section 5.4). This study would include a comparison with other applicable constitutive models.

- A similar study to the one of the present thesis but using the transversal macroelement of the church of Santa Maria del Pi (SMPi) in order to complete the seismic assessment.

- In order to obtain the collapse mechanisms and the influence of the Vaults Infill material in SMPi's behaviour a limited similar study using the 3D model is recommended.

- One remaining question is the real seismic influence of the rubble material layer found in the soil below the foundations of SMPi (section 4.5.2). In the present thesis a conservative approach has been used, but a detailed study on the soil characteristics and behaviour may lead to more precise results.

8. Bibliography

Advisory Committee on Technical Recommendations for Construction (2013) *Guide for the Probabilistic Assessment of the Seismic Safety of Existing Buildings*. National Reserch Council of Italy (CNR).

Basílica de Santa Maria del Pi (2017). Available at: http://basilicadelpi.com/ (Accessed: 22 May 2018).

Batlle & Mascareñas Geoprojectes SL (2007a) *Estudi Geotècnic en Primera Fase per a la Diagnosi de Patologies Afectant Determinats Sectors de la Basílica de Santa Maria del Pi, a Barcelona*. (In Catalan).

Batlle & Mascareñas Geoprojectes SL (2007b) *Estudi Geotècnic en Primera Fase per a la Diagosi de Patologies Afectant Determinats Sectors de la Basílica de Santa Maria del Mar, a Barcelona*. (In Catalan).

Cattari, S., Lagomarsino, S. and Ottonelli, D. (2014) 'Fragility Curves for Masonry Buildings from Empirical and Analyitical Models', in *Second European Conference on Earthquake Engineering and Seismology*. Istambul.

Contrafatto, F. R. (2017) *Vulnerability assessment of monumental masonry structures including uncertainty*. Universitat Politècnica de Catalunya.

Costa, A. A., Penna, A. and Magenes, G. (2011) 'Seismic Performance of Autoclaved Aerated Concrete (AAC) Masonry: From Experimental Testing of the In-Plane Capacity of Walls to Building Response Simulation', *Journal of Earthquake Engineering*. Taylor & Francis Group, 15(1), pp. 1–31.

D'Ayala, D. and Speranza, E. (2003) 'Definition of Collapse Mechanisms and Seismic Vulnerability of Historic Masonry Buildings', *Earthquake Spectra*, 19(3), pp. 479–509.

Dymiotis, C., Kappos, A. J. and Chryssanthopoulos, M. K. (1999) 'Seismic Reliability of RC Frames with Uncertain Drift and Member Capacity', *Journal of Structural Engineering*, 125(9), pp. 1038–1047.

Elyamani, A. *et al.* (2017) 'Seismic safety assessment of historical structures using updated numerical models: The case of Mallorca cathedral in Spain', *Engineering Failure Analysis*. Pergamon, 74, pp. 54–79.

Endo, Y. *et al.* (2015) 'Comparison of seismic analysis methods applied to a historical church struck by 2009 L'Aquila earthquake', *Bulletin of Earthquake Engineering*. Springer Netherlands, 13(12), pp. 3749–3778. doi: 10.1007/s10518-015-9796-0.

Euro-International Comitee for Concrete (1990) *CEB-FIB Model Code 1990*.

European Committee for Standardization (2004) *Eurocode 8: Design of structures for earthquake resistance - Part 1: General rules, seismic actions and rules for buildings (EN 1998-1:2004)*. Brusels.

European Seismologic Commission (1998) *European macroseismic scale 1998 : EMS-98*. Edited by G. Grünthal. Luxembourg: Centre Européen de Géodynamique et de Séismologie.

Fajfar, P. (2000) 'A Nonlinear Analysis Method for Performance-Based Seismic Design', *Earthquake Spectra*, 16(3), pp. 573–592.

Galasco, A., Lagomarsino, S. and Penna, A. (2006) 'On the use of pushover analysis

for existing masonry buildings', in *First European Conference on Earthquake Engineering and Seismology (a joint event of the 13th ECEE & 30th General Assembly of the ESC)*. Geneva, Switzerland.

Griera i Cura, A. and Artime Alem, L. (2007) *Aixecament per l'estudi de l'estat estructural de l'església de Santa Maria del Pi a Barcelona*. Sabadell.

ICOMOS (2003) 'ICOMOS Charter- Principles for the Analysis, Conservation and Structural Restoration of Architectural Heritage', in *ICOMOS 14th General Assembly*. Victoria Falls, Zimbaue.

Institut Cartogràfic i Geològic de Catalunya (2018). Available at: http://www.icc.cat/vissir3/ (Accessed: 29 May 2018).

Italian Ministry of Infrastructure (2008) 'Approvazione delle nuove norme tecniche per le costruzioni', *Gazzetta Ufficiale della Repubblica italiana*. 4 febbraio. Rome (in Italian), 29(Serie Generale), p. Supplemento Ordinario n.30 (In Italian).

Italian Ministry of Infrastructure and Transport (2009) 'Istruzioni per l'applicazione delle «Nuove norme tecniche per le costruzioni» di cui al decreto ministeriale 14 gennaio 2008', *Gazzetta Ufficiale della Repubblica italiana*, p. Supplemento Ordinario n.27 (In Italian).

Jalayer, F., Iervolino, I. and Manfredi, G. (2010) 'Structural modeling uncertainties and their influence on seismic assessment of existing RC structures', *Structural Safety*. Elsevier, 32(3), pp. 220–228.

Karbassi, A. and Lestuzzi, P. (2012) 'Fragility Analysis of Existing Unreinforced Masonry Buildings through a Numerical-based Methodology', *The Open Civil Engineering Journal*, 6(1), pp. 121–130.

Kernler, D. (2014) *File:Empirical Rule.PNG - Wikimedia Commons*. Available at: https://commons.wikimedia.org/wiki/File:Empirical_Rule.PNG (Accessed: 3 June 2018).

Krawinkler, H. (1999) 'Challanges and Progress in Performance-Based Earthquake Engineering', in *International Seminar on Seismic Engineering for Tomorrow – In Honor of Professor Hiroshi Akiyama*. Tokyo, Japan.

Lagomarsino, S. and Giovinazzi, S. (2006) 'Macroseismic and mechanical models for the vulnerability and damage assessment of current buildings', *Bulletin of Earthquake Engineering*. Kluwer Academic Publishers, 4(4), pp. 415–443.

Lang, K. (2002) *Seismic vulnerability of existing buildings*. vdf, Hochschulverlag an der ETH Zürich.

Lantada, N. *et al.* (2010) 'Seismic hazard and risk scenarios for Barcelona, Spain, using the Risk-UE vulnerability index method', *Bulletin of Earthquake Engineering*. Springer Netherlands, 8(2), pp. 201–229.

Lourenço, P. B. (2001) 'Analysis of historical constructions: From thrust-lines to advanced simulations', in Lourenço, P. B. and Roca, P. (eds) *Historical Constructions 2001: Possibilities of numerical and experimental techniques (Proceedings of the 3rd International Seminar)*. Guimarães, Portugal: University of Minho, pp. 91–116.

Lourenço, P. B. (2009) 'Recent Advances in Masonry Modelling: Micromodelling and Homogenisation', in *Multiscale Modeling in Solid Mechanics*. London: Imperial College Press (Computational and Experimental Methods in Structures), pp. 251–294.

Lourenço, P. B. *et al.* (2011) 'Analysis of Masonry Structures Without Box Behavior', *International Journal of Architectural Heritage*. Taylor & Francis Group, 5(4–5), pp. 369–382.

Manie, J. and Kikstra, W. P. (eds) (2017) *DIANA – Finite Element Analysis, User's Manual release 10.1, Material Library*. Delft: DIANA FEA BV.

Mouroux, P. and Le Brun, B. (2006) 'Presentation of RISK-UE Project', *Bulletin of Earthquake Engineering*. Kluwer Academic Publishers, 4(4), pp. 323–339.

Mouyiannou, A. *et al.* (2014) 'Identification of Suitable Limit States from Nonlinear Dynamic Analyses of Masonry Structures', *Journal of Earthquake Engineering*. Taylor & Francis Group, 18(2), pp. 231–263.

Murcia, J. (2008) *Seismic Analysis of Santa Maria del Mar Church in Barcelona*. Universitat Politècnica de Catalunya.

Navarro, A. *et al.* (2013) *1714 Santa Maria del Pi, una Comunitat Assetjada*. Edited by J. Sacasas, V. Martín, and F. X. Monjo. Barcelona: Arxiu Parroquial de Santa Maria del Pi (in Catalan).

Ortega, J. *et al.* (2018) 'Assessment of the influence of horizontal diaphragms on the seismic performance of vernacular buildings', *Bulletin of Earthquake Engineering*. Springer Netherlands, pp. 1–34.

Park, J. *et al.* (2009) 'Seismic fragility analysis of low-rise unreinforced masonry structures', *Engineering Structures*. Elsevier, 31(1), pp. 125–137.

Pelà, L., Aprile, A. and Benedetti, A. (2009) 'Seismic assessment of masonry arch bridges', *Engineering Structures*. Elsevier, 31(8), pp. 1777–1788.

Pelà, L., Aprile, A. and Benedetti, A. (2013) 'Comparison of seismic assessment procedures for masonry arch bridges', *Construction and Building Materials*. Elsevier, 38, pp. 381–394.

Petromichelakis, I., Saloustros, S. and Pelà, L. (2014) 'Seismic assessment of historical masonry construction including uncertainty.', in Cunha, A. et al. (eds) *Proceedings of the 9th International Conference on Structural Dynamics, EURODYN 2014*. Porto: European Association for Structural Dynamics (EASD), pp. 297–304.

Politecnico di Milano (2010) 'Deliverable 3.1: Inventory of earthquake-induced failure mechanisms related to construction types, structural elements, and materials', in *European Collaborative Project: NIKER (WORKPACKAGE 3: Damage based selection of technologies)*.

Riks, E. (1979) 'An incremental approach to the solution of snapping and buckling problems', *International Journal of Solids and Structures*. Pergamon, 15(7), pp. 529–551.

Rota, M., Penna, A. and Magenes, G. (2010) 'A methodology for deriving analytical fragility curves for masonry buildings based on stochastic nonlinear analyses', *Engineering Structures*. Elsevier, 32(5), pp. 1312–1323.

Rots, J. G. (1988) *Computational Modeling of Concrete Fracture*. Delft University of Technology.

Saloustros, S. *et al.* (2015) 'Numerical analysis of structural damage in the church of the Poblet Monastery', *Engineering Failure Analysis*, 48, pp. 41–61. doi:

10.1016/j.engfailanal.2014.10.015.

Saloustros, S. *et al.* (2018) 'Vulnerability Assessment of Monumental Masonry Structures Including Uncertainty', in *11th International Conference on Structural Analysis of Historical Constructions*. Cusco, Perú.

Singhal, A. and Kiremidjian, A. S. (1996) 'Method for Probabilistic Evaluation of Seismic Structural Damage', *Journal of Structural Engineering*, 122(12), pp. 1459–1467.

Spanish Ministry of Public Works (ed.) (2003) *Norma de construcción sismorresistente: Parte general y edificación (NCSE-02)*. 1st edn. Madrid (In Spanish).

StijnDeVuyst (2016) *File:Lognormal Distribution.svg - Wikipedia*. Available at: https://en.wikipedia.org/wiki/File:Lognormal_Distribution.svg (Accessed: 2 June 2018).

Sýkora, M. and Holický, M. (2010) 'Probabilistic Model for Masonry Strength of Existing Structures', *Engineering MECHANICS*, 17(1), pp. 61–70.

Tomaževič, M. (2007) 'Damage as a measure for earthquake-resistant design of masonry structures: Slovenian experience.', *Canadian Journal of Civil Engineering*, 34(11), pp. 1403–1412.

Tomaževič, M. and Klemenc, I. (1997) 'Seismic behaviour of confined masonry walls', *Earthquake Engineering & Structural Dynamics*. Wiley-Blackwell, 26(10), pp. 1059–1071.

Tomaževič, M., Turnšek, V. and Terčelj, S. (1978) *Computation of the shear resistance of masonry buildings.*, *Report ZRMK-IK*. Ljubljana (in Slovene).

Tomaževič, M. and Žarnič, R. (1984) 'The effect of horizontal reinforcement on the strength and ductlility of masonry walls at shear faliure', *Report ZRMK-IK*, 2, pp. 1291–1302.

Vamvatsikos, D. and Fragiadakis, M. (2009) 'Incremental dynamic analysis for estimating seismic performance sensitivity and uncertainty', *Earthquake Engineering & Structural Dynamics*. Wiley-Blackwell, 39(2).

Vergés, T. (1992) *Santa Maria del Pi i la Seva Història*. Barcelona: La Formiga d'Or (in Catalan).